Residual Voltage in Biphasic Electrical Stimulation: Cause, Clues, and Control

Submitted in partial fulfillment of the requirements for

the degree of

Doctor of Philosophy

in

Electrical and Computer Engineering

Ashwati Krishnan

Master of Science, Electrical & Computer Engineering, December 2010

Carnegie Mellon University, Pittsburgh, USA

Bachelor of Technology, Electronics & Instrumentation Engineering, June 2009

Vellore Institute of Technology, Vellore, India

Carnegie Mellon University

Pittsburgh, PA, USA

Supervisor: Dr. Shawn K. Kelly
Institute of Complex Engineered Systems
Carnegie Mellon University

Committee Members: Dr. Gary K. Fedder
Electrical and Computer Engineering
Carnegie Mellon University

Dr. Jeffrey Weldon
Electrical and Computer Engineering
Carnegie Mellon University

Dr. Tracy Cui
McGowan Institute for Regenerative Medicine
University of Pittsburgh

Dr. Peter Gilgunn
Dynamics Inc., Pittsburgh, PA, USA

Dedicated to my grandmother,

Saradha Venkataraman *(9 July, 1933 - 4 February, 2016)*,

who always believed that I was the best engineer she knew.

Acknowledgements

"Cultivate the habit of being grateful for every good thing that comes to you, and to give thanks continuously. And because all things have contributed to your advancement, you should include all things in your gratitude."

Ralph Waldo Emerson

My academic and personal growth at Carnegie Mellon University is due to an amalgamation of a lot of people and experiences. I would like to acknowledge the Pennsylvania Infrastructure Technology Alliance for funding a large part of this research, as well as the Sigma Xi Grants-In-Aid of Research for supplementary funding. I would like to first thank Dr. Shawn Kelly for all his guidance and support over the years, and helping me develop and mature into a more confident researcher. I have had the privilege of having his undivided attention, and I appreciate the times he has allowed me to barge into his office with ideas and questions. I am grateful for the fact that he has allowed me to work independently and given me the time to understand concepts at my own pace. Most importantly, I am thankful for the support he has given me over the years, both personal and professional.

I feel my entry into the Ph.D. program in the ECE Department at CMU happened under unique circumstances, and I would not be here if not for the support of Dr. Gary Fedder, with a lot of help from Elaine Lawrence. Dr. Fedder has provided very appropriate and insightful comments at critical stages of my work. A very useful statement that has stuck with me for over 4 years now, came when I was taking up my qualifier exam, and it goes, "Don't wonder why they are asking you the question, just answer the question." There is a

raw efficiency to following that statement, which has made all my technical confrontations since then, straightforward. I am grateful for his guidance.

One of my earliest impressions of Dr. Peter Gilgunn was when he walked into the office on (what may have been) a Friday afternoon, and exclaimed aloud to a student (on purpose), "Have the brains arrived yet?" He wasn't joking - apart from his sense of humour, his enthusiasm for neuroscience was contagious. While he was a professor in ECE, I also had the privilege of being a teaching assistant for one of his courses. He is never hesitant to give me well-meaning constructive criticism. I am grateful for all the conversations we have had about life, research and education.

It is very encouraging to have a committee member who is insightful and curious at the same time. When I first spoke to Dr. Jeff Weldon about being on my committee, he was intrigued about the direction of my research, and understood its significance. Even though he was more familiar with circuit design than neural stimulation, he was receptive and asked questions and picked up key aspects of my work. A lot of times his questions have given me ideas to further develop the work. It has been a pleasure having him as a committee member.

In the field of bio-electronics, it is very easy to work on the electronics without proper insight into the biological aspects of the work. While Dr. Shawn Kelly's course on Neural Technology provided a good foundation, I am very glad I got to work with Dr. Xinyan (Tracy) Cui and her students. The biggest question I had in my research about residual voltage in biphasic stimulation for about 4 years was - "Can this really be a problem in a tissue environment?". She helped me set up preliminary animal experiments, which is uncommon for most electronics engineers, and along with Zhanhong (Jeff) Du, we found that residual voltage can increase to unsafe voltage levels in tissue. She is enthusiastic and encouraging, and has provided sound technical feedback for my experiments.

My first taste of research was under the guidance of Dr. Mel Siegel, and I continue to follow up with him occasionally, even today. He has a very practical view of the world and he always shares his observations. I have also had conversations with Dr. Charles

Neuman, who checked up on me at regular intervals and Dr. Bhiksha Raj, who has seen me grow from a naive, young student to what I am today - a not-as-naive, older student. I am grateful to my graduate course professors at CMU - Dr. Larry Pileggi, Dr. Tamal Mukherjee, Dr. Rick Carley, Dr. Jeyanandh Paramesh, who have helped me hone my skills and professional interests. Back in India, at a time when the majority of students would take up a job after their undergraduate education, my interests were in research. In this regard, I would like to thank my college professors from Vellore Institute of Technology (VIT, Vellore) - Mr. Ruban, Dr. Arulmozhivarman, Mr. Sivabalan and Dr. Elizabeth Rufus, for their support and encouragement. I owe my intellectual development to some of the many influential teachers I have had at school - Prema Shekar Ma'am, Geeta Rajendran Ma'am, Praveena Ma'am, Shyamala Ma'am, Ananthan Sir and Ravishankar Sir, Srimathi Ma'am and Narayanaswamy Sir.

Life in the MEMS office was always fun, and I will cherish the conversations I have had with Kristen Dorsey, Nathan Lazarus, Congzong Guo and Dylan Fang. They were ready to give advice about their experiences and in the same way I share my experiences with Sean Yen, Mats Forssell, Erdinc Tatar, Albert Patterson, Metin Guney, Mary Beth Galanko, Xiao Chuan Ong and Lionel Wong. I hope the conversations on seemingly-useless topics on Friday afternoons never end. I had the opportunity to help start-up a lab from scratch, right from finding a room, to see it move to its new space in a new building. I have appreciated the opportunity to mentor people in the Neural Devices Engineering Lab (NDEL), Varsha Shetty, Xuetong Mao (Amy), Enqun Zhou (Gabby), Mohsin Shahmohmadi, Chi Hua Lin (Dale) and Aziz Yousif. Additionally, I am ever grateful to Mohmammed Omar Darwish for teaching me a lot about integrated circuit design and guiding me through my designs. To all the students I have been a teaching assistant for, it has been a pleasure teaching you, and learning from you as well.

The ECE department has undergone a lot of changes during my time here, and I am grateful to the administrative staff for helping with the little things, like keeping out a snack during stressful times. In particular, I would like to thank Elaine, Samantha, Lyz, Debbie,

Susan, Jeff Zayas and Nathan Snizaski. I was lucky to be part of two departments with amazing staff, and I am grateful to Christina, Alicia, Rhonda, Becca and Charlie over at the ICES department. I have enjoyed all our hallway conversations.

I have had a fulfilling life here in Pittsburgh, and there are so many groups of people that have been responsible for it. Firstly, I would like to thank all the members of the Shotokan Karate Club - Daemon, Konstantin, Dante, Mridula, Nobu, Alan and Zach. In particular, to Bruce Schmidt, for making me strive for perfection, and teaching me about balance and consistency in life. To the Quiz Club - Utsav, Nishtha, Suyash, Apurva, Keshav, Varun, Abhijeet, Samrat, Aranya, Supreeth, Lavanya, Harini, Chitra, Satya, Vinod, Toupie, Uday, Krishna, Ranjini, Maddali, Erle, Sudarshan, Sekhar, Mike, Saurabh and Ji. Friday evenings without the Quiz Club will never be the same again. Thanks to my friends in the Taza coffee group - Vivek, GC, Shane, Aravindan, PJ, Harsha, SKB, Joy, Sudhanshu, Arvind and Niranjini - I have enjoyed and learned from the interesting conversations we have had over coffee. To the people I got to know through Indian Graduate Student Association, Vishnu, Vignesh, Madhu, Meghana, Bhavana, Ruta, Sumon and Arun for helping me express my creativity and leadership. I learned a lot about administration and working with people during my time at the IGSA. To the Drama Club, Mudit, Sudipto, Aditya, Madhu, Ankita and Pushkala for all the laughs we have had during rehearsals. To 5826 Darlington Road, and all the housemates I have had there - Usha, Shravya, Aishwarya, Lavanya, Jyoti, Divya Hariharan and most importantly, Divya Sharma(ji). To all the people I have had the pleasure of knowing and hosting at home - Kota, Vinay Krishna, Kaushik, Navin, Vikram as well as Varoon, Abhinav, Jajoo, Anirban and Deepa. I would like to thank Mary aunty and Geeta aunty, and their respective families, for making me feel like I have a home away from home.

Over the years, I have had the privilege of sharing my thoughts with a lot of my close friends from high school and college - Priyanka, Shivangi, Sujitha, Harish, Maruthi, Mahesh, Subho, Gaurav, Varenya and Zach. I am very grateful for the fact that they lent an ear through the ups and downs of what can seem like an endless process.

I consider myself one of the luckiest people in the world because I have the love and

support of my family. Words are not enough to express my gratitude to my parents, Dr. K.V. Krishnan and Dr. Lalitha Krishnan, for showing me what hard work really means, and if I am at least half as dedicated as they are, I would consider myself worthy. To my sister, Anjali Krishnan, for being the strong and loving character she is. She has taught me a lot about strength and persistence, and I know that we will always support each other when we need it. To my brother-in-law, yet who is more like a brother, Bharath Prithiviraj, for constantly encouraging me to take up new and interesting opportunities, and for tolerating my sister and I, with our sibling eccentricities. To Uday, who made the last year of my graduate studies so colourful, and I hope to see many vibrant years in the future. To my little nephew, Vedu, for being the most entertaining little human being I have ever met and for providing my family with so much happiness, at a time when we all needed it the most. To my grandmother, Saradha Venkataraman, who I will miss very much.

Ashwati Krishnan

> "I may not have gone where I intended to go, but I think I have ended up where I needed to be."
>
> Douglas Adams

Abstract

Electrical stimulation of neural tissue has been known to evoke functional responses in animals. Stimulation is primarily performed by passing controlled, symmetric biphasic current pulses to an electrode placed near the neural tissue. The biphasic current pulse consists of a negative pulse, followed by a positive pulse to maintain charge neutrality. A theoretical analysis on a first order electrode-electrolyte (tissue) interface model has shown that perfectly balanced input current signals do not ensure net neutrality at the interface, due to an unrecoverable loss of charge via the faradaic impedance. In chronically implanted devices, there is currently no practical way to quickly identify changes that occur at the electrode-tissue interface, especially in high-density electrode arrays. This work explores the extent to which the residual voltage can act as a preliminary indicator of electrode degradation, because residual voltage is essentially a characteristic of the interface. While residual voltage provides timely feedback when sampled at regular intervals, it can accumulate and a DC voltage on a stimulation electrode can be potentially unsafe in a chronically implanted device. The method of delivering current signals has traditionally been implemented as an open loop system. This work also demonstrates that one can control the residual voltage by correcting the positive pulse of the biphasic signal based on the existing state of the electrode-electrolyte/tissue interface. While the resulting biphasic stimulation waveform is imbalanced, the interface is electrochemically neutral. The updated value of the imbalanced anodic pulse width can provide us meta-data about the interface, in case there is any degradation. By controlling the residual voltage at the electrode actively with feedback, the proposed closed loop system will improve the safety of neural stimulator systems.

Contents

List of Figures

List of Tables

Chapter 1

Introduction

Functional Electrical Stimulation

Artificial electrical stimulation is the use of electrical charge to induce a physiological response in neural tissue. Recent research developments suggest that electrical stimulation of retinal tissue can evoke rudimentary vision in blind humans. An interesting, and challenging space for electrical stimulation is the development of a retinal implant for vision impairment. Two medical conditions that stand to benefit from a retinal prosthesis are retinitis pigmentosa (RP) and age-related macular degeneration (AMD) [1]. These diseases correlate to a degeneration of the retina, ultimately leading to vision impairment. With the advent of microelectronics, we are now able to target smaller areas of tissue for functional electrical stimulation. A retinal implant typically comprises an electronic circuit that injects charge into the retinal tissue via an array of electrodes. There are at least 15 research groups currently working on developing a high-density electrode array based implant retinal prosthesis [2].

Implantable biomedical devices need to make sure that chronic use of the device does not cause any harm or damage to the target area. Stimulation devices can change the nature of the electrode-tissue interface by electrochemical corrosion or by the development of scar tissue. For high density stimulation electrodes ($>$ 100 electrodes) it can be very

useful to know, at the earliest, if there is any degradation at the electrode-tissue interface. Residual voltage, which is a leakage voltage that occurs at the end of a biphasic stimulation pulse, is a function of the impedance of the electrode-tissue interface. The work presented in this thesis focuses on measurement of the residual voltage to monitor the health of the electrode. Additionally, it is imperative to ensure that electrical stimulation devices are safe. The presence of a net direct current leakage through the electrode can result in long-term damage to the tissue surrounding the electrode. The second part of this thesis suggests an active feedback stimulation method to ensure that there is electrochemical neutrality at the interface. Active anodic feedback allows us to monitor the neural interface, and compensate for any charge error that might arise during biphasic stimulation.

To garner some perspective, this chapter explores the approaches to electrical stimulation over the years. Particularly, there have been several major scientific and engineering advances that have resulted in the ability for a new generation of high-density electrode stimulation devices.

1.1 Brief History of Functional Electrical Stimulation

The earliest documented use of electrical stimulation for medical treatment dates back to the 50 A.D., when a Roman physician Scribonius Largus used torpedo fish to treat headache and gout (Figure 1.1). The patient was to 'apply' the fish to the painful region until the area become numb [3]. In the middle of the 18th century, it was discovered that the nervous system can be a sensitive electrical detector. Benjamin Franklin arrived at the empirical observation that electric shocks cause muscle contraction. In 1791, Luigi Galvani induced muscular contractions in frog's legs using a metallic device constructed from dissimilar metals[1]. The invention of the electric generator and alternating current by Michael Faraday in 1831, saw the use of a plethora of animal experiments to study electrical stimulation.

[1]While Galvani thought the muscle discharged onto the metal, Alessandro Volta thought otherwise, realizing that the frog's leg served as a conductor of electricity, and went on to discover the electrochemical series, and the battery! [4]

In 1848, German physiologist Emil du-Bois Reymond discovered the nerve action potential and demonstrated the stimulation of nerves in frog legs. He also demonstrated that the time-varying nature of faradaic current was important for efficient electrical stimulation [5]. In 1852, Guillaume-Benjamin Duchenne became the first person to systematically use electricity to study disease, and used faradaic current to treat facial palsy via electrical stimulation [6]. A chronological history of electrical stimulation used for treatment of chronic pain can be found in [7].

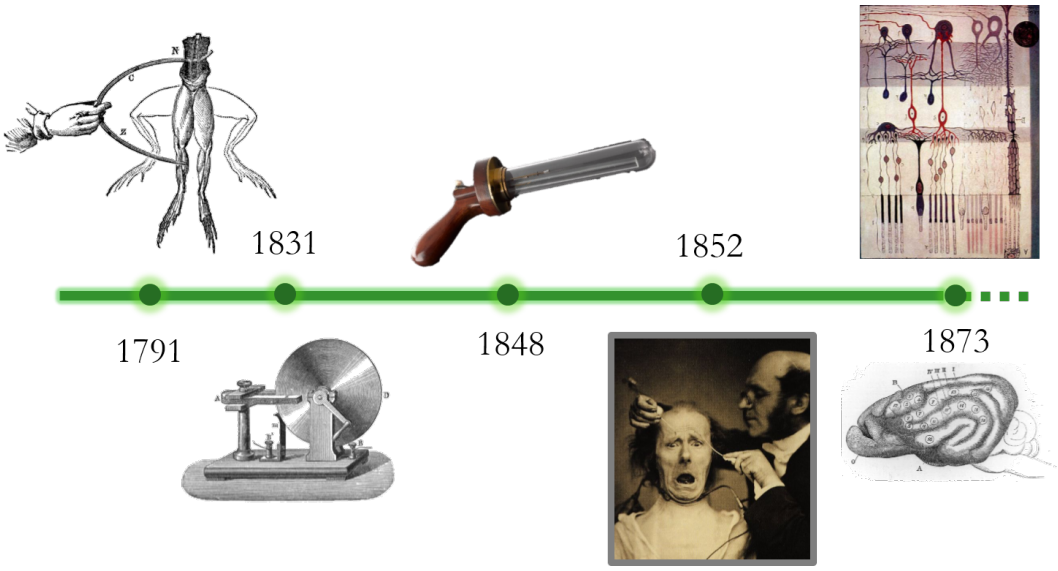

Figure 1.1: Chronological development of functional electrical stimulation: Early years from 1791 to 1852.

In 1873, David Ferrier, a Scottish neurologist had the opportunity to stimulate and lesion the brains of birds, cats, dogs, guinea pigs and rabbits, and was one of the first experimentalists to produce publications on the cortical map of a dog [8]. Also in 1873, Camillo Golgi invented a method of staining that allowed people to visualize individual neurons for the first time. Using the Golgi technique, Spanish anatomist Santiago Ramn y Cajal characterized the neuron in elegant detail. Both Golgi and Ramn y Cajal shared the Nobel Prize in Physiology and Medicine in 1906 for their contributions. Going forward a few years, in 1939, Hodkgin and Huxley successfully recorded the intracellular action potential and published their work in Nature in October of that year. They repeatedly measured the action potential

in the giant axon of a squid and developed a mathematical equation for the action potential in 1952[2] [9]. The Hodgkin-Huxley equation earned them the Nobel Prize in Physiology and Medicine in 1963.

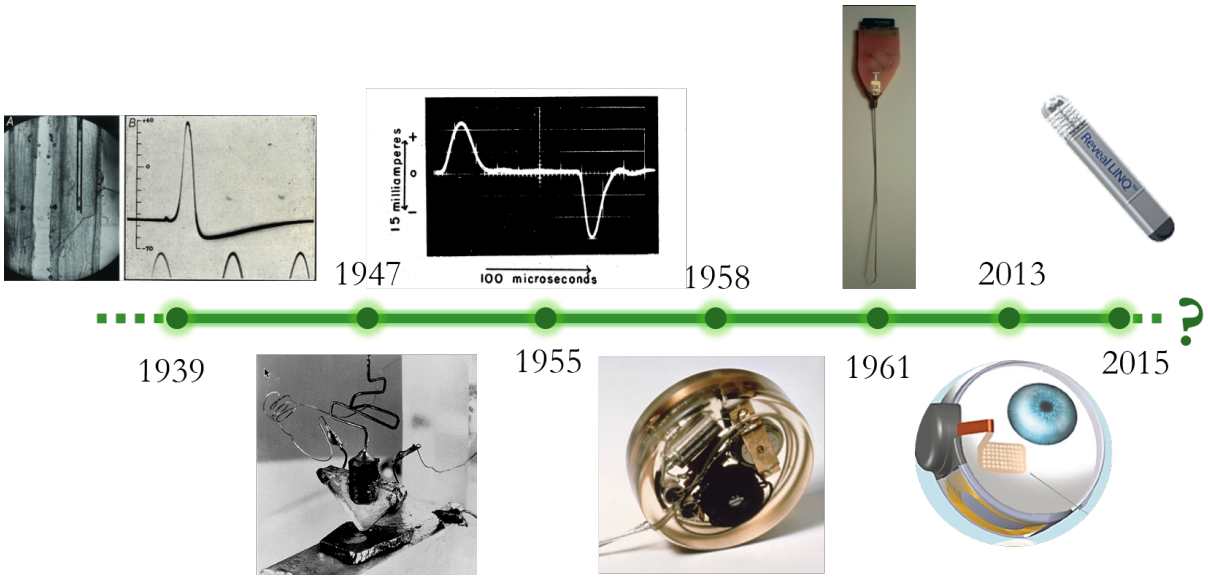

Figure 1.2: Chronological development of functional electrical stimulation: 20th century and after.

The development of stimulation devices occurred predominantly in the later half of the 20th century (Figure 1.2). In 1955, American neurologist John C. Lilly created a methodology for safe electrical stimulation using the notion of charge balanced biphasic waveforms, or "Lilly's pulses" [10]. With the invention of the transistor in 1947 [11], and the subsequent development of integrated circuits, it became easier to target smaller areas, and to design smaller implantable devices. In 1958, Wilson Greatbatch developed the first implantable medical device, a cardiac pacemaker [12], setting the stage for medical device design as an industry. The first cochlear implant was implanted by William House and John Doyle of Los Angeles, California, in 1961 [13]. This development eventually paved the way for other stimulation-based implants, such as retinal implants to come to the fore, mainly for retinal diseases such as retinitis pigmentosa and age-related macular degeneration [1], with the first retinal implant, Argus II by Second Sight, to be approved by the United States Food and Drug Administration (FDA) in 2013 [14].

[2]The numerical calculations for the equation were done on mechanical computers, or by hand!

Electrical stimulation has come a long way in efficiency and usability. In April 2015, Medtronic Inc., one of the world's largest medical device companies, released an implantable cardiac monitor (Reveal LINQ) [15], that can diagnose and treat irregular heartbeats. Reveal LINQ is a cardiac monitor that can record abnormal heart rhythms for upto 3 years and is comparable to the size of a AAA battery. However, in the era of miniaturization, electrical stimulation comes with its own set of limitations: direct contact with electrodes which could result in tissue or electrode damage, low spacial specificity due to the size of the electrode, and cross-coupling effects from stimulation on adjacent areas. There have been developments in the use of non-electrical stimulation for functional physiological responses, mainly using optical methods. Optogenetic stimulation is a new method that involves the injection of a light-sensitive protein into neural tissue, which then activates neurons when exposed to light [16]. Optogenetic methods have proven to be very insightful in exploratory neuroscience research, but it will take a few years before the method is ready for functional, high resolution and safe stimulation devices.

To understand residual voltage in biphasic current stimulation and thereby design safe stimulation systems, it is imperative to study the characteristics of the electrode-electrolyte (tissue) interface, which is discussed in the following chapter.

Chapter 2

Background

Stimulation at the Electrode-Tissue Interface

Artificial electrical stimulation is fundamentally achieved by an electrode injecting charge into an electrically excitable biological cell, such as a neuron. Because electrical stimulation involves the interaction of two different materials (electrode and tissue), the electrical properties of the interface needs to be understood. Biological cells exist in aqueous, electrolytic environments. The advent of microtechnology has allowed us to fabricate microelectrode arrays with closely spaced electrodes for experimental stimulation of neural cells [17]. One of the main challenges in developing a stimulation system for a biological application, is the dynamic nature of the electrode-tissue interface, growth and death of tissue around the location of the electrode. Understanding the electrochemical properties of stimulation electrodes helps establish a model which can be used to design stimulation systems.

2.1 Stimulation at the Electrode-Tissue Interface

When an electrode is placed in a conducting medium, such as an electrolyte or tissue, current flow is determined by the flow of electrons in the electrode and flow of ions in the electrolyte. Ions in the electrolyte or tissue align across the interface, to oppose the charge present on

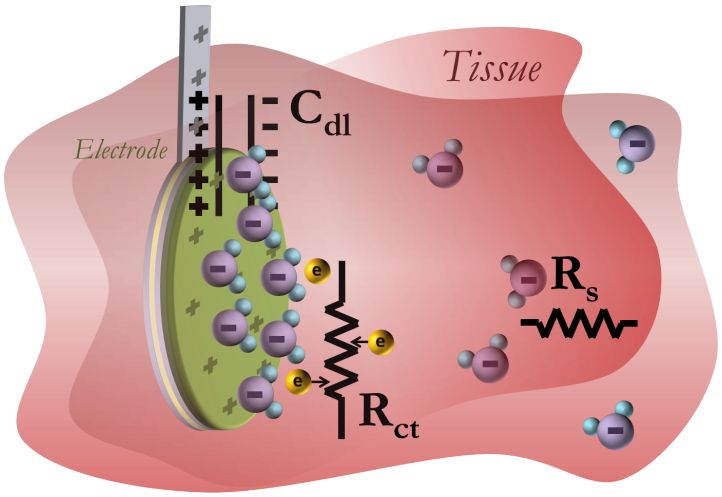

Figure 2.1: Pictorial representation of the electrode-tissue interface: The electrode-tissue interface is a region of neural tissue with different ions in the medium. C_{dl} is the double-layer capacitance, R_{ct} is the charge transfer resistance and R_s models the solution resistance.

the electrode, thereby forming a double layer of charge, mimicking a parallel plate capacitor. The dielectric of the *double layer capacitance* can be the result of a layer of certain chemical species that tend to adsorb onto the surface of the electrode. Additionally, polar molecules such as water orient themselves at the interface, and the net orientation thereby creates a charge separation. Because the thickness of the dielectric is on the order of the diameters of water molecule, the capacitance can be very large ($10\mu F/cm^2$). Earlier forms of the electrode model comprised predominantly of the double layer capacitance, C_{dl}, and the solution resistance, R_s, as shown in Figure 2.1.

The movement of electrons in a reversible electrochemical reaction at the electrode-tissue interface is modeled as a charge-transfer resistance,R_{ct}, shown in Figure 2.1. Electrical stimulation is achieved by establishing charge-transfer across the electrode-tissue interface, which can be achieved via two main mechanisms: *capacitive* and *faradaic*.

2.1.1 Mechanism of Electrical Stimulation

Capacitive (or *non-faradaic*) mechanisms involve the charging and discharging of the electrical double layer that is present at the interface. The maximum amount of charge that can be

injected via capacitive double layer charging and discharging is about $1mC/cm^2$ [18]. A perfectly capacitive charge transfer mechanism does not involve any electrochemical reactions at the electrode-electrolyte (tissue) interface.

Faradaic mechanisms of charge transfer involve the movement of electrons across the electrode-tissue interface through chemical reactions. Charge injection capacity can be increased by introducing an insulation material with a large dielectric constant at the metal electrolyte interface [19]. Stimulation electrodes use faradaic mechanisms because the amount of charge required to elicit a physiological response is greater than what can be achieved with a capactive mechanism (about $5mC/cm^2$) [18]. During a faradaic reaction, chemical species are either oxidized or reduced at the interface. When the species are bound to the electrode surface, the reaction is said to be *reversible*. Reversible faradaic reactions do not add or change chemical species in the electrolyte. The extent of reversibility depends on the rate of electron transfer at the interface (*chemical kinetics*), and movement of intermediate chemical species near the interface (*mass transport*) [20]. When the chemical species do not remain bound to the electrode surface, the process is said to be an *irreversible* faradaic reaction, and the species move into the bulk of the electrolyte. Irreversible processes lead to electrode corrosion and are usually undesirable for stimulation electrodes because they can produce biologically toxic products, or alter the chemical nature of the tissue. The *electrochemical window* is the applied voltage range where a substance does not get irreversibly oxidized or reduced. Electrical stimulation in aqueous environments has empirical limits in the electrode potential across an electrode-electrolyte (tissue) interface. If the applied electrode potential is greater than the electrochemical water window of the electrode, water gets oxidized/reduced to oxygen/hydrogen (Equations 2.1, 2.2).

$$2H_2O + 2e^- \rightarrow H_2 \uparrow + 2OH^- \tag{2.1}$$

$$2H_2O \rightarrow O_2 \uparrow + 4H^+ + 4e^- \tag{2.2}$$

The water window is defined as the potential range between the oxidation of water to form

oxygen and the reduction of water to form hydrogen [20]. When gas bubbles are formed at the electrode-tissue interface due to stimulation, the molecules are not spatially limited to the region around the interface (*mass transport limited*), they move away and are chemically unrecoverable. The oxidation/reduction process alters the pH of the environment, which is unnatural and potentially unsafe. Typically, the electrode potential must not greatly exceed the water window. Water window voltage limits are observed and reported during the development of materials developed for electrochemical applications.

2.1.2 Electrode-Tissue Interface Models

Basic equivalent electrical circuit models of the electrode-electrolyte (tissue) interface are shown in Figure 2.2. The solution resistance, R_s, models the resistance of the bulk of the electrolyte (tissue). The capacitor models the double layer of charge that exists at the electrode-electrolyte interface. The charge transfer resistance, or faradaic resistance, R_{ct}, in parallel with the capacitance, accounts for the conduction of charged particles across the interface. More than one faradaic reaction can occur at the interface, which is generally modeled by several branches of R_{ct}, in parallel with the double-layer capacitance. The conduction of these charged particles can occur through various mechanisms, mainly through oxidation-reduction reactions at the electrode [20]. More complex models of the electrode-electrolyte (tissue) that incorporate the effects of the transport of ions in solution models exist, but are not required for this work. A chronological evolution of electrode-electrolyte (tissue) models can be found in [21].

2.1.3 Discussion on Electrode Voltages

Because electrical potential is always specified between two points in space, it is physically impossible to measure the interphase electrode potential for a single electrode. When charge is injected into the *working* electrode, electrically there needs to be a return path for the current. The electrode placed in the tissue to provide a path for injected charge is the

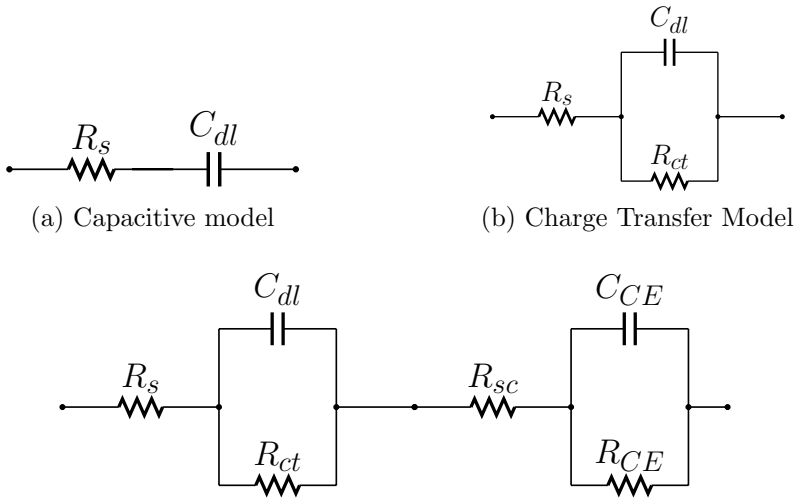

(a) Capacitive model

(b) Charge Transfer Model

(c) Interface Model with Counter Electrode ($C_{CE} >> C_{dl}$)

Figure 2.2: First order electrode-electrolyte/tissue interface models: (a) Purely capacitive charge transfer model (b) Capacitive and faradaic transfer model (c) First order electrode model including the counter electrode

counter electrode. The *reference* electrode is an electrochemical cell that remains at constant potential, and the electrode voltages across the working electrode and the counter electrode are reported with respect to the reference electrode. Electrical stimulation can alter the potential of the working electrode, as well as the counter electrode, when measured with respect to a reference point.

In most electrochemical applications, changes in potential across the working electrode is considered most relevant, therefore the material for the counter electrode is typically made much larger in area than the working electrode used in the application. The area, and therefore capacitance, of the counter electrode is much greater than that of the stimulation electrode. Therefore, for the same charge per unit time driven through the stimulation and counter electrode, the voltage changes across the larger counter electrode may be neglected. The term *electrode potential* or *electrode voltage* in this work refers to the voltage *measured* across the working electrode with respect to a known reference voltage, or a large counter electrode. The complete interface model for monopolar electrical stimulation includes the electrode-tissue interface model for the counter electrode (Fig. 2.2c).

Electrode materials for neural stimulation are chosen based on their charge density and charge per phase of the stimulation pulse for a given geometry. For neural stimulation with a small target area (for example, retinal stimulation) it is required that the electrodes have a high charge injection capacity and a high charge density. Among the different tested stimulation electrode materials (a review of which can be found in [18]), in this work, all the experiments conducted have been performed with working electrodes that have **S**puttered **IR**idium **O**xide **F**ilms.

2.1.4 Sputtered Iridium Oxide Film (SIROF) Electrodes

Capacitive charge injection is the ideal method of stimulation because no chemical changes occur in the tissue. Moreover, to inject a large amount of charge, the electrode would have to have a large surface area, and such an electrode would target too many neuronal cells in a given tissue. Moreover, large electrode arrays are not scalable for applications like a cochlear implant or a retinal implant. Faradaic materials such as **S**puttered **IR**idium **O**xide **F**ilm (SIROF) electrodes were developed to achieve higher charge injection capacities [18]. The SIROF electrodes used in this work were developed by Shire et al at Cornell University as part of the Boston Retinal Implant Project [1].

The microelectrode arrays were fabricated by first depositing polyimide (PI-2611) on a 100mm-diameter silicon wafer (Figure 2.3a, with three metalization layers (titanium-gold-titanium) deposited by physical vapor deposition. The contact pads (square of side 250 μm) are accessed via the gold layer and titanium acts as an adhesion layer. The electrode sites were coated with 300 nm of reactive DC-sputtered iridium oxide film from an iridum metal target. The details of the fabrication process of the electrodes are described in [1]. A schematic cross section of the sputtered iridium film electrodes used in this work is shown in Figure 2.4.

SIROF electrodes achieve higher charge-injection capacity via a reversible faradaic process that involves a valence transition between the Ir^{3+} and Ir^{4+} states and H^+/OH^- transfers

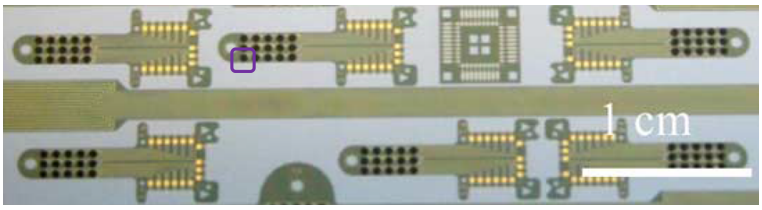

(a) SIROF array on Silicon

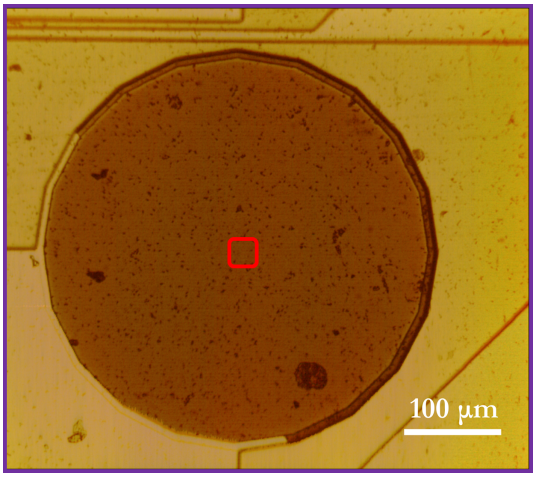

(b) SIROF electrode 10X magnification

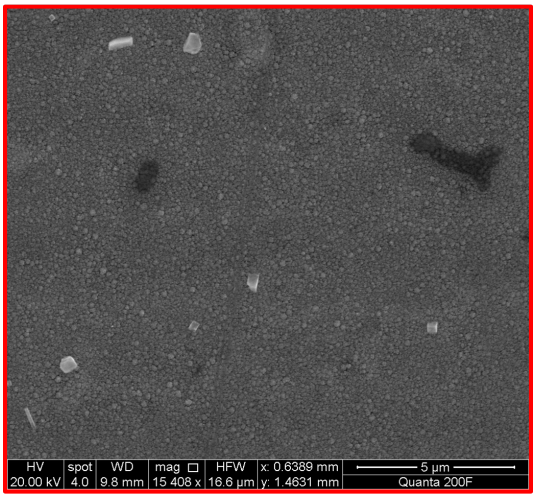

(c) SEM image of SIROF under 15000X magnification

Figure 2.3: (a) SIROF micro-electrode arrays on silicon wafer (Images obtained from [1] with permission.) (b) Single SIROF electrode under 10X magnification (c) SEM image of SIROF electrode surface at 15000X magnification.

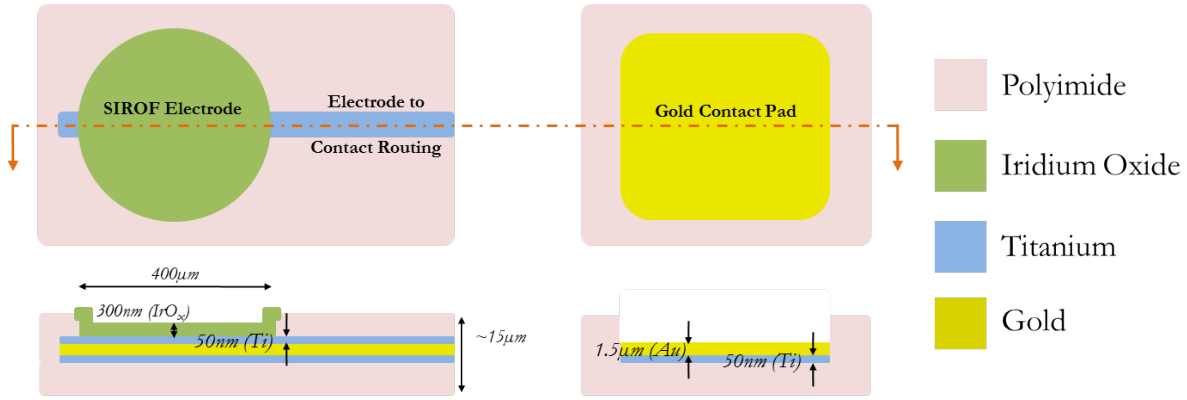

Figure 2.4: Schematic cross section of a sputtered iridum oxide film electrode, which is 400 μm diameter. The gold contact pads have an edge of 250μm, titanium is used as an adhesion layer (Image adapted from [1] and not drawn to scale)

[20]. The operating equations for a sputtered iridium oxide film are:

$$Ir^{3+}(OH)_3 + H_2O \Leftrightarrow Ir^{4+}(OH)_4 + H^+ + e^- \tag{2.3}$$

$$Ir^{3+}(OH)_3 + OH^- \Leftrightarrow Ir^{4+}(OH)_4 + e^- \tag{2.4}$$

The transfer of electrons in the set of Equations 2.3,2.4 is modeled as a resistance (as shown in Figure 2.2b). Stimulation electrodes are designed to have large electron tansfer, so this parameter is a relevant inclusion for these electrode models.

Because only SIROF electrodes have been used in this work, the discussion on the electro-analytical methods is centered around the characterization of these electrodes. Characterization of electrode materials are typically performed using **C**yclic **V**oltammetry (CV) and **E**lectrochemical **I**mpedance **S**pectroscopy (EIS), which will be briefly described in Chapter 4.

Given a stimulation electrode, there are many ways of driving charge into the electrode, and the tissue. The following sections covers a brief overview of the different stimulation waveforms, and the eventual decision to use biphasic current stimulation as the *de facto* standard for electrical stimulation.

2.2 Electrical Stimulation Waveforms

Electrical stimulation is realized by driving charge into the electrode, which enters the tissue environment through two main mechanisms, capacitive and faradaic, as described in Section 2.1.1. Capacitive involves the charging and discharging of the electrical double layer at the interface. Faradaic reactions indicate the movement of electrons across the interface via chemical reactions. While designing safe electrical stimulation systems, it is best to avoid irreversible faradaic reactions. Stimulation to trigger an action potential are predominantly achieved by voltage stimulation and current stimulation. Voltage-controlled stimulation is performed by driving a current between the working electrode and the counter electrode, such that the required voltage is set on the working electrode with respect to a reference electrode. Voltage-controlled (potentiostatic) stimulation requires three electrodes, and it is used more for electrochemical characterization than for stimulation experiments. A variant of this method, adapted for experimental implementation, is to apply a voltage between the working electrode and the counter electrode. While voltage stimulation has better power efficiency [22], we cannot control the amount of charge that is being delivered into the tissue. In voltage stimulation, the load draws as much current as it requires. The electrode-electrolyte/tissue interface is not a well-defined "load". Therefore, we cannot control the amount of charge delivered into the electrode with voltage stimulation. Current stimulation has been the established norm because of its high controllability. Balanced biphasic waveforms were first introduced as a safe method of stimulation by Lilly et. al. in 1955 [10]. For stimulation electrode material that involve faradaic reactions, a charge balanced waveform ensures that electrochemical reactions that occur in the first phase are reversed in the second phase. More recently, switched capacitor stimulation [23] and high frequency current-switching stimulation [24] have been proposed as charge delivery methods, but have not been extensively used for physiological experiments. Current stimulation has been the long established norm [25] because the amount of charge delivered during current stimulation is controllable.

The background presented in this chapter aims to bring the reader to a point where a discussion on the evidence and applications of residual voltage can be understood. In particular, the following are notable points of interest.

- The discussion uses the first order model (Figure 2.2b) [20] (Figure 2.2b) to understand the concept of residual voltage. The scope of this work is targeted to engineers who work with biological systems, and who require a higher level, simplified model to develop an efficient stimulation system. In reality, the electrode-tissue interface can be very complex, and varies with electrode material and electrolyte (tissue) interface [21]. The purpose of this research is to form a bridge of understanding between the electrochemical aspect of stimulation and the design of efficient neural stimulators.

- We begin our discussion with current-controlled, balanced, biphasic, cathodic-first waveforms as the basis of efficient electrical stimulation. However, this work questions the requirement of *balanced* biphasic stimuli, and whether or not it guarantees safe electrical stimulation. Specifically, it has been shown with the first order electrode model shown in Figure 2.2b, that a *residual voltage* exists at the end of the anodic pulse, even with balanced biphasic pulses. Residual voltage is a characteristic of the electrode-tissue interface when stimulated with biphasic current pulses. However, depending on the frequency of stimulation, the residual voltage can build up over several stimulation pulses, and potentially reach the water window of the electrode. There have been several system level advances in stimulation methodologies to balance the charge in a biphasic current pulse.

The main contributions of the work in this thesis are (1) to identify and characterize residual voltage (Chapter 3) and demonstrate its usefulness in early detection of electrode-tissue interface changes (Chapter 5), and (2) to use imbalanced biphasic pulses as a way to prevent the build-up of residual voltage, without losing damage information in the process (Chapter 6), and (3) to corroborate the discussions on residual voltage through preliminary in vivo experiments (Chapter 7).

Chapter 3

Residual Voltage

Leakage Phenomenon from Biphasic Stimulation

The most prevalent method of delivering artificial electrical stimulation is through current-controlled, balanced biphasic pulses. Residual voltage is a by-product of biphasic current stimulation. This chapter explains the origin of residual voltage using simulations with ideal biphasic signals, assuming the first order electrode-electrolyte (tissue) interface model consisting of the solution resistance, R_s, double-layer capacitance, C_{dl}, and the charge transfer resistance, R_{ct}. Using idealized models, the characteristics of residual voltage are described, followed by a motivation for the two main contributions of this work, which are (1) using residual voltage as a status indicator for electrode damage, and (2) controlling residual voltage growth by active anodic feedback. Along with the electrode-electrolyte (tissue) interface model in Chapter 2, to describe and derive residual voltage, we first need to understand the current-based biphasic stimulation waveform.

3.1 Biphasic Current Stimulation

Artificial triggering of an action potential can be achieved by voltage stimulation, current stimulation and more recently, switched capacitor stimulation [23] and high frequency

current-switching stimulation [24]. While voltage stimulation has better power efficiency [22], we cannot control the amount of charge that is being delivered into the tissue because the load draws as much current as it requires. The electrode-electrolyte/tissue interface is not a well-defined "load". Therefore, current stimulation has been the established norm because of its high controllability. Electrical stimulation for neural prosthesis devices is typically performed using biphasic pulses. Balanced biphasic waveforms were first introduced as a safe method of stimulation by Lilly et. al. in 1955 [10]. For stimulation electrode materials that involve Faradaic reactions, a charge balanced waveform ensures that electrochemical reactions that occur in the first phase, are reversed in the second phase, ensuring a net zero injection of charge for safety.

The *stimulation* phase is the phase that elicits the action potential in the neuronal cell. An *interphase delay* is introduced to allow the action potential to propagate and a *recovery* phase is used to neutralize the charge sent in the first phase. The stimulation phase of biphasic waveforms is cathodic-first (negative-first) because it more power efficient in eliciting an action potential from an excitable cell, based on a model calculation found in [26]. The *recovery* phase is the anodic (positive) phase, used to electrically neutralize the chrage inject byt he cathodic phase, after the generation of the action potential. If the charge in the stimulation phase equals that charge in the recovery phase, i.e., $Q_c = Q_a$, then the stimulation is said to *balanced*. The mismatch in charge (or current) between the cathodic and anodic phases in a biphasic stimulation pulse is termed as the *biphasic mismatch error*. While it is important to have zero biphasic mismatch betweent he two pahses, we shall see in Chapter 6 that the goal of safe electrical stimulation is not electrical neutrality, but *electrochemical* neutrality. A generic current-based, cathodic-first, square, biphasic stimulation waveform is shown in Figure 3.1a. Normal experimental conditions in this work use a maximum stimulation current of 100 μA, with initial cathodic (stimulation) and anodic (recovery) pulse widths of 1 ms. The interphase delay is 100 μs.

Residual voltage can be observed when a biphasic current stimulation passes though an electrode-electrolyte (interface). For the theoretical discussions in this work, we assume the

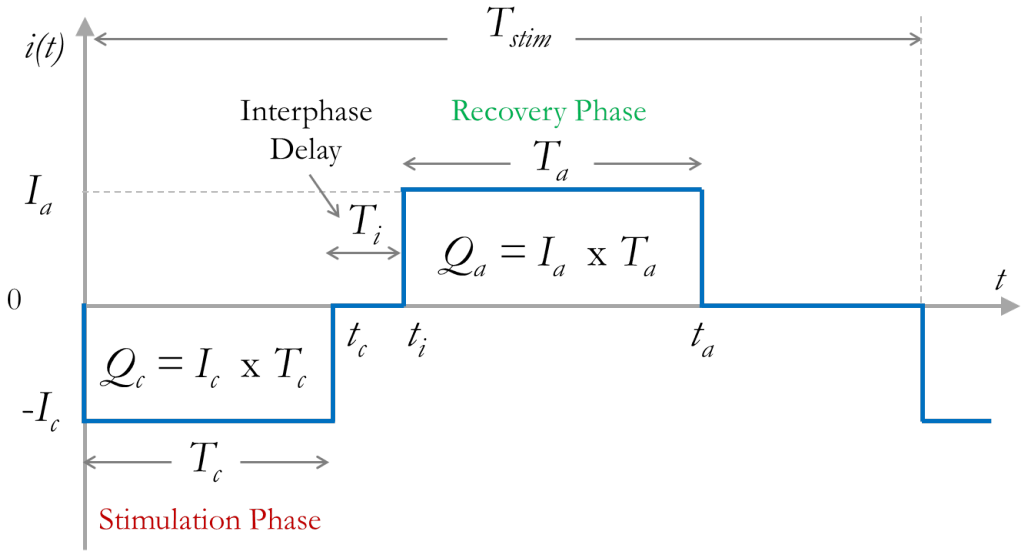

(a) Current-based Biphasic Stimulation Waveform

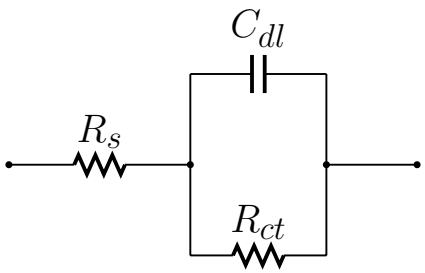

(b) First order model of the electrode tissue interface

Figure 3.1: (a) Biphasic current stimulation waveform: Biphasic waveforms are said to be *balanced* when $Q_c = Q_a$. In this work, the stimulation phase is assumed to be cathodic (negative) and the recovery phase is anodic (positive). T_c, T_i and T_a are cathodic, interphase and anodic pulse *widths*. Stimulation time period is given by T_{stim}. Absolute time is denoted by t_c, t_i, t_a. The magnitude of cathodic current is expressed as I_c, and anodic current by I_c (b) R_s is the solution resistance, R_{ct} is the charge-transfer resistance and C_{dl} is the double-layer capacitance (detailed description in Section 2.1). The relaxation time constant is $\tau = C_{dl} \times R_{ct}$.

first order model of the electrode tissue interface, shown in Figure 3.1b, is being driven by current-controlled biphasic pulses. The notations used in this chapter are described in Figure 3.1a.

3.2 Origin of Residual Voltage

Residual voltage (RV) is an accumulation of charge that manifests as a voltage when biphasic current pulses are applied across an electrode-electrolyte (tissue) interface. Consider a ***balanced*** biphasic current stimulation pulse (Figure 3.1a), applied across the electrode-electrolyte (tissue) model shown in Figure 3.1b. The cathodic phase of the biphasic current pulse negatively charges the double-layer capacitance, C_{dl}, and the *balanced* anodic phase discharges the capacitor. Observe from Figure 3.2, that the double layer capacitance is always negatively charged (because the stimulation pulse is cathodic-first). Due to the presence of the charge-transfer resistance, R_{ct}, there is a unidirectional leakage across R_{ct} for the duration of the stimulation pulse, even if the phases of the stimulation pulse are perfectly balanced [27].

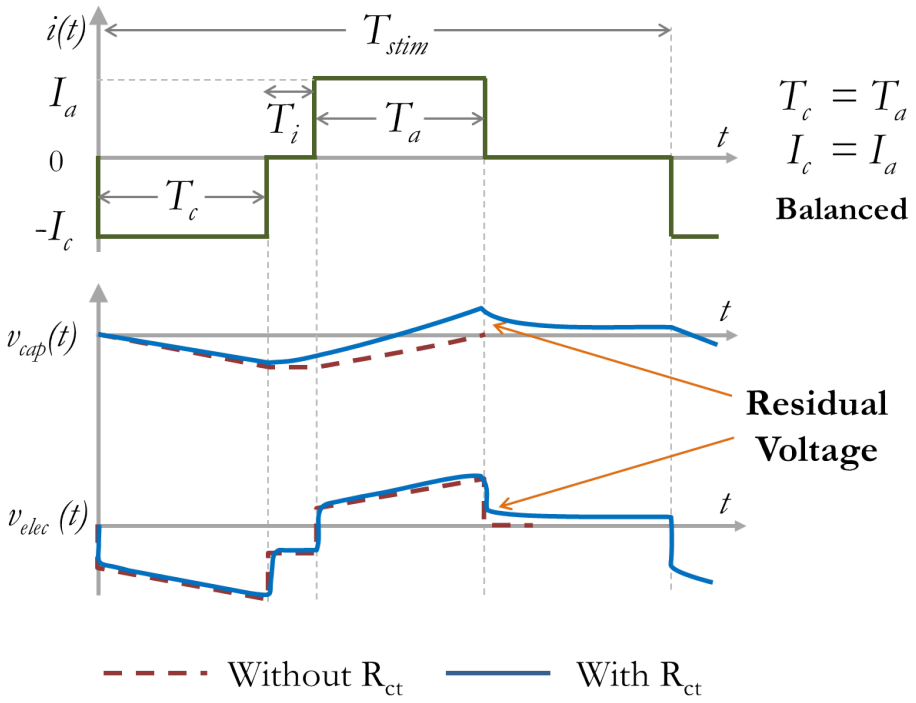

Figure 3.2: Schematic representation of residual voltage arising from balanced biphasic stimulation. The dashed line shows the voltage across C_{dl} if R_{ct} was not present in the model, there would be no leakage. Balanced biphasic pulses have zero biphasic mismatch, i.e., $Q_c = Q_a$, and unidirectional leakage across R_{ct} occurs even with zero biphasic mismatch.

A mathematical proof of the non-zero voltage at the end of the anodic pulse is shown in Appendix A. For a *balanced* biphasic signal, $Q_a = Q_c$. The notations are described in Figure 3.1a. The residual voltage at the end of the recovery (anodic) pulse is given by,

$$v_c(t_a) = -I_c R_{ct}[e^{-(t_a - t_c)/\tau} - e^{-t_a/\tau}] + I_a R_{ct}[1 - e^{-(t_a - t_i)/\tau}], \tag{3.1}$$

where $\tau = R_{ct} \times C_{dl}$. Observe from Equation 3.1 that the voltage at the end of the anodic pulse of a biphasic stimulation pulse contains the parameters R_{ct} and C_{dl}, which captures information about the electrode-electrolyte (tissue) interface, and not just the biphasic mismatch error between anodic and cathodic pulses. While this is a first order model of the electrode-electrolyte (tissue) interface, it allows us to understand the characteristic nature of the residual voltage, with respect to the electrode model parameters. The residual voltage at the end of the anodic pulse width, in terms of the biphasic stimulation pulse-widths is:

$$v_c(t_a) = -I_c R_{ct}[e^{-(T_i + T_a)/\tau} - e^{-(T_c + T_i + T_a)/\tau}] + I_a R_{ct}[1 - e^{-(T_a)/\tau}]. \tag{3.2}$$

3.2.1 Biphasic Mismatch in Residual Voltage

The physiological response of tissue to artificial electrical stimulation depends on the charge injected into the tissue [20]. As discussed in Section 3.1, current based stimulation allows us to control the charge more accurately when compared to voltage stimulation. It is appropriate to define biphasic mismatch, β, as the relative error in charge between the cathodic and anodic phases, β_Q,

$$\beta_Q = \frac{Q_c - Q_a}{Q_c}, \tag{3.3}$$

where β_Q is defined with respect to cathodic-first stimulation pulses. For stimulation methods that involve switched capacitor circuits [23], *biphasic charge mismatch* (Equation 3.3) is sufficient to measure the mismatch, albeit this method is not very widely used. For

stimulation using current pulses, charge is defined as the product of current and time, $Q = I \times t$, which implies that the two components of the mismatch are,

$$\beta_I = \frac{I_c - I_a}{I_c} \qquad \beta_T = \frac{T_c - T_a}{T_c} \tag{3.4}$$

The relationship between charge mismatch and the relative errors in current and time is,

$$\beta_Q = \beta_I + \beta_T - \beta_I \beta_T. \tag{3.5}$$

The algebraic steps arriving at Equation 3.5 can be found in Appendix C. An ideal biphasic stimulator will have zero charge mismatch between the cathodic (negative) and anodic (positive). A positive biphasic mismatch between the two phases will result in an increase in residual voltage.

3.2.2 Definition of Residual Voltage

Residual Voltage (RV) in biphasic electrical stimulation is the voltage that appears at the end of the recovery phase of a biphasic stimulation waveform. Residual voltage occurs due to a combination of two factors: one, the mismatch in charge between the stimulation and recovery phases and two, the unidirectional leakage of the double layer capacitance across the charge-transfer resistance for the duration of the pulse.

When the mismatch between the stimulation phase and the recovery phase of the biphasic stimulation pulse is *zero*, the biphasic stimulation waveform is said to be *balanced*, and the residual voltage is solely a function of the electrode-electrolyte (tissue) interface impedance, and shall be called the *intrinsic residual voltage*.

Using the definition of residual voltage (Section 3.2.2), the intrinsic residual voltage (Equation 3.2) and the expressions for biphasic mismatch (Equation 3.4), the generalized expression for the residual voltage from the first biphasic current stimulation pulse, defined at the end

of the anodic phase, for a first-order electrode model is,

$$RV|_{T_c,I_c,\beta_I,\beta_T} = -I_c R_{ct}\left[exp\left(\frac{-(T_i+(1-\beta_T)T_c)}{\tau}\right) - exp\left(\frac{-(T_i+(2-\beta_T)T_c)}{\tau}\right)\right] + (1-\beta_I)I_c R_{ct}\left[1 - exp\left(\frac{-(1-\beta_T)T_c}{\tau}\right)\right] \tag{3.6}$$

Biphasic stimulation waveforms are periodic, and are more often characterized by pulse widths than in terms of absolute time. The cathodic pulse width (T_c) and the interphase pulse delay (T_i) are fixed, because they are directly related to the physiological response. The current and pulse-width mismatch parameters (β_I, β_T) are quantities that can be determined by testing. The relaxation time constant (τ) is a characteristic of the interface, and represents the electrode-electrolyte (tissue) interface model.

$$RV|_{T_a} = -I_c R_{ct}\left[exp\left(\frac{-(T_i+T_a)}{\tau}\right) - exp\left(\frac{-(T_c+T_i+T_a)}{\tau}\right)\right] + (1-\beta_I)I_c R_{ct}\left[1 - exp\left(\frac{-T_a}{\tau}\right)\right] \tag{3.7}$$

In Equation 3.7, RV is represented as a function of the anodic pulse width (T_a), and the anodic current amplitude (I_a) has been represented as a function of the cathodic pulse width and mismatch parameter (β_I). This is because the anodic pulse is used for charge-balancing, and while it is usually fixed and equal to the cathodic pulse (both time and current), there are several approaches in research that suggest adjusting the anodic pulse charge using feedback [27], [28], [29]. This approach is described in more detail in Chapter 6.

3.2.3 Residual Voltage Growth

The expression for residual voltage in biphasic current stimulation for a first-order model shown in Equation 3.6 is the voltage that appears at the end of the *first* pulse. While

theoretically, the time required for the double-layer capacitance to completely discharge is infinite, the time constant of discharge via the charge transfer resistance is $\tau = R_{ct} \times C_{dl}$. If the frequency of the stimulation pulse is low, then there is negligible net residual voltage growth. In the absence of any charge balancing methods, the stimulation electrode will operate at different bias voltages, higher bias voltages being potentially harmful. Therefore, it is of interest to theoretically understand the model of residual voltage growth in a stimulation electrode over several stimulation pulses.

The residual voltage including the effects of the intrinsic leakage, as well as biphasic mismatch at the end of the anodic pulse of the first biphasic waveform, is shown in Equation 3.6. This voltage, $RV|_{T_a,\beta}$, represented in terms of pulse widths and mismatch coefficients, discharges for the time after the anodic pulse, until the next biphasic stimulation pulse (refer Case 5 from Appendix Section A),

$$RV_0 = RV|_{T_a}.exp\left(-\frac{T_{stim} - t_a}{\tau}\right). \tag{3.8}$$

If we follow through the differential equation assuming the same input waveform (Appendix Section B), we get the residual voltage right before the *third* biphasic stimulation pulse to be,

$$RV_1 = RV_0 + RV_0 e^{\frac{-T_{stim}}{\tau}} \tag{3.9}$$

By recursively applying Equation 3.9 for subsequent stimulation pulses, with the same input biphasic stimulation pulse, we get

$$RV_n = RV_0\left[1 + e^{\frac{-T_{stim}}{\tau}} + e^{\frac{-2T_{stim}}{\tau}} + ... + e^{\frac{-nT_{stim}}{\tau}}\right] \tag{3.10}$$

The value of the stimulation time period, T_{stim}, is typically 10ms and the relaxation time constant, τ, of a stimulation electrode can be of the order of 20ms or higher [22]. Therefore,

Equation 3.10 is the sum of a geomteric series, where the common factor is $exp(\frac{-T_{stim}}{\tau})$. The sum of n terms for such a series is,

$$RV_n = RV_0 \frac{1 - (exp(-T_{stim}/\tau))^{n-1}}{1 - exp(-T_{stim}/\tau}), \tag{3.11}$$

which as $n \to \infty$, converges to,

$$RV_{sat} = \lim_{n\to\infty} RV_n = RV_0 \left[\frac{1}{1 - exp\left(\frac{-T_{stim}}{\tau}\right)} \right] \tag{3.12}$$

From Equation 3.12, one can say that residual voltage depends on the stimulation frequency and the relaxation time constant. A theoretical discussion on the method of measurement of the relaxation time constant is shown in Appendix F. The existence of a saturated residual voltage on the electrode dynamically changes the operating point of the stimulating electrode. Simulations were performed using an ideal biphasic stimulator and the first-order model, to understand the dynamics of residual voltage and residual voltage growth.

3.3 Simulations

For theoretical simulations, an ideal biphasic current source, characterized by an infinite output impedance and infinite power supply is connected to the electrode model. The purpose of using ideal current sources for simulations is to isolate the dependence of the residual voltage on the electrode parameters from biphasic current mismatch errors. An ideal biphasic stimulator was constructed using components from analogLib in Cadence Virtuoso Schematic and the simuations were run using Spectre. Theoretical modeling was done via scripts in MATLAB, the pseudocodes are present in Appendix I.2. The discussions and results in this section aim to describe the characteristics of residual voltage in biphasic electrical stimulation through simulation experiments.

3.3.1 Intrinsic Residual Voltage

The variation of intrinsic residual voltage ($\beta_Q = 0$) for the first stimulation signal (RV_0) was examined by systematically sweeping through a wide range of values of the electrode model parameters. Although some values may not physically viable in practice, the simulation results give us some insight into the empirical bounds on the charge transfer resistance and the implications it has on the residual voltage. Moreover, with the appearance of feedback methods in electrical stimulation systems [30], [27], the simulation results help the feedback circuit designer understand the dependence of the residual voltage on the sampling time and the stimulation frequency of the application. The conditions for the intrinsic residual voltage in the simulations are as follows:

- the ideal biphasic stimulator has **zero** biphasic mismatch,
- the biphasic waveform input is current-based and cathodic-first,
- the intrinsic residual voltage is measured 1μs after the end of the anodic pulse, for one biphasic pulse.

The initial values for the system parameters are shown in Table 3.1. While the values for the electrode parameters are obtained as approximations for a SIROF retinal electrode in tissue [22], in this chapter they serve as initial and/or typical parameter values, based on the type of parameter sweep that is being performed.

Table 3.1: Initial Simulation Parameter Values

Parameter	**Symbol**	**Typical Value**
Stimulation Time Period	T_{stim}	10 ms
Cathodic Pulse Width	T_c	1 ms
Anodic Pulse Width	T_c	1 ms
Interphase Delay	T_i	0.1 ms
Cathodic Current Amplitude	I_c	100 μA
Anodic Current Amplitude	I_a	100 μA
Solution Resistance	R_s	2 - 10 $k\Omega$
Double Layer Capacitance	C_{dl}	$200nF$
Charge Transfer Resistance	R_{ct}	100 $k\Omega$

3.3.2 Transient Biphasic Simulation

Using the first-order model of the electrode-electrolyte (tissue) interface, and an ideal biphasic stimulation waveform generated in MATLAB, the simulated transient response is shown in Figure 3.3. The plot also shows the transient response for a stimulator with a current mismatch of 1%.

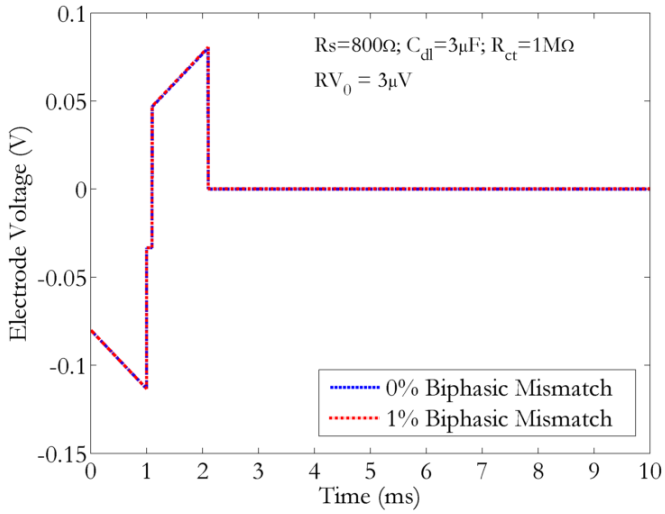

Figure 3.3: Simulated transient biphasic response: For an electrode model with parameters $R_s = 800\Omega$, $C_{dl} = 3\mu F$ and $R_{ct} = 1M\Omega$. The transient response for the same model with a stimulator with $\beta_I = 1\%$ is also shown. The residual voltage at the end of the stimulation pulse for this model is $RV_0 = 3\mu V$.

3.3.3 Variation of Intrinsic RV with C_{dl} and R_{ct}

To understand the dynamic range of intrinsic residual voltage with respect to the electrode-electrolyte (tissue) parameters, a parametric sweep of the charge-transfer resistance, R_{ct} and the double layer capacitance, C_{dl} was performed using the system parameters provided in Table 3.1.

The results in Figure 3.4 show that the intrinsic residual voltage *peaks* at a particular value of the parameters. When the charge-transfer resistance is very low, the pathway acts

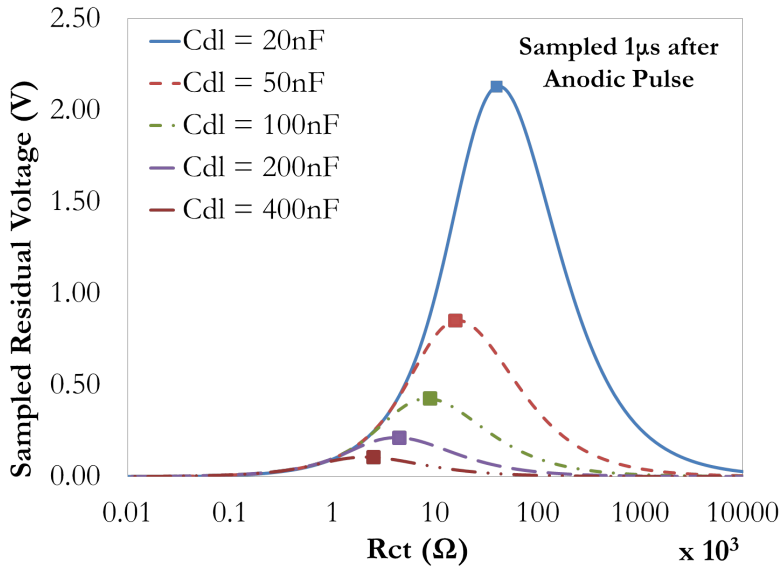

Figure 3.4: Variation of intrinsic RV with C_{dl} and R_{ct}: Residual voltage (sampled after $1\mu s$) with parametric sweeps of R_{ct} and C_{dl}. The values of C_{dl} and R_{ct} depends on the electrochemical reactions, the geometric area and the medium in which the electrode is placed. For the same charge-transfer resistance, if the capacitance is low, the residual voltage increases.

like a short and the residual voltage is zero. Electrochemically, this situation models only Faradaic charge transfer across the electrode tissue interface. On the other hand, when R_{ct} tends towards infinity, the mechanism of stimulation is purely via charging and discharging of the double layer capacitance, which implies that the residual voltage will be zero due to the absence of faradaic reactions (Figure 3.5). For a given value of R_{ct}, lower values of C_{dl} have a higher residual voltage. An interesting characterization of the the electrode interface model parameters is the time constant, $\tau = R_{ct} \times C_{dl}$, called the *relaxation time*.

3.3.4 Residual Voltage Growth

Using an ideal biphasic stimulator, the residual voltage growth curves for a for a first-order electrode model was simulated. The electrode model parameters described here are $R_s = 900\ \Omega$, $C_{dl} = 3.6\ \mu F$ and $R_{ct} = 400\ M\Omega$. The biphasic mismatch simulated here are based on current mismatch only (β_I), and pulse widths are assumed to be perfectly matched ($\beta_T = 0$). The contribution of biphasic mismatch to the residual voltage (and, thereby the

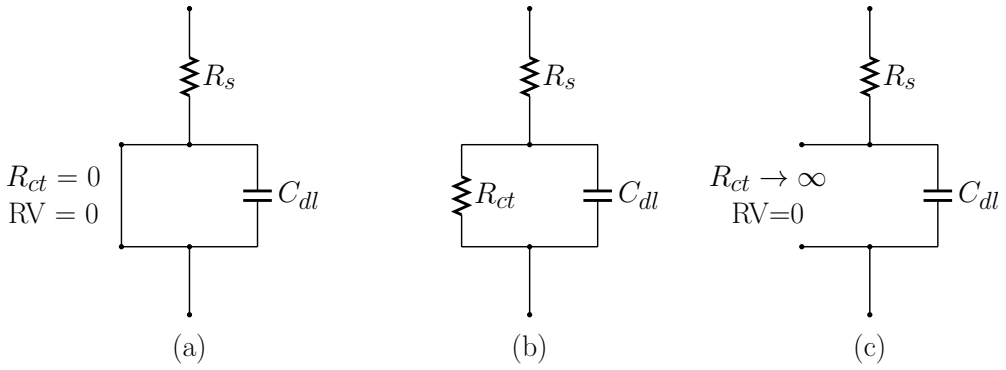

Figure 3.5: Understanding RV peaking between R_{ct} limits: (a) When the R_{ct}=0, C_{dl} is effectively shorted, so there is no leakage from C_{dl} via R_{ct}, thereby zero residual voltage, (b) the nominal case, where there is a non-zero residual voltage, (c) When the $R_{ct} \to \infty$, C_{dl} charges and discharges perfectly, and there is no leakage from C_{dl} via R_{ct}, thereby resulting in zero residual voltage.

saturated residual voltage) is more significant ($> 50\%$).

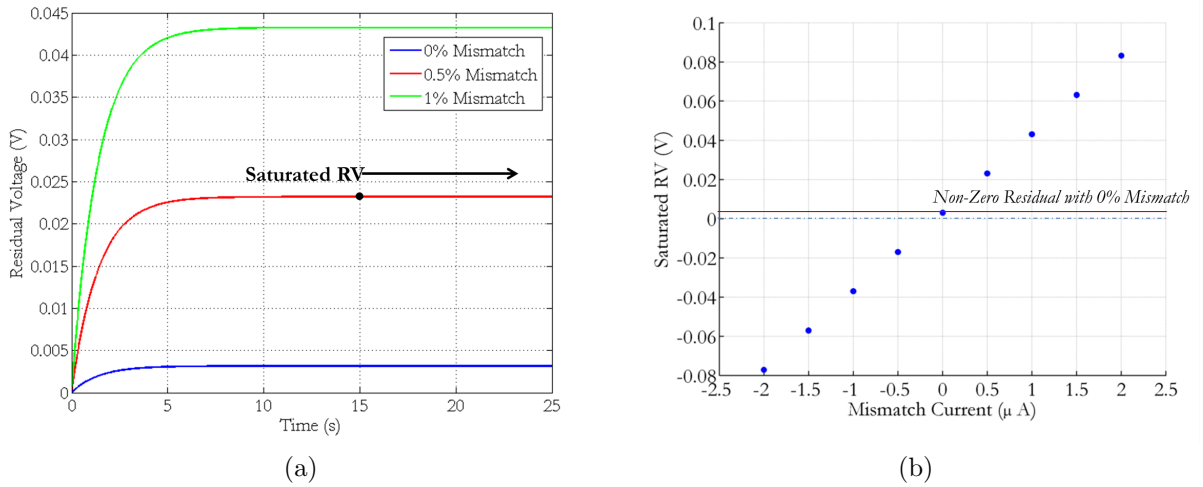

Figure 3.6: (a) Illustration of the contribution of Biphasic mismatch in residual voltage (simulated in MATLAB using $R_s = 900\Omega, C_{dl} = 3.6\mu F, R_{ct} = 400k\Omega$). (b) Because the model we assumed is linear and first-order, the effect of biphasic mismatch is linear. The contribution of intrinsic residual voltage is not as significant as biphasic mismatch to the total residual voltage.

Chun et al. derive the required matching between the cathodic and anodic phases in single and multichannel stimulators [31]. While their work does not consider the leakage across the charge transfer resistance as a source of residual charge, they provide a very useful metric for the practical design of biphasic stimulators. If we allow the residual voltage to grow over

several stimulation pulses, theoretically we can envision a plot shown in Figure 3.6, which was generated by MATLAB using Randle's electrode model (Figure 2.2b). The simulation mismatch plot in Figure 3.6 allows us to draw three main inferences. Firstly, as suggested in [31], it is important to match the anodic and cathodic phases as closely as possible, because the contribution to residual voltage is a function of the biphasic mismatch (linear, if we assume the linear model). Secondly, the residual voltage discharge is representative of the electrode-electrolyte (tissue) interface, even if the biphasic mismatch causes a part of the charge build-up. Thirdly, regardless of how accurately one matches the charge delivered by the stimulator in the two phases, there will be a net residual voltage across the electrode, which is a characteristic of the interface.

3.4 Discussion

One of the contributions of this work is to theoretically identify and define residual voltage. More specifically, *intrinsic residual voltage* is caused due to a unidirectional leakage of the charge across the double-layer capacitance via the charge-transfer resistance during a biphasic current pulse. In the absence of charge-balancing methods during electrical stimulation (discussed in Chapter 6), residual voltage growth can grow, but the first order model assumption indicates there is a bound on the voltage growth. The equations for residual voltage growth reveal that the saturated residual voltage growth depends on the stimulation frequency and the relaxation time constant. The stimulation frequency is controlled by physiological requirements and the relaxation time constant ($R_{ct} \times C_{dl}$) is representative of the stimulation electrode characteristics. In line with prior research in biphasic current stimulation, biphasic mismatch should be minimized for safe stimulation. However, because intrinsic residual voltage exists with zero biphasic mismatch, design effort must concentrate on efficient correction of residual voltage, rather than perfect matching between the cathodic (stimulation) and anodic (recovery) pulse.

The following chapter (Chapter 4) discusses all the generic methods used in this work

to prepare and study stimulation electrode characteristics, as well as the development of a programmable biphasic current stimulator with feedback. Using the methods and apparatus from Chapter 4, the dissertation proceeds to validate the applications of understanding residual voltage. Two aspects of the theoretical discussion of residual voltage presented thus far can be applied to the design of efficient neural stimulation systems. One, because residual voltage is an outcome of the characteristic of the electrode-electrolyte (tissue) interface, measuring the residual voltage can indicate changes in the electrode-electrolyte (tissue) interface (Chapter 5). Two, efficient stimulation systems should aim to correct the underlying cause of residual voltage *before* creating it (Chapter 6).

Chapter 4

In Vitro Experimental Methods

Methods

Residual voltage is a leakage phenomenon that arises from biphasic current stimulation waveforms. A theoretical discussion on the existence of residual voltage was discussed in Chapter 3. Experimental verification of the existence, applications and control of residual voltage involve,

- ionic mediums,
- electrochemical measurement instrumentation,
- characterized stimulation electrodes,
- a programmable biphasic stimulator, and
- adjustable control mechanisms

This chapter covers all the relevant details of experimental methods used in subsequent chapters. The material and cross section of the SIROF electrodes are described in Chapter 2.1, section 2.1.4. This chapter focuses on the methods used to prepare and characterize of these electrodes, prior to the application of any experimental hypothesis.

4.1 Electrochemical Setup

Electrochemical characterization measurement systems typically employ a *three electrode* cell, which comprises of the SIROF working electrode, and a coiled platinum (Pt) counter electrode and a silver/silver chloride reference electrode saline solution. The three electrode setup was used for Cyclic Voltammetry (CV) and Electrode Impedance Spectroscopy (EIS) experiments with the Metrohm Autolab measurement system, to characterize the electrode array.

4.1.1 Ionic Medium

In order to repeatedly study and model the behavior of any electrode material, there needs to be an ionic medium that can imitate the electrolytes that is present in living organism. While there are variations between different types of tissues and electrolytes, the predominant method of testing the electrochemical response of electrodes, and electrophysiological systems is to use ionic solutions. Experiments that are performed with biological entities outside their normal biological environment are known as *in vitro* experiments. On the other hand, experiments with biological environments performed within the living being, are called *in vivo* experiments, which will be briefly discussed in Chapter 7. The electrochemical characterizations and feedback experiments described in this, and subsequent chapters use *in vitro* methods, specifically buffered saline solutions. Physiological saline solutions are used to maintain an iostonic environment with the cells present in living tissue. Phosphate buffered saline (PBS) is an isotonic buffer solution used in biological research because the osmolarity and ion concentrations match those of the human body.

The *in vitro* experiments performed in this work all use 1X Phosphate Buffered Saline (1X PBS). The components of phosphate buffered saline, by weight, are water (88.6%), sodium chloride (8.0%), sodium phosphate dibasic (1.4%), potassium chloride (0.02%), dihydrogen potassium phosphate (0.024%) [32] at a pH value of 7.4. Commercially, concentrated versions of PBS are available, and can be diluted to the required concentration by adding distilled

water. For the experiments in this work, we use Fisher Scientific Phosphate Buffered Saline (10X). To make up 500mL of 1X PBS, 50mL of 10X PBS is diluted with 450mL of distilled water. The prepared solution is used as the electrolyte for stimulation experiments as well as for electrochemical characterization of working electrodes.

4.1.2 Electrodes

Electrochemical measurement systems typically consist of a working electrode, which is the electrode of interest, a counter electrode and a reference electrode.

Working Electrode

The working electrodes used in this work are circular **S**puttered **Ir**idium **O**xide **F**ilm (SIROF) electrodes, which have a diameter of $400\mu m$ and were developed for retinal prosthesis devices by the Boston Retinal Implant Project [1]. The empirical water window potential limits of SIROF electrodes are +0.8V/-0.6V [18]. The geometric surface area of each SIROF electrode is $0.125mm^2$. We used a polyimide-base electrode array (Figure 4.1), with numbers identifying each of the 15 electrodes.

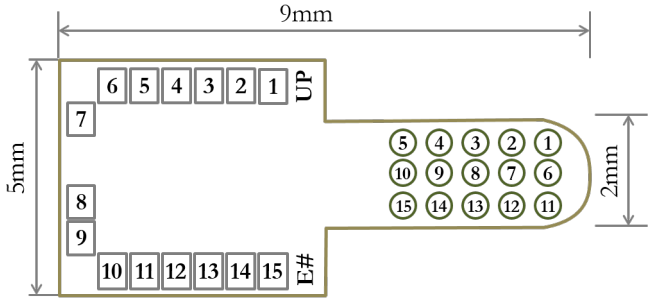

Figure 4.1: SIROF electrode array with 15 electrodes. Each array has an array number on it, denoted by E# on the figure.

Counter Electrode

A coiled platinum counter electrode (Basi Inc. MW1033) is used as the counter electrode for all *in vitro* experiments in this work. Platinum (Pt) is an electrochemically inert material and has a total geometric surface area of $360mm^2$ when completely immersed in the electrolyte, which is more than 2000X when compared to the area of the SIROF working electrode. Because of the relative electrochemical inertness of platinum, and large surface area ratio with respect to the SIROF working electrode, the potential difference variations across the counter electrode is negligible when compared to the working electrode.

Reference Electrode

A reference electrode is an electrode that has a stable and known electrode potential. The reference electrode is used as an electrochemical half-cell in an electrochemical setup, such that the potential of the working electrode can be determined, or set. A reference electrode is made stable by using a reduction-oxidation (redox) system with saturated concentrations of the entities in the redox reaction. For example, the standard hydrogen electrode (SHE) is based on the redox reaction that involves a state shift between $H^+(aq)$ and $H_2(g)$ through the equation,

$$2H^+(aq) + 2e^- \leftrightarrow H_2(g), \tag{4.1}$$

and the internationally accepted primary reference electrodes [33]. Because of the gaseous product involved, these electrodes can be cumbersome to work with, thereby giving rise to the conventional use of secondary electrodes. This work uses a silver/silver chloride (Ag/AgCl) reference electrode, manufactured by Basi Inc. (MF-2052). The redox reactions occurs between silver (Ag) and silver chloride (AgCl), governed by the equations,

$$Ag^+ + e^- \leftrightarrow Ag(s) \tag{4.2}$$

$$AgCl(s) \leftrightarrow Ag^+ + Cl^- \tag{4.3}$$

The standard electrode potential of an Ag/AgCl reference electrode as compared to a standard hydrogen electrode (SHE) is 0.230V ± 10mV. A schematic of the three electrode setup is shown in Figure 4.2.

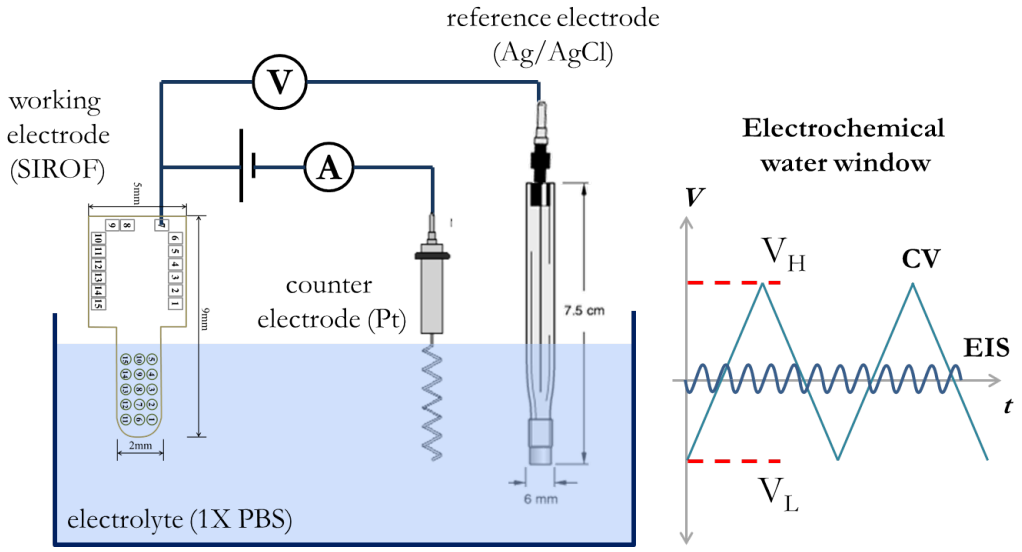

Figure 4.2: Three electrode measurement setup, used for cyclic voltammetry and electrochemical impedance spectroscopy. For stimulation experiments and applications, the reference electrode is not used, only the working electrode and a relatively large counter electrodes (usually Pt) is used.

Electrochemical analysis uses a three electrode measurement system as shown in Figure 4.2. If the potential of the working electrode is varied linearly and cyclically between large values, the measurement is called cyclic voltammetry. On the other hand, small (sinusoidal) signals are used to measure the electrochemical impedance of the working electrode. The following section describes both these methods briefly.

4.2 Electrochemical Analysis Methods

Electrochemical methods are used as a tool to study the characteristics of different materials in order to assess them for different applications. This section briefly describes the electrochemical methods of cyclic voltammetry (CV) and electrochemical impedance spectroscopy (EIS) using sputtered iridum oxide films (SIROF) as the main example. Detailed

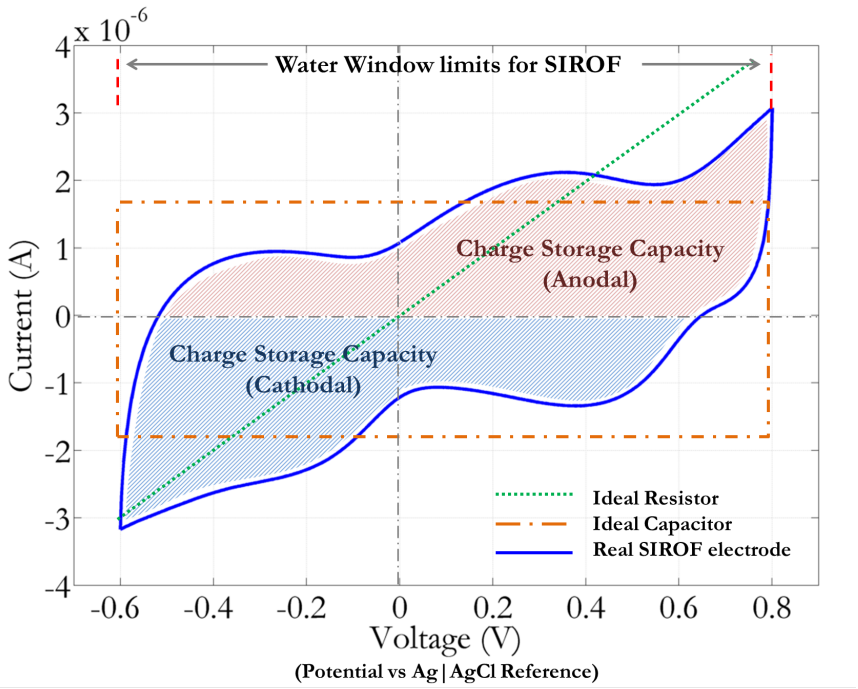

Figure 4.3: Cyclic Voltammetry (CV) curve for a SIROF electrode: The enclosed area in the plot indicates charge storage capacity. The SIROF curve shows peaks at +0.4V and around -0.1V indicating redox reactions, that also contribute to charge storage capacity. A stimulation electrode is designed to have high charge capacity [18], depending on the physiological application.

descriptions of these methods are available in [33], [34].

4.2.1 Cyclic Voltammetry (CV)

Cyclic voltammetry consists of the measurement of current passing through a test electrode, while cycling the potential linearly at a known rate. Cyclic voltammetry curves are used to understand the nature of electrochemical reactions that occur during a linear sweep of electrical potential across the electrode in a known electrolyte medium, against a known reference. The potential is changed linearly between two potential limits, typically the water window. The water window of SIROF is -0.6V/+0.8V vs Ag/AgCl [35]. A typical current versus potential curve for a SIROF electrode in 1X Phosphate Buffered Saline (PBS) solution, measured against an Ag/AgCl reference electrode is shown in Figure 4.3.

A comparison of the SIROF CV curve, shown against ideal linear components in Figure 4.3 provides an intuitive approach to interpreting a CV curve. For stimulation electrodes, CV measurements are used to extract the *charge storage capacity* of the electrode. The charge storage capacity is the amount of charge that is available for a stimulation pulse. An ideal capacitor stores charge and exhibits hysteresis, and conversely, an ideal resistor does not store any charge. The regions where the current is fairly constant corresponds to the double layer capacitance. SIROF electrodes have a high charge storage capacity, typically the values reported for stimulation electrodes are cathodic charge storage capacity (CSC_c), and it is the area under the negative region of the CV curve. While it is evident from Figure 4.3 that SIROF electrodes do have the ability to store charge, the peaks and dents in the curve indicate that the charge storage is largely due to faradaic reactions, involving the reactions described in Chapter 2, Equation **??**. The average cathodal charge storage capacity for a circular SIROF electrode of $400\mu m$ in diameter is $3.4mC/cm^2$. A detailed description on the performance of stimulation electrodes is presented by Cogan et al in [18]. Cyclic voltammetry curves depend on the frequency of the linear voltage sweep used in the measurement, which is usually a slow sweep. Characterization measurements are also performed using high frequency sinusoidal measurements, called Electrochemical Impedance Spectroscopy.

4.2.2 Electrochemical Impedance Spectroscopy (EIS)

Electrochemical impedance spectroscopy (EIS) is the method of determining the magnitude and phase of the impedance of an interface, by sweeping the frequency of a small amplitude sinusoidal signal. The theoretical impedance of the electrode-tissue interface, based on the model in Figure 2.2b, is given by Equation 4.4.

$$Z(s) = R_s + \frac{R_{ct}}{1 + sC_{dl}R_{ct}} \tag{4.4}$$

The magnitude and phase responses of the SIROF electrodes used in this work are shown

in Figure 4.4. Frequency measurements are made over a frequency range from 0.1 Hz to 100 kHz. The sinusoidal voltage excitation is within the range of $5 - 50mV$, so that the operating bias across the electrode during measurement does not alter significantly. The purpose of EIS studies of electrode-tissue interfaces is to better approximate electrode model parameters (Figure 2.2b) [36].

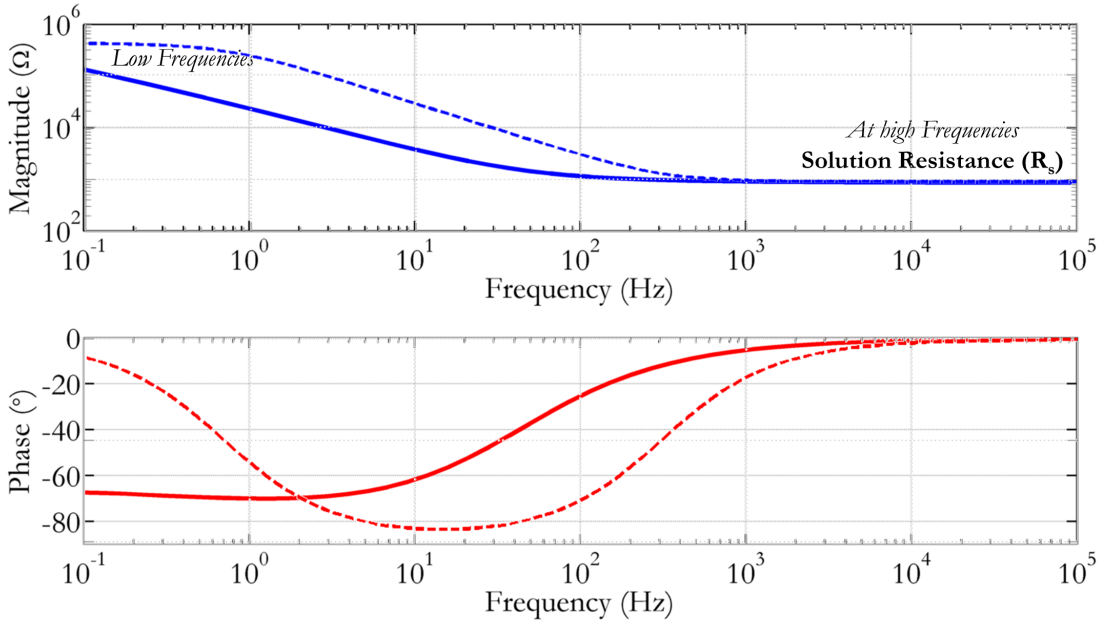

Figure 4.4: Electrochemical Impedance Spectroscopy (EIS) Magnitude and Phase plots: The magnitude plot is about 1kΩ at high frequencies. At low frequencies, it is harder to determine the charge-transfer resistance, R_{ct} using a first-order model. The phase plot shows a 70° increase in phase back to zero. The plots in the dashed line show the Bode plot simulation for an ideal first-order model with $R_s = 900\Omega$, $C_{dl} = 3.6\mu F$ and $R_{ct} = 400k\Omega$. The slope of the magnitude plot for the real data is not at -20dB/decade, and the phase plot does not reach -90° due to the Warburg impedance, often modeled as a constant phase element.

At very high frequencies (>1MHz), the double layer capacitance (C_{dl}) in the model charges (and discharges) very quickly, thereby effectively behaving like a short across the charge transfer resistance (R_{ct}). Therefore, the solution resistance R_s, which models the conductivity of the tissue or electrolyte, can be estimated at high frequencies (about 860Ω for this electrode). At very low frequencies (< 0.01Hz), the capacitor blocks current, and can be approxmiated by an open circuit. From the EIS magnitude plot at $0.1Hz$, the exact value of R_{ct} cannot be determined because the impedance of the capacitor dominates the total

impedance. However, we know that the electrode conducts DC, which implies that R_{ct} does exist, but can be very large [37], in this case, R_{ct} must be greater than $100k\Omega$. When plotted against a Bode plot simulation for a first order electrode-electrolyte (tissue) interface model (with parameters $R_s = 900\Omega$, $C_{dl} = 3.6\mu F$ and $R_{ct} = 400k\Omega$), the model does have a low frequency impedance of $R_s + R_{ct}$, which can be observed as a leveling on the dashed magnitude plot (Figure 4.4). The difference between the measured data (solid line) and first-order model simulation (dashed line) in the magnitude plot is the slope of the real data is not at -20dB/decade, as it is in the Bode plot. This also corresponds to the fact that the phase plot does not reach -90° in the measured data. This discrepancy between the first order model and the measured data response is often modeled as a constant phase element or as Warburg impedance [20].

As described, electrochemical characterization experiments conventionally use a three-electrode system. In most neural stimulation environments, however, two electrodes are sufficient to enable a flow of current between the working electrode and the counter electrode. To observe the *in vitro* response to a current-based, biphasic stimulation waveform (Figure 3.1a), one of the contributions of this work was to develop an open-source, programmable 8-bit biphasic stimulator with the option of active feedback. While the details of the feedback system will be elaborated in Chapter 6, a detailed description of the **Bi**phasic **C**urrent stimulator with **A**ctive **F**eedback (BiCAF), is described in the next section.

4.3 Biphasic Stimulation

To study the effects of residual voltage and long term anodic feedback across the electrode-electrolyte interface, several versions of a programmable stimulator were developed at the Neural Devices Engineering Lab. The **Bi**phasic **C**urrent Stimulator with **A**ctive **F**eedback (BiCAF) board is a programmable, controllable high impedance biphasic current source with provision to implement active feedback algorithms in neural stimulation systems. The components of the board can be modified to suit different magnitudes of current. The Arduino

Micro, an open-source, cross-platform microcontroller board based on the ATmega32u4, controls the functionality of the system, and interfaces with the PC via a Serial USB protocol. The stimulation system parameters can be adjusted via a Python based graphic user interface (Figure 4.7). The default stimulation parameter values that were used for experimentation are shown in Table 4.1. The sequence diagram for the operation of the board is shown in Figure 4.8.

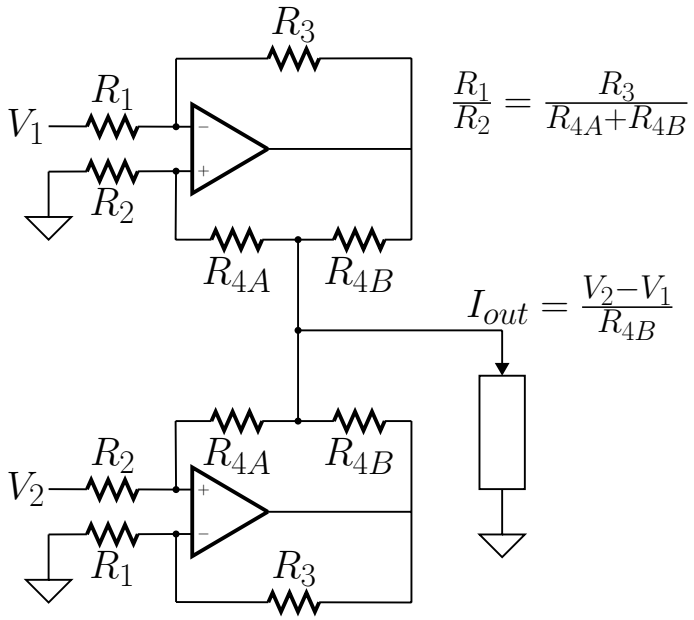

Figure 4.5: Modified Howland current pump circuit: a versatile current pump that can has been designed to accommodate bidirectional current, with the capability of supplying different current ranges based on the power supply, and resistor values.

4.3.1 Biphasic Mismatch in the BiCAF System

Perfect charge balancing of the cathodic and anodic phases of a biphasic stimulation pulse is only theoretically possible. Practically, there exists a biphasic mismatch offset in the stimulator that was developed for this work. When the cathodic bit value and the anodic bit value are both at full scale (255), the currents are not equal and opposite. The change in mismatch was measured using a capacitive load (100nF) and the transient data was captured by an oscilloscope and analyzed for deviations in the output voltage in MATLAB.

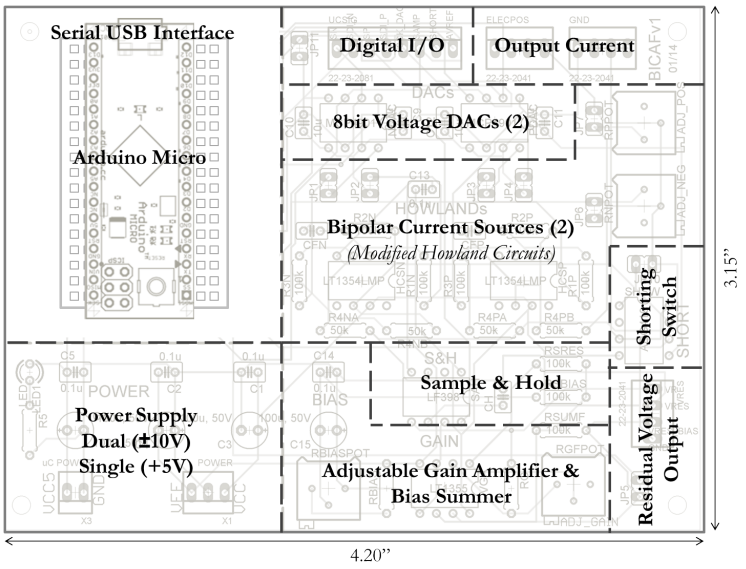

Figure 4.6: BiCAF board level layout: The Arduino Micro is a microcontroller that interfaces between the PC and the programmable current source, as well as performs the active feedback control.

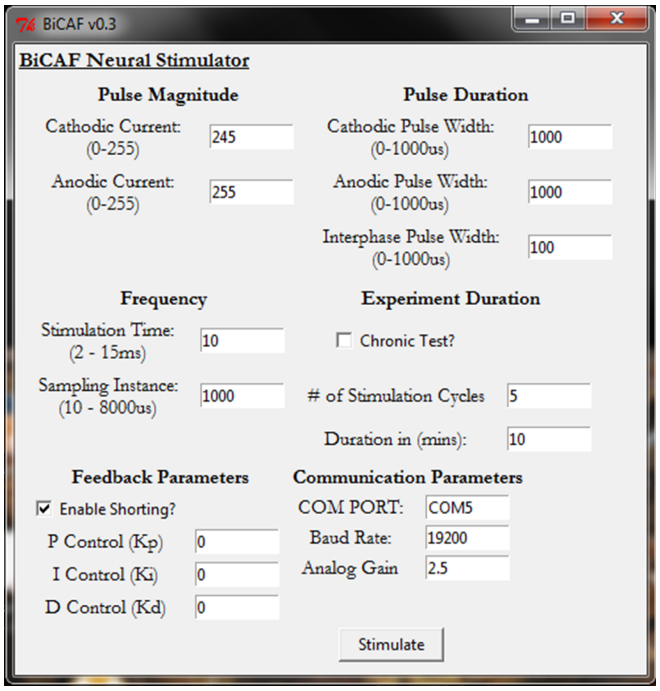

Figure 4.7: **Bi**phasic **C**urrent stimulator with **A**ctive **F**eedback (BiCAF) System Control Interface, designed to manipulate the control parameters for active anodic feedback.

Table 4.1: BiCAF Performance Parameters

System Block	Parameter	Value
Power Supply	Dual Power Supply	$> \pm 10\ V$
	Min. Voltage Compliance	$2.5\ V$
Current Source	Current DAC Resolution	8 bit
	Pulse Rise/Fall Time	$10\ \mu s$
	Pulsewidth Resolution	$1\ \mu s$
	Max. Current Amplitude	$\pm 100 \mu A$
	Biphasic Charge Mismatch	1.5%
Microcontroller	Clock Frequency	$16\ MHz$
	ADC Conversion Time	$< 250\ \mu s$
	ADC Resolution	10 bit
	Min. Voltage Measurement Resolution	1mV

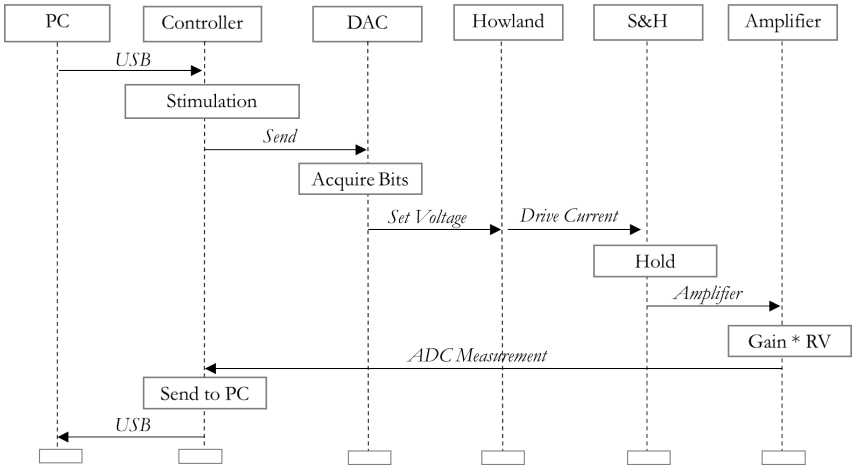

Figure 4.8: BiCAF operational sequence diagram outlining the sequential relationships between different blocks in the BiCAF system.

The mismatch variation was linear and the near-zero mismatch point was found at a cathodic value of 245 and anodic value of 255 (Figure 4.9). Any biphasic stimulator circuit must be tested for a stable biphasic mismatch value, because residual voltage measurements are best characterized when measured close to zero biphasic mismatch.

4.3.2 SIROF Electrode Response to Biphasic Pulses

A typical response to a balanced biphasic pulse to a Sputtered Iridium Oxide Film (SIROF) electrode is shown in Figure 4.10, highlighting the parameters in the electrode model de-

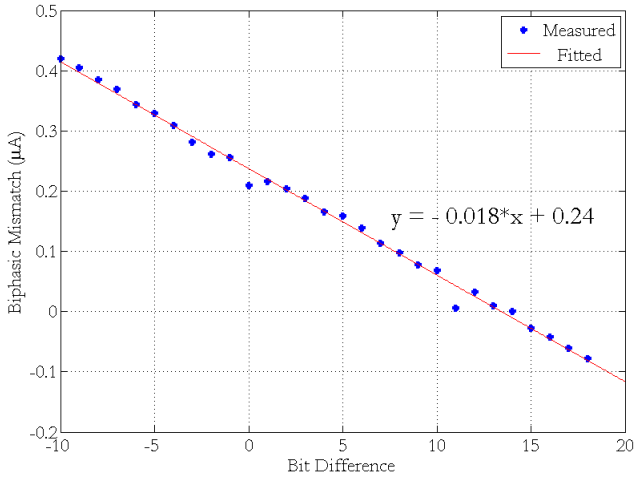

Figure 4.9: Measured biphasic mismatch in the BiCAF system: The average mismatch is shown versus (anodic bit - cathodic bit) values, deviating from fullscale value at (255-255=0). For example, a bit difference of -5 implies the anodic current was set at 250 and the cathodic current is set at 255. The mismatch measured at this setting was found to be $+0.33\mu$A, when it should be -2μA, for an 8-bit current stimlator with a full scale current of 100μA.

scribed in Section 2.1.2.

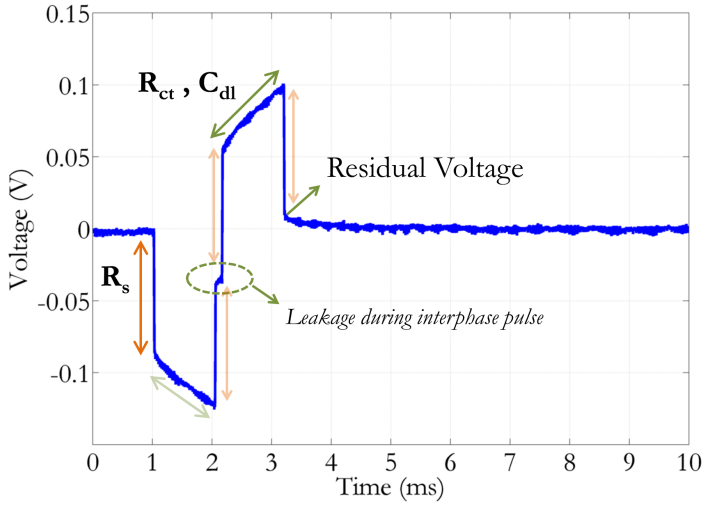

Figure 4.10: Transient response of a SIROF electrode to a balanced biphasic current pulse for the parameters shown in Table 4.1. Transient measurement data was obtained using an Agilent DSO7012B with a minimum sampling rate of $20kS/s$.

The ohmic drop in voltage is predominantly due to solution resistance, R_s. Leakage across

the charge-transfer resistance, R_{ct}, from the double-layer capacitance, C_{dl}, occurs throughout the stimulation pulse. It is particularly evident from the leakage during the interphase pulse, eventually leading upto the residual voltage at the end of the anodic pulse.

4.4 Discussion

The methods provided in this chapter cover electrochemical characterization methods of cyclic voltammetry (CV) and electrode impedance spectroscopy (EIS). CV and EIS methods are used for validation and comparison of residual voltage measurements. The residual voltage generation and measurement setups are done using biphasic current stimulation pulses, generated by a modified-Howland current source circuit, along with a 16MHz microcontroller based control system. In particular, the methods presented in this chapter are used to understand:

- how the residual voltage changes when the electrode-electrolyte (tissue) interfaces changes (Chapter 5),
- how the residual voltage grows when subject to continuous stimulation pulses (Chapter 6, 7),
- how the anodic pulse width can be controlled by measuring the residual voltage such that the electrode-electrolyte (tissue) interface voltage is constant at a safe potential (Chapter 6).

Chapter 5

Residual Voltage as a Status Indicator

Application of Residual Voltage

Chronically implantable electrical stimulation mechanisms have been the focus of physiological engineering research for the last decade. With the advent of microelectronics, large stimulation electrode array designs are becoming the norm. Therefore, it is imperative, and challenging, to look into the criticality of safe functional electrical stimulation for large electrode arrays. In this chapter, we explore the idea that the residual voltage from a biphasic electrical stimulation pulse can serve to recognize damage at the electrode-tissue interface. Sputtered iridium oxide film electrodes are systematically damaged and characterized. Residual voltage values from these electrodes are then compared to measurements made using cyclic voltammetry (CV) and electrode impedance spectroscopy (EIS).

5.1 Damage at the Electrode-Tissue Interface

When microelectrode arrays are chronically implanted into tissue for stimulation, there are a multitude of mechanisms that affect their performance. Animal tissue environments are responsive to the presence of a foreign body. While the stimulation electrode may be effective over acute time periods, the prolonged use of chronically implanted electrodes often exhibit

erratic behaviour. As outlined by Merrill and Tresco [36], some of the mechanisms that describe electrode-tissue interface damage on prolonged use include:

- a change in the electrical impedance due to the formation of a barrier following encapsulation of fibrous growth,
- movement of the electrode from the original implantation site,
- mechanical breakage (or delamination) of the electrode,
- effects of neural plasticity around the electrode [36],
- and changes in the stimulation electrode characteristics due to electrode dissolution [38].

While it is advantageous to individually analyze each damaged/degraded electrode, it is practically inefficient to do so when the number of electrodes increases. There needs to be a way to diagnose the problem and disconnect any substandard electrode before further damage can occur. One of the main contributions of this work is to highlight the usefulness of measuring the residual voltage after a biphasic stimulus, as a way of detecting any changes to the electrode/electrolyte (tissue) interface in a chronic stimulation implant [39].

5.2 Why Use Residual Voltage for Damage Detection?

There are several advantages to using residual voltage as an early indicator of electrode damage: Firstly, the residual voltage is one of the most accessible measurements that is a function of R_{ct} and C_{dl}. Secondly, the dynamic range for detection of residual voltage is smaller than measuring the entire stimulation waveform. Residual voltage values after a biphasic stimulation pulse, range in the order of a few millivolts, as opposed to solution resistance (R_s) measurements, which can be in the order of volts. This makes it easier to develop low-power hardware circuits for the measurements. Thirdly, the measurement is performed *after* the stimulation pulse. Because the stimulation frequency of most applications is of the order of

$100Hz$, state of the art microelectronics can acquire fairly accurate samples at frequencies that are greater by at least 2 orders of magnitude.

Currently, the only established mechanism for safety in an electrode is to short the electrode immediately after stimulation. The elegance of the shorting method lies in its simplicity, because the electronic switch is the most inexpensive hardware that could be added to a circuit. However, the method is very brute-force, and it essentially nulls a voltage measurement that may give us a clue about the health of the interface. Shorting the electrode out may prevent us from detecting early damage in implanted electrodes. The shorting mechanism uses a switch to bypass any residual charge in the form of current away from the electrode after the stimulation is complete. When the shorting switch is active, the voltage on the electrode will be clamped at zero, we thereby lose information about the electrode/electrolyte (tissue) interface. Cogan et al. suggest that a measurement of the voltage during the interphase pulse is a direct measure of the voltage across the double layer capacitance [40]. While a measure of a charged C_{dl} is very beneficial, the order of biphasic interphase pulse widths is around 100 μs and the voltage across the capacitance may be 0.5V, depending on the size and material of the electrode. These constraints make the design of electrode measurement circuits less scalable and energy inefficient.

In an *in vitro* tissue study performed by Merrill and Tresco [36], it was found that the variation of electrode impedance with different biological cell cultures *in vitro* typically increased 20-80%, which is a broad range. Residual voltage measurements provide an indication of whether the stimulation circuit sees the same load circuit that is was designed for. If there is any change, the stimulation system can be designed to shut down or adapt to a different configuration. The work presented in this chapter describes the methods used to establish the use of residual voltage for feedback information during electrical simulation.

In this work, the following steps were used to validate the measurement of residual voltage from biphasic stimulation to detect evidences of change at the electrode-electrolyte (tissue) interface. A detailed description of **c**yclic **v**oltammetry (CV) and **e**lectrochemical **i**mpedance **s**pectroscopy (EIS) have been described in Chapter 4.

1. Break-in of SIROF electrodes[1]
2. Characterization of electrodes using CV and EIS
3. Measurement of **r**esidual **v**oltage (RV) pulses using a biphasic current stimulator with known mismatch
4. Extraction of cathodal charge capacity from CV
5. Degradation of electrodes using CV cycling above the water window
6. Characterization of electrodes using CV and EIS, as well as RV
7. Comparison of characterization data with RV measurements using cathodal charge storage capacity

5.3 Characterization Methods

The electrochemical setup used in this work comprised of the SIROF working electrode in an array of 15 electrodes (Figure 5.1(c)), and a coiled platinum (Pt) counter electrode, in 1X physiological buffered saline (PBS) saline solution. Phosphate buffered saline is an isotonic buffer solution used in biological research because the osmolarity and ion concentrations match those of the human body. A three electrode setup was used for Cyclic Voltammetry (CV) and Electrode Impedance Spectroscopy (EIS) experiments with the Metrohm Autolab measurement system, with an Ag/AgCl reference electrode (Basi Inc. MF2052) to characterize the electrode array (Figure 5.1(b)). The Autolab analyzer was also used to perform switch time constant measurements. Practical electrical stimulations typically employ a two electrode setup (Figure 5.1(c)). The details of the electrochemical measurement setup is described in Section 4.1.

[1] a process of activation for sputtered iridum oxide film (SIROF) electrodes prior to regular use

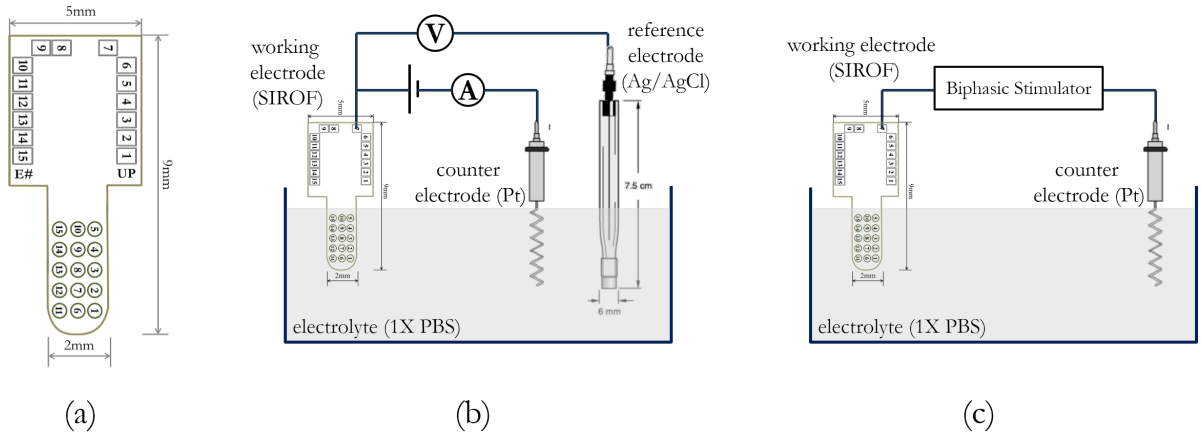

(a) (b) (c)

Figure 5.1: Experimental setup for RV validation experiments: (a) SIROF working electrode array of 15 electrodes obtained from [1] with each electrode of 400μm diameter. The working electrode array was bonded to a circuit breakout board using cellophane tape, and sealed in a container using silicone glue. (b) Three electrode measurement setup for Autolab Metrohm (c) Two electrode measurement setup for stimulation. The counter electrode (Basi Inc. MW1033) is made of platinum and has a surface area 2000 times the area of the SIROF electrode, which is sufficient to neglect any potential changes across the counter electrode.

5.3.1 Preparation & Break-in SIROF electrode array

The polyimide base electrode array, containing 15 electrode sites, was lifted-off from the silicon die substrate. Once removed, the array was adhered to a circuit breakout board using cellophane tape, such that the contacts on the array aligned with the the contacts on the board. In order to hold the electrode in place with respect to the circuit board, a 3D printed clamp was used to press the electrode against the circuit board. The clamp was sealed in silicone to prevent seepage of saline up the electrode, which can cause shorting of electrode pads. The complete electrochemical setup for the break-in is represented in Figure 5.1(b) where they are characterized for first use using cyclic voltammetry (CV) and electrochemical impedance measurements (EIS). The parameters used for typical CV and EIS characterizations are described in Table 5.1.

After initial characterization, the electrodes were subject to potential cycling (repeated CV cycles) to activate the iridium oxide film. Activation by means of repeated cyclic voltammetry measurements causes the initial monolayer of iridium oxide to become extended as

Parameter	Value
Scan Rate	0.1 V/s
Lower Potential Limit (V_L)	-0.6V
Upper Potential Limit (V_H)	+0.8V
# Zero Crossings	6

Parameter	Value
Sinusoidal Input	10mV$_{RMS}$
Lower Frequency Limit	0.1Hz
Upper Frequency Limit	100kHz
# Frequency Values	50

Table 5.1: Typical CV and EIS parameters for electrochemical characterization, the potential limits for the CV measurement are water window limits [18]

a thicker, hydrated oxide [41]. The CV cycles were performed at a scan rate of $0.1V/s$, between the limits of -0.6V/+0.8V [18] for 14 minutes. For these experiments, the number of zero-crossings was adjusted to set the duration of the CV cycling. All the electrodes were characterized using cyclic voltammetry (CV) and electrochemical impedance spectroscopy (EIS) with typical parameters shown in Table 5.1. The SIROF electrodes were obtained from the Boston Retinal Implant research lab, and were designed for retinal implants. The electrodes are identical in design. Of the 15 electrodes present in the electrode array, 13 electrodes were prepared for use and characterized using CV and EIS (Figure 5.1(a)).

5.3.2 Biphasic Stimulation Responses

All the electrodes were driven by closely balanced[2] biphasic pulses generated by the BiCAF system, described in Chapter 4, Section 4.3. Transient responses for one pulse were obtained using the Agilent DSO7012B with a minimum sampling rate of $20kS/s$, the data was smoothed in MATLAB using a moving average filter when required.

5.3.3 Extraction of Physical Parameters

Cathodal Charge Storage Capacity

The charge capacity of an electrode is a measure of the maximum charge that can be injected into the electrolyte (tissue) through the electrode. The cathodal charge capacity was

[2]No biphasic stimulator is going to have biphasic mismatch of zero, the tested biphasic mismatch of the BiCAF system used in this work is shown in Chapter 4, Figure 4.9.

obtained by numerically integrating the curve under the negative half of the CV curve, and dividing it by the area of the electrode (refer Section 4.2.1, Figure 4.3). The units of cathodal charge capacity are typically coulombs per square centimeter (C/cm^2).

Solution Resistance

The high frequency impedance, obtained from the magnitude plot of the EIS data, is a measure of the solution resistance, R_s, of the electrode-electrolyte (tissue) interface (Chapter 4, Figure 4.4). The solution resistance can also be graphically estimated from the step change in voltage in the biphasic response plot (Chapter 4, Figure 4.10).

5.4 Electrode Degradation Protocol

One of the objectives of the work presented in this dissertation is the idea that one can use residual voltage (RV) from biphasic current stimulation, as an early indicator of changes at the electrode-electrolyte (tissue) interface. The most useful application of measuring residual voltage is to detect damage at the electrode-electrolyte (tissue) interface (Section 5.1). The main reasons to use residual voltage are the fact that it is a function of the charge-transfer resistance and the double-layer capacitance, and there is sufficient time for measurement after stimulation (Section 5.2). From a high-density stimulation electrode systems standpoint, if there is any indication of damage at the interface, the channel can be disconnected if there is any problem.

In order to validate the usefulness of measuring RV, the approach followed in this work is to systematically degrade stimulation electrode, in a way that is repeatable. There is empirical evidence that exposing sputtered iridium oxide film electrodes (SIROF) above the electrochemical water window limits of -0.6V/+0.8V, can cause damage to the film [18]. Using these limits as a premise, the electrodes were subject to CV cycling at limits that are above these limits, each for a duration of 1 hour, in 1X PBS. The electrodes were charac-

Degradation Protocol	Electrodes #	V_L	V_H	# Zero Crossings	Deviation from Water Window (WW)
I	5,10,15	-0.4V	+0.6V	360	Within WW
II	3,4,6	-0.6V	+0.8V	257	At WW
III	7,8,9	-1.2V	+1.4V	200	Above WW by $\|0.6V\|$
IV	12,13,14	-1.6V	+1.8V	105	Above WW by $\|1V\|$
V	11	-1.8V	+2.0V	100	Above WW by $\|1.2V\|$

Table 5.2: Degradation Protocol using Cyclic Voltammetry, by using the potential limits for the CV measurement above water window limits for SIROF[18]. The electrode numbers are based on the numbers marked in Figure 5.1(a). The values of zero crossings are adjusted to make sure all the electrodes are exposed to the saline under each condition for the same duration of 1 hour. V_H and V_L are the set upper and lower limits of the CV cycle.

terized and imaged after the degradation. The total of 13 electrodes were damaged, with 3 electrodes for each experimental condition. To illustrate an extreme case of degradation, 1 electrode was exposed to a very high potential limit window. The experimental details for the degradation protocol are described in Table 5.2. The nominal cycling was performed at regular intervals during the degradation of each electrode, to include the effect of exposure to saline for long duration.

Note on Degradation Protocol

The degradation protocol was designed to expedite a change in the electrode-electrolyte (tissue) interface. In reality, while it may not be common that a stimulation electrode gets exposed to high voltages, the final state of the electrode can be degraded in similar ways. The types of damage that are observed are cracking of the electrode surface, corrosion and delamination. The experiment was used primarily to achieve a non-standard operating state for a stimulation electrode. The results and images described in Section 5.5.3 will elucidate the different types of damage achieved through the use of the protocol, and discuss how residual voltage can be used to detect some of these changes.

eSEM Imaging

Preliminary optical imaging of the electrodes to view the systematic degradation was done using the ScopeTek MD560 Digital Microscope. To study the nature of degradation, the elec-

trodes were imaged using an **e**nvironmental **S**canning **E**lectron **M**icroscope (eSEM) The SEM model used was the Quanta 200 (FEI). An environmental scanning eletron microscope allows the collection of electron micrographs of specimens that are uncoated (non-conducting), because of a gaseous environment in the specimen chamber.

5.5 Results

For the 13 electrodes that were subject to the degradation protocol described in Table 5.2, biphasic responses were made for all electrodes before and after applying the protocol. All the electrodes were also characterized by cyclic voltammetry and electrochemical impedance, before and after the application of the protocol. For each category of the protocol, 3 electrodes were tested. This section reports the results of all the electrodes. The average transient biphasic response for 13 electrodes *before* degradation is shown in Figure 5.2, along with error bars, with a maximum error range of 80mV.

5.5.1 Pre-Degradation Characterization

Stimulation electrodes are typically characterized by their cathodal charge storage capacity. Cathodal charge storage capacity is calculated by numerically integrating the area enclosed by the negative Y-axis curve of a cyclic voltammetry (CV) plot (described in Chapter 4, Section 4.2.1). CV plots consist of multiple zero-crossings, as shown in Figure 5.3a. In this work, a total of 6 zero-crossings were used for a typical characterization, which implies there are 3 complete CV scans. To calculate the charge storage capacity, the second and third scans (Figure 5.3b) were averaged, and the cathodal charge storage capacity was obtained from Figure 5.3c. Henceforth, all CV plots reported are averaged CV plots.

The break-in procedure for SIROF electrodes (described in Section 5.3.1) involves cycling the electrode between the water window limits. This process increases the real surface area of the SIROF material, thereby increasing the charge storage capacity. Charge storage capacity

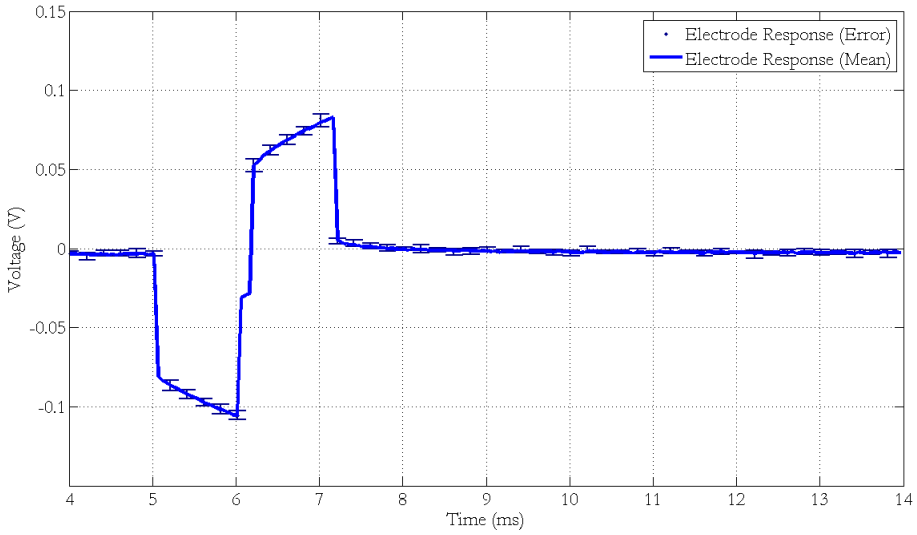

Figure 5.2: Average biphasic transient response of SIROF electrode array: The graphs shows the mean of the transient biphasic response of electrodes #3-#15, along with error bars for different time points (downsampled for clarity).

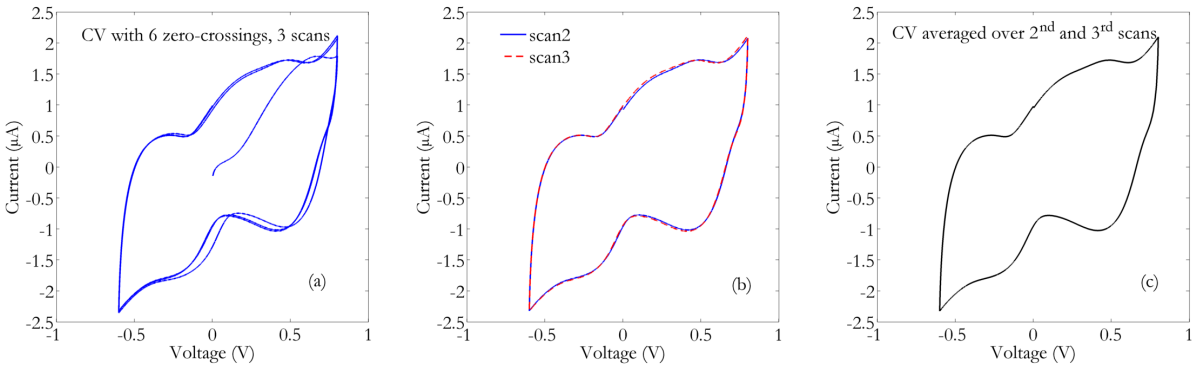

Figure 5.3: CV Averaging Example: (a) CV response with 6 zero crossings (b) Extracted two scans (2,3) from the full CV curve shown in (a) and (c) Average CV curve from the two curves shown in (b). The curve shown in (c) is typically reported for this work and is used for calculating the cathodal charge storage capacity.

is the area enclosed by the CV curve, and can be seen in Figure 5.4. The mean and error of the magnitude and phase of all the electrodes, from the break-in to the electrode state before applying the degradation protocol is shown in Figure 5.5.

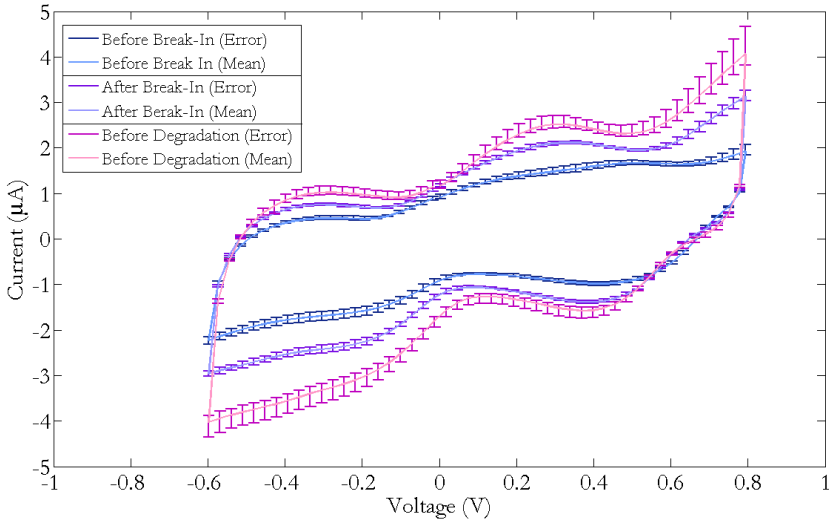

Figure 5.4: CV curves before Degradation Protocol: The data here show the mean and error for the averaged CV cycle (Figure 5.3) for electrodes #3 - #15. The break-in of the electrodes by potential cycling activates the iridium oxide, thereby increasing the charge storage capacity of the electrodes (Section 5.3.1).

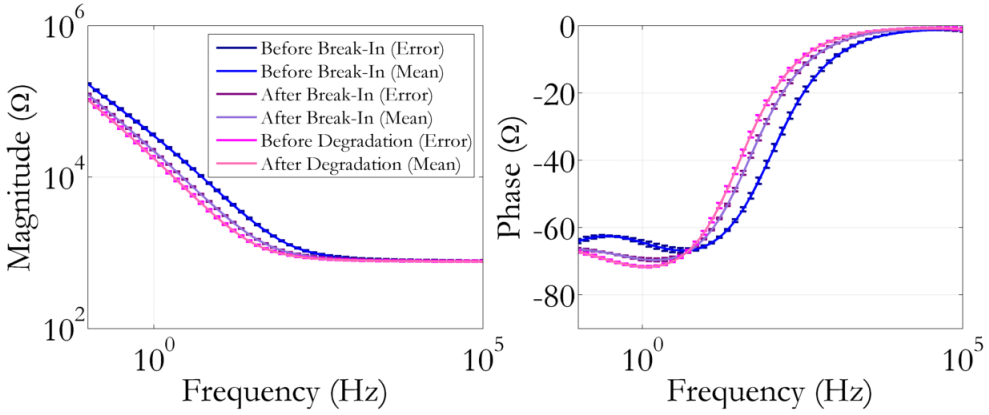

Figure 5.5: EIS curves before Degradation Protocol: The data here show the mean and error of the magnitude and phase plots for electrodes #3 - #15. The break-in of the electrodes by potential cycling activates the iridium oxide, increasing the capacitance, thereby decreasing the low-frequency impedance on the magnitude plot.

5.5.2 Degradation Protocol

The degradation protocol was applied on a total of 13 electrodes (Table 5.2), with 3 electrodes testing protocols DP-I to DP-IV, and one electrode for degradation protocol V (DP-V). CV curves for each protocol is shown in Figure 5.6. As the voltage range increases, the current conducted across the interface increases by more than one order of magnitude. The degradation procedure was used primarily to *alter* the characteristics of the electrode-electrolyte interface, to study residual voltage measurements on altered stimulation electrodes.

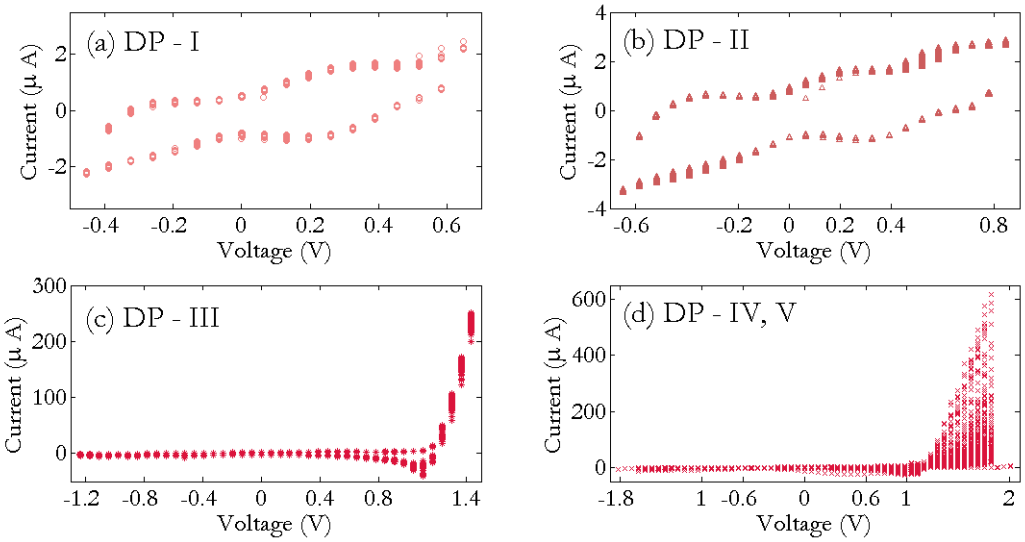

Figure 5.6: CV-based electrode Degradation Protocol: Running CV cycles higher than the specified water window potentials (-0.6/+0.8V for SIROF) in order to systematically, repetitively and expeditiously induce a variation in the electrode characteristic (ref Table 5.2) (a) Degradation Protocol I (Nominal) (b) Degradation Protocol II (At Water Window) (c) Degradation Protocol III ($|0.6V|$ Above Water Window) (d) Degradation Protocol IV ($|1V|$ Above Water Window). As the applied voltages increases, the conduction of the electrodes increases due to irreversible electrochemical reactions, thereby damaging the electrode.

5.5.3 Post-Degradation Protocol Results

Wet scanning electron microscope (eSEM, 50000X magnification) images of the electrodes after the degradation protocol are shown in Figure 5.7. The protocol enabled the simulation of several degraded electrode structures, such as corrosion, mechanical damage, re-deposition and delamination. Images taken at 50kX magnification are presented in Appendix Section H. It is interesting to note that the cases which show cracking or lifting-off of the SIROF layer, also exhibit an increase in the real surface area of the electrode that is in contact with the electrolyte.

A comparison of the biphasic responses with cyclic voltammetry characterization for each of the degraded electrodes are shown in Figures 5.8 - 5.11. Recall that the biphasic stimulation pulse is a rectangular current pulse (Chapter 3, Figure 3.1a). When a rectangular current pulse passes through a capacitor (C_{dl}), the resulting waveform is a straight line, with a slope of ($1/C_{dl}$). Therefore, a decrease in the slope of the biphasic response, indicates an increase in the double-layer capacitance. The double-layer capacitance is proportional to the charge storage capacity of the electrode material, which is the area enclosed by the cyclic voltammetry (CV) curve. A culmination of the results shown in Figures 5.8 - 5.11 is depicted as the charge storage capacity (Figure 5.12) along with the electrochemical impedance spectroscopy (EIS) magnitude and phase plots (Figure 5.13). Figures 5.14a and 5.14b show the residual voltage values sampled 1μs and 1ms after the anodic pulse of the biphasic response.

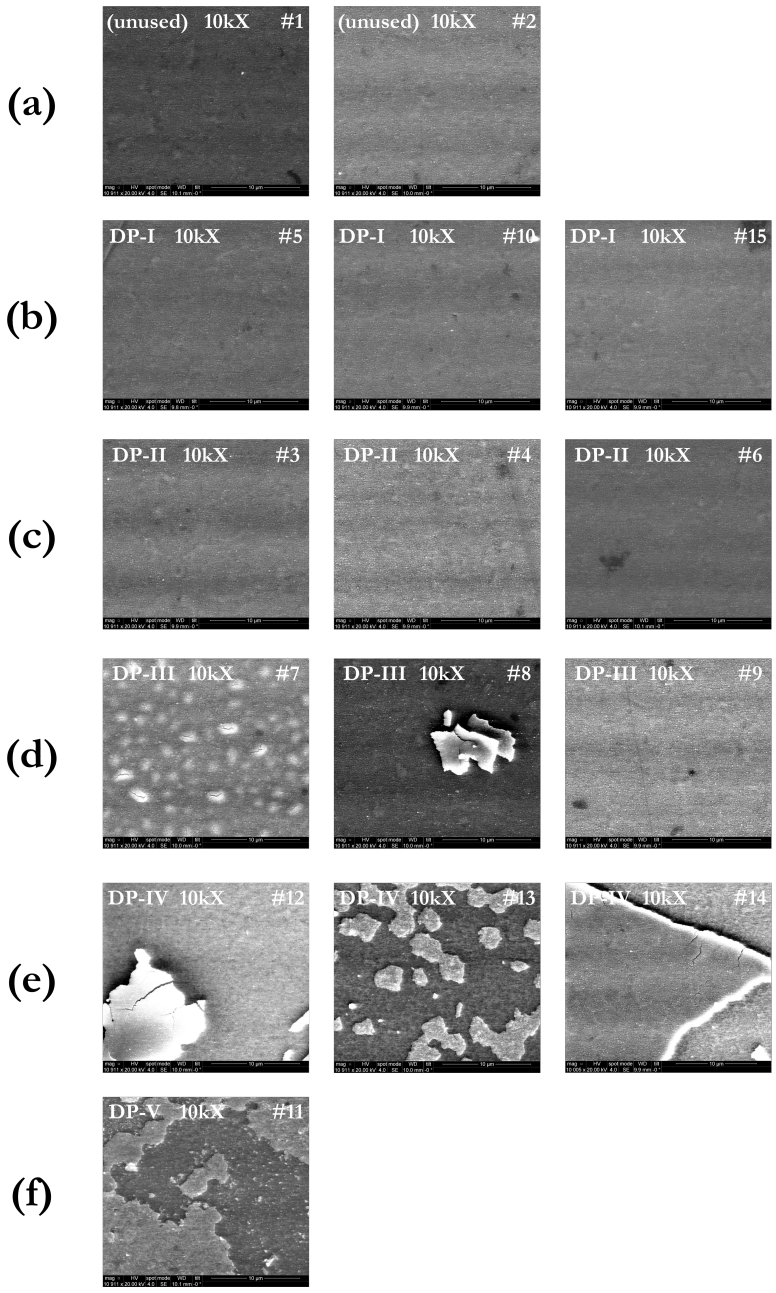

Figure 5.7: Wet SEM images after Degradation Protocol 10kX magnification (DP, Table 5.2): (a) Unused electrodes showing the general structure of SIROF film (b) DP - I, nominal voltage range, within the water window, there is no significant texture change in all electrodes (c) DP - II, operated at the water window limits, cracks start to appear on the surface (d) DP - III, operated above the water window, the SIROF film starts to rupture (#7), #8 shows a redeposition of SIROF film, these cases can exhibit an increase in charge storage capacity, #9 shows an absence of SIROF film (e) DP - IV, operated above the water window, shows delamination, resulting in absence of SIROF material in most areas, #12, #13 shows absence of SIROF film (f) DP - V, test case for very high voltage range, resulting in delamination

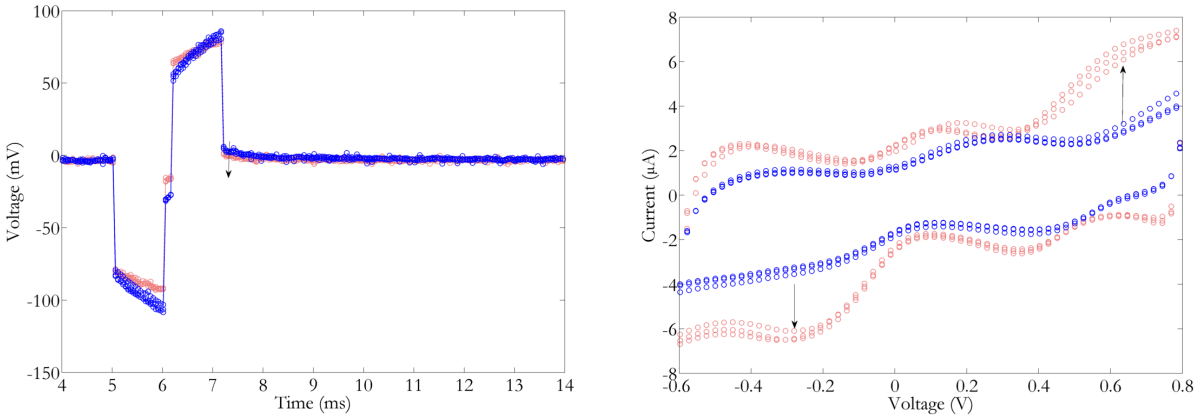

(a) (b)

Figure 5.8: Outcome of Degradation Protocol - I (Nominal): (a) Biphasic response (b) CV curve. An increase in capacitance is indicated by the increase in the area enclosed by the CV curve.

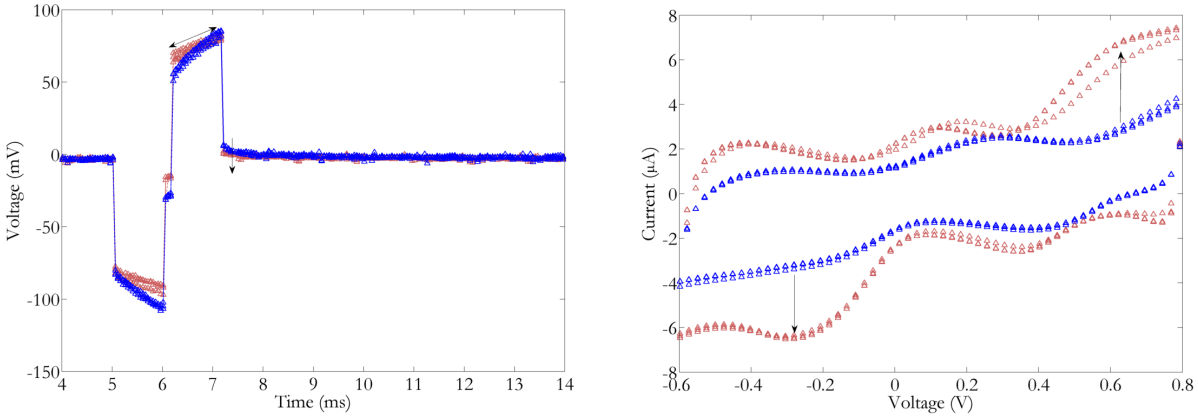

(a) (b)

Figure 5.9: Outcome of Degradation Protocol - II (At WW): (a) Biphasic response (b) CV curve. There is a noticeable decrease in the slope of the biphasic response, indicating an increase in the double-layer capacitance, corroborated by the increase in the enclosed area of the CV curve.

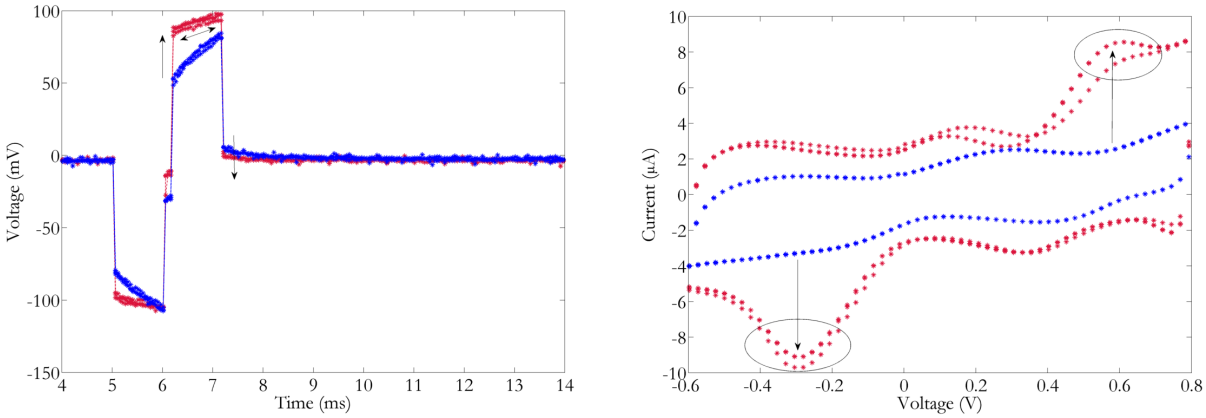

(a) (b)

Figure 5.10: Outcome of Degradation Protocol - III (Above WW by $|0.6V|$): (a) Biphasic response (b) CV curve. There is an increase in the solution resistance, indicated by the step change in the biphasic response. The CV curve, while showing an increase in area, also shows a lot more electrochemical reactions, based on the sharp peaks at higher voltage ranges. Surface cracking exhibited in Figure 5.7(d) can exhibit an increase in the real surface area.

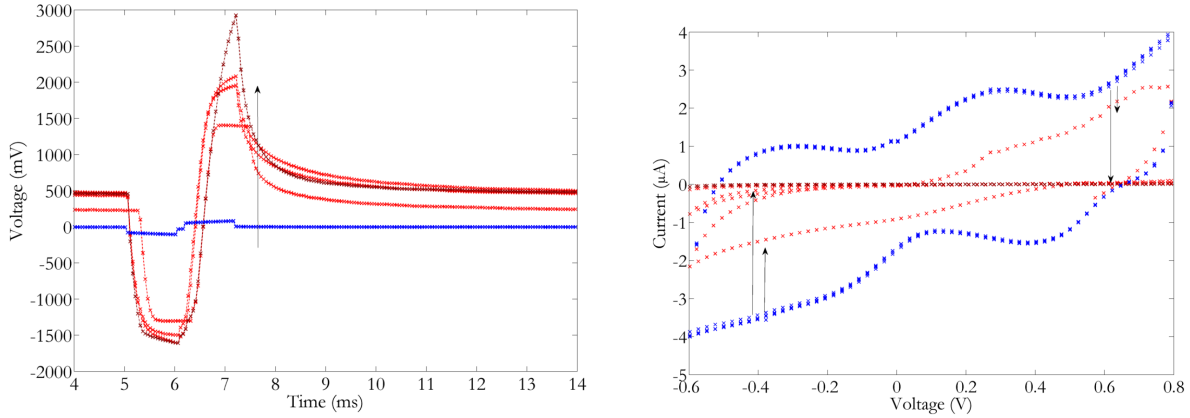

(a) (b)

Figure 5.11: Outcome of Degradation Protocol - IV (Above WW by $|1V|$): (a) Biphasic response (b) CV curve. The responses for this case can be erratic, but mostly involve a complete delamination of the SIROF material, thereby drastically reducing the storage capacity, and increasing the dynamic range of the biphasic response, thereby the residual voltage.

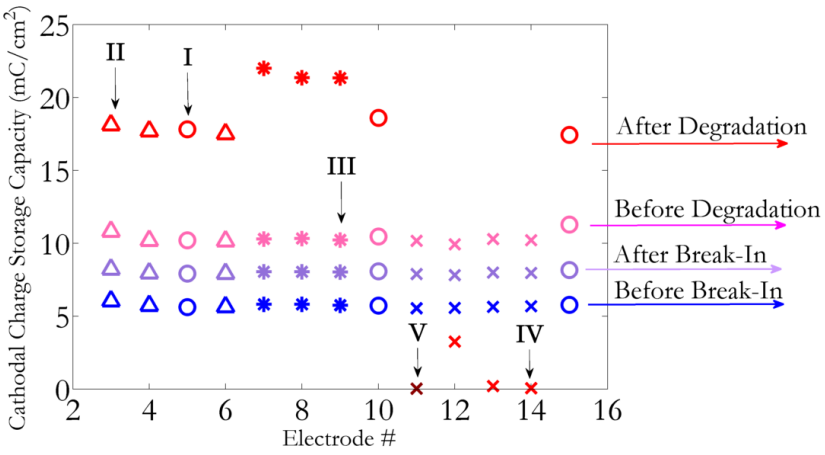

Figure 5.12: Cathodal charge storage capacity response: The figure shows the cathodal charge storage capacity for the electrodes before and after applying our degradation protocol. The electrodes exhibit a mean charge storage capacity of $5.7mC/cm^2$. All the electrodes were subject to potential cycling for 60 minutes at voltage ranges described in Table 5.2. The degradation procotol (DPI-V) is marked with a different symbol, shown in the figure. The potential cycling increases the charge storage capacity, indicating an increase in the value of the double-layer capacitor. Damaged electrodes, however, show a drastic reduction in charge storage capacity, due to delamination of the SIROF electrode.

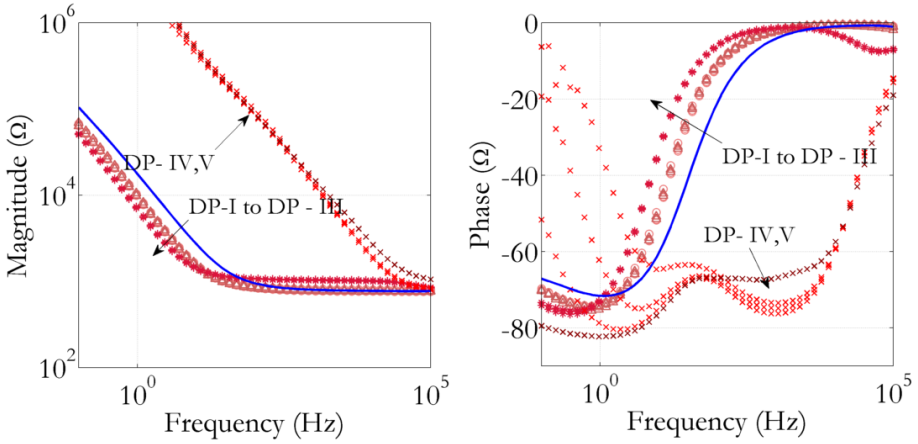

Figure 5.13: EIS magnitude and phase after Degradation Protocol: The solid blue line shows the mean plot from all electrodes before degradation. For protocols DP-I, DP-II and DP-III, there is no significant change in the magnitude plot between them, but they decrease from the pre-degraded response. The degraded cases, DP-IV and DP-V show a large increase in impedance, thereby increasing the measured residual voltage.

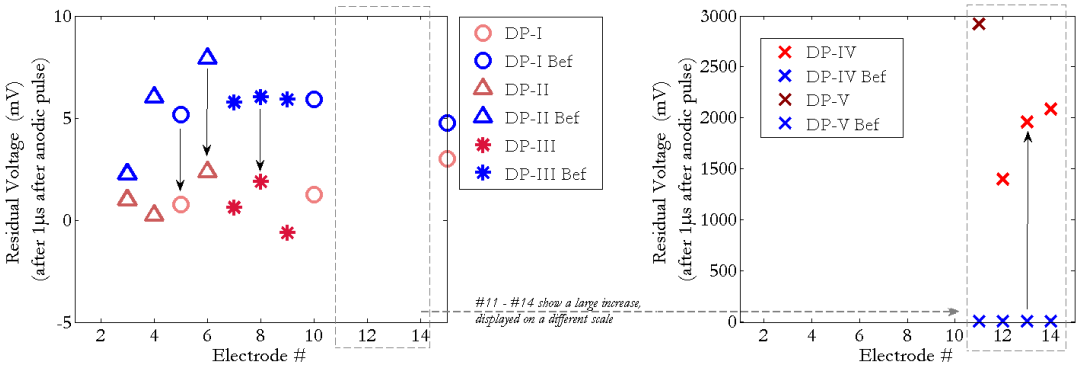

(a) Post Degradation: Residual Voltage after $1\mu s$ after the anodic pulse

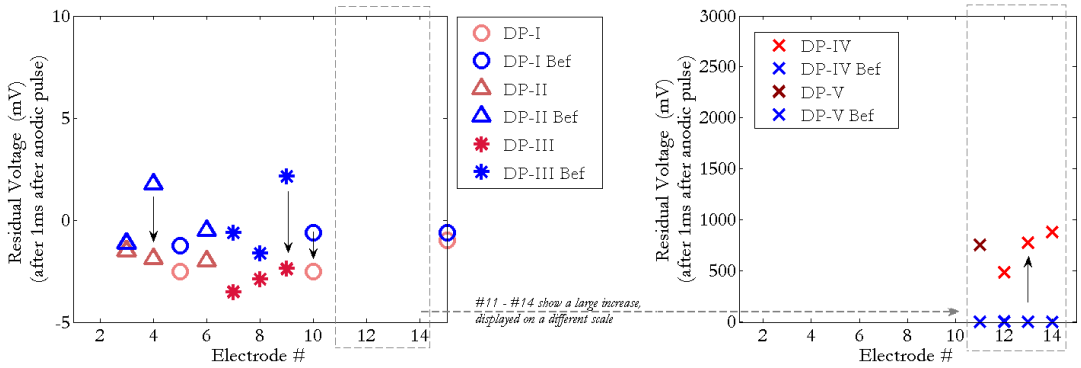

(b) Post Degradation: Residual Voltage after $1ms$ after the anodic pulse

Figure 5.14: Post degradation: Residual Voltage measurement (a) Measured after $1\mu s$ (b), after the anodic pulse: An increase in charge storage capacity (shown in Figure 5.12) indicates a decrease in residual voltage measurement. Measurement of residual voltage further away in time from the end of the anodic pulse is more prone to noise interference.

5.6 Discussion

Residual voltage (RV) is a leakage phenomenon that occurs during biphasic electrical stimulation due to discharge of the double-layer capacitance via the charge-transfer resistance. Because it is representative of the electrode-electrolyte (tissue) interface, measurement of residual voltage is a useful tool to identify changes that occur at the interface. While the theoretical characteristics of residual voltage are described in Chapter 3, this chapter uses a demonstrative degradation protocol on SIROF electrodes to illustrate the usefulness of residual voltage measurements for real-time feedback on electrode characteristics. Stimulation electrodes are typically coated with an electrochemically active material, like iridium oxide, in order to enhance the charge injection capacity for stimulation applications. The charge-transfer resistance (R_{ct}) is more relevant when discussing stimulation electrodes, due to the reversible redox reactions that occur at the interface. The double-layer capacitance (C_{dl}) is a function of the material and the area that is in contact with the electrolyte (tissue). From Chapter 3, we have seen that the RV peaks at a certain value of C_{dl}, R_{ct}, with higher values of RV for smaller values of C_{dl}, at a given value of R_{ct} (Figure 3.4).

In this work, sputtered iridium oxide film electrodes were used to demonstrate the relevance of RV measurements through controlled degradation experiments. There are three cases of electrode surface changes that are distinct in the context of RV measurements: (1) activation of SIROF film (2) cracking of the SIROF film and (3) delamination of the SIROF film. Potential cycling of iridium oxide activates the material, increasing the real surface area, and thereby increasing the charge storage capacity. Therefore, for electrodes tested with degradation protocols DP-I (#5,#10,#15) and DP-II (#3,#4,#6), which are within and at the water window limits, an increase in charge storage capacity is observed (Figure 5.12), without a significant change in the surface topology (Figure 5.7(b),(c)). For DP-III (#7,#8,#9), the damage is more pronounced, causing visible cracking on the surface (Figure 5.7(d)), and redeposition of SIROF material. This case is interesting because it causes an *increase* in the charge storage capacity, but this increase is not sustainable. If there is a large

deviation from the standard charge storage capacity, a *decrease* in RV can imply cracking on the electrode surface. For the last case of complete delamination, at that point, there is no SIROF material remaining, which decreases the capacitance significantly. Smaller C_{dl} values correspond to a higher residual voltage, which is evident from the residual voltage sampled after $1\mu s$ (Figure 5.14a). Therefore, it is imperative to measure the transient response of different layers of the electrode so that it is easier to diagnose the problem identified by the residual voltage.

Through this work, we have seen that residual voltage has its application in diagnosing faulty electrodes, particularly in high-density electrode stimulation systems. The residual voltage measurements made in this chapter are for one biphasic stimulation pulse. However, if residual voltage remains uncontrolled for several stimulation pulses, it can rise and possibly saturate at a voltage value that is unsafe for electrical stimulation. In prior work, any occurrence of residual voltage has been controlled by charge balancing methods, described in the following chapter (Chapter 6). One of the contributions of this work is to use active anodic feedback based stimulation to prevent residual voltage growth. In active anodic feedback, the anodic pulse width of the biphasic stimulation pulse is corrected such that the residual voltage is minimized. The advantage of this method is that the closed loop system can also acquire information about the interface, while keeping the residual voltage controlled. Chapter 6 shows the experimental evidence of residual voltage growth, as well as discusses the methods of control.

Chapter 6

Active Anodic Feedback

Safe Electrical Stimulation

We have so far established that the residual voltage is a characteristic of the electrode-tissue interface by mimicking damage in an high charge density stimulation electrode. A good stimulation system must ensure that the electrode potential does not reach levels where unwanted irreversible chemical reactions may occur. Depending on the frequency of stimulation and the impedance of the electrode-electrolyte/tissue interface, the residual voltage can build up over several stimulation pulses, and potentially reach the water window of the electrode. The water window is the applied voltage range when a substance does not get irreversibly oxidized or reduced.

6.1 Safe Electrical Stimulation

The *electrochemical window* is the applied voltage range when a substance does not get irreversibly oxidized or reduced. Electrical stimulation in aqueous environments has empirical limits in the electrode potential across an electrode-electrolyte/tissue interface. If the measured electrode potential is greater than the water window of the electrode, water gets oxidized/reduced to oxygen/hydrogen. The oxidation/reduction process, that occurs

through Equations 2.1, 2.2 alters the pH of the environment, which is unnatural and potentially unsafe. This process is irreversible because it leads to the formation of non-recoverable gas bubbles at the interface. Fundamentally, the electrode potential must not exceed the water window. The water window of SIROF is -0.6V/+0.8V [35]. Apart from electrochemical limits, McCreery et al. also identified charge per phase and charge density of stimulation as *cofactors* in biological neuronal damage [42]. The empirical boundary between safe and unsafe stimulation for different charge density and charge per phase values is approximated by Equation 6.1:

$$log(D) = k - log(Q) \tag{6.1}$$

Shannon [43] built upon this work to identify that a value of $k = 1.5$ as a proposed safe limit for stimulation. Cogan et al. show via cyclic voltammetry studies, that the safe electrochemical charge density limit for SIROF electrodes is $\approx 1\ mC/cm^2$ [35]. This work uses electrodes that have a diameter of $400\mu m$. For these electrodes, the safe biological charge limit is $200nC$, while the electrochemical safety limit is 1256 nC. Charge is delivered to the stimulation electrode by driving the electrode with electrical stimulation waveforms, notably current-based stimulation.

While it has been shown that measurement of residual voltage is useful to understand the nature of the interface, the existence of a long-term voltage across the electrode-tissue interface can be potentially harmful. In a chronic implant, a slow leakage current can cause irreversible reactions at the interface. Currently, the *de facto* for safety in an electrode is to short the electrode immediately after stimulation. The elegance of the shorting method lies in its simplicity, because the electronic switch is inexpensive in terms of hardware area, when compared to correction circuits. Relying on one mechanism to prevent electrode or tissue damage in a medical device designed for chronic use is a precarious approach. In the event that the switch fails, there will be an accumulation of charge over time. Charge balancing methods have been studied as a way of keeping the interface within safe limits of potential limits.

6.2 Charge Balancing Mechanisms

Charge balancing mechanisms can be broadly classified as passive and active mechanisms. Passive methods are typically open-loop methods, and active methods are closed loop feedback systems. Passive methods include the use of a large DC blocking capacitor and/or shorting the electrode after every stimulus pulse. Active methods are currently being explored as a more intelligent method for controlling the stimulation environment.

6.2.1 Passive Methods

A simple and safe idea to ensure that no DC current enters the tissue is to include a large blocking capacitor in series with the electrode (Figure 6.1a). The capacitance of the blocking capacitor must be much greater than that of the electrode-tissue interface, to ensure that the voltage drop across the blocking capacitor is small. There are several disadvantages to this technique. The inclusion of the capacitance increases the voltage compliance requirement of the current stimulator. Secondly, for applications that require large arrays of electrodes such as retinal stimulation, one capacitor is required per stimulator. Capacitors occupy a large portion of the area on integrated circuit stimulators and hence, DC blocking capacitors are impractical. The DC blocking capacitor also requires frequent discharging for optimal functionality of the mechanism. Moreover, the DC blocking capacitor only protects against circuit mismatch, and not against leakage across the charge-transfer resistance.

The frequency of neural stimulation pulses is approximately 100 Hz. The achievable frequency of operation of contemporary integrated circuits is at least 5 orders of magnitude higher than this frequency of stimulation. Therefore, a simple mechanism of shorting the electrode to ground after the stimulation pulse is widely used for charge balancing (Figure 6.1b). However, the shorting switch introduces glitches into the system. The discharge time for the shorting switch depends on the time constant determined by the solution resistance (R_s) and the double layer capacitance, C_{dl} [22]. If the electrode is not given sufficient time to discharge between stimulation pulses, then the purpose of shorting the electrode will be

defeated.

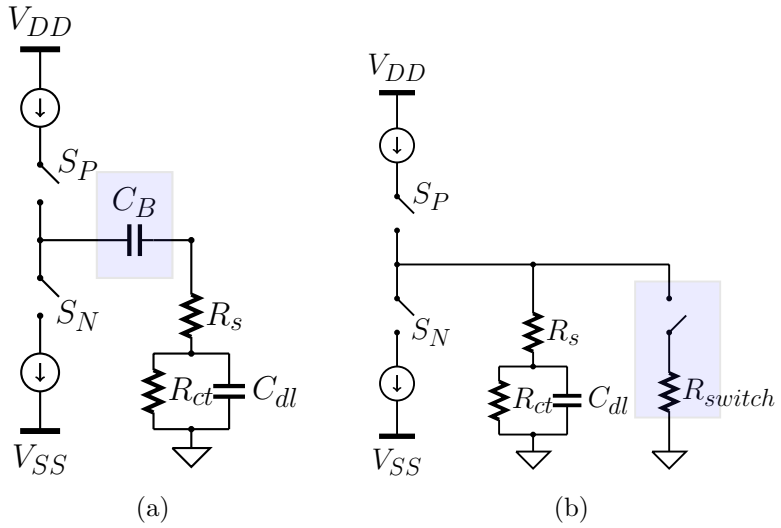

Figure 6.1: Passive charge balancing mechanisms: (a) DC blocking capacitor (b) Electrode shorting: DC blocking capacitors protect the electrode from mismatch errors of the stimulator. The shorting switch shorts the electrode after each stimulation pulse.

6.2.2 Active Methods

Active charge balancing mechanisms monitor the output voltage on the electrode at the end of one stimulation pulse and incorporate a correction mechanism during subsequent pulses. The extent of correction varies across different mechanisms. While electrode shorting has been the long established norm, active mechanisms have recently been introduced into the field due to the improved performance of integrated circuits.

The pulse insertion mechanism (Figure 6.2a) monitors the residual voltage at the end of the charge balanced pulse and inserts pulses of charge until the residual voltage is regulated to lie within pre-defined safe limits [25]. While this is a feasible idea, it involves the introduction of additional current pulses, which in turn could potentially excite neural tissue.

In the pulse insertion method, the correction for the residual voltage is implemented on every stimulation cycle. An approach presented in [44] is to ensure that the residual voltage over several stimulation pulses is within the safety limit. The long term offset regulation

method (Figure 6.2b) uses an offset current source to augment the biphasic stimulator. The advantage of using long term offset regulation is that the control mechanism does not introduce rapid changes in the stimulation system. However, by using an additional current source in parallel with the main biphasic stimulator, the output impedance of the current source will effectively decrease. Moreover, the offset current source will have to remain powered throughout the lifetime of the stimulator.

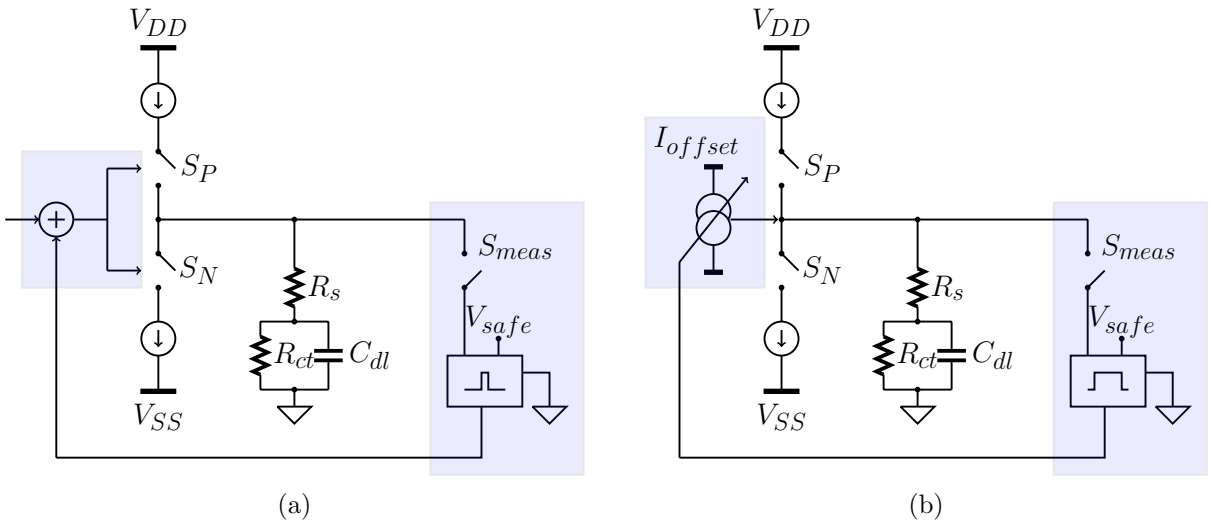

Figure 6.2: Active charge balancing mechanisms: (a) Pulse insertion method (b) Long term offset method: Pulse insertion uses repeated corrective pulses of current to correct the residual voltage. Long terms offset regulation uses an alternative current source to adjust the residual voltage over several stimulation pulses.

6.3 Active Anodic Feedback for Biphasic Stimulation

The *de facto* standard for stimulation is to deliver balanced biphasic current pulses. The matching accuracy required between the phases for safe levels of DC current (< 100nA) must be within 3% [31]. Theoretically, perfectly matched biphasic signals will not result in a zero residual voltage at the end of the anodic pulse [27]. The primary purpose of the anodic pulse is to neutralize the charge injected by the cathodic pulse. There are studies performed *in vivo* to show that imbalanced stimulation is not necessarily harmful to tissue [45]. Moreover, as

suggested by Merrill et al. in [20], "The electrode potential must be kept within a potential window where irreversible Faradaic reactions do not occur at levels that are intolerable to the physiological system or the electrode". An active anodic feedback mechanism corrects the width of the anodic pulse based on the residual voltage present on the electrode (Figure 6.3).

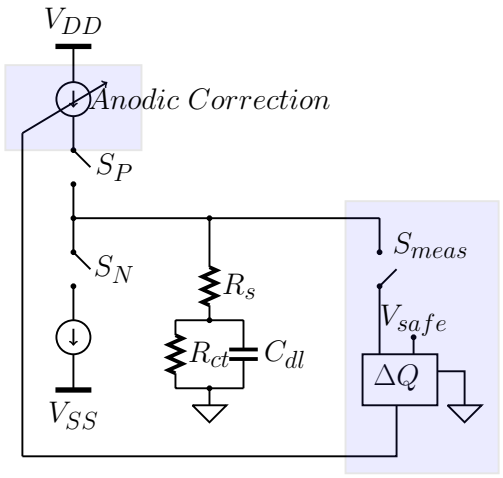

Figure 6.3: Active anodic feedback mechanism: the charge delivered by the anodic pulse width is adjusted such that the electrode-electrolyte (tissue) interface is electrochemically neutral.

The residual voltage is measured after every anodic pulse and the work presented in this paper uses digital **P**roportional **I**ntegral **D**erivative feedback control methods to adjust the anodic pulse width such that it maintains the electrode voltage near the desired set point. Active anodic feedback simulations algorithms have emerged in neural stimulation applications [28], [29]. Zheng et. al. [29] derive a simulation model for active anodic feedback , and use a system approach to outline a set of general guidelines for the feedback design, which are given below.

- Dynamic system performance shall be evaluated based on speed and accuracy
- An integrator is used in the feedback path to reduce the steady state offset of the system
- Settling time of the system is the time taken for the feedback system to attain 1%

error from the desired output set point.

The work presented in this thesis uses proportional, integral and derivative control to experimentally verify active anodic feedback based electrical stimulation in *in vitro* saline solution.

6.3.1 PID Control

To demonstrate the effect of active anodic feedback in electrical stimulation, this work implements the digital version of the traditional **P**roportional-**I**ntegral-**D**erivative control. Feedback control measures the output variable, and compares the output variable to a desired set point. The error signal, $e(t)$, is the difference between the output variable and the set point. The continuous form of the PID control equation for a general input, p, is,

$$p = \bar{p} - \left[k_p e(t) + k_i \int_0^t e(\tau) d\tau + k_d \frac{de(t)}{dt} \right], \tag{6.2}$$

where $\bar{p}$ is the bias value for the controller [46]. Sampling the residual voltage after every anodic pulse implies that the process of controlling the residual voltage over several pulses is not continuous. The digital version of the PID controller is obtained by replacing the integral and derivative expressions with their numerical equivalents. The sampling period, Δt, is the time between successive samples of the controlled variable. Therefore, Equation 6.2 becomes,

$$p[n] = \bar{p} - \left[k_p e[n] + k_i \Delta t \sum_{k=1}^{n} e[k] + \frac{k_d}{\Delta t} (e[n] - e[n-1]) \right], \tag{6.3}$$

The compensated feedback model is shown in Figure 6.4. The equation for residual voltage is linearized with respect to the anodic pulse-width, so that the parameter can be controlled. A discrete proportional-integral-differential controller is designed to correct the next anodic pulse width based on the previous value of the residual voltage. The derivation of the system

model is shown in Appendix G.

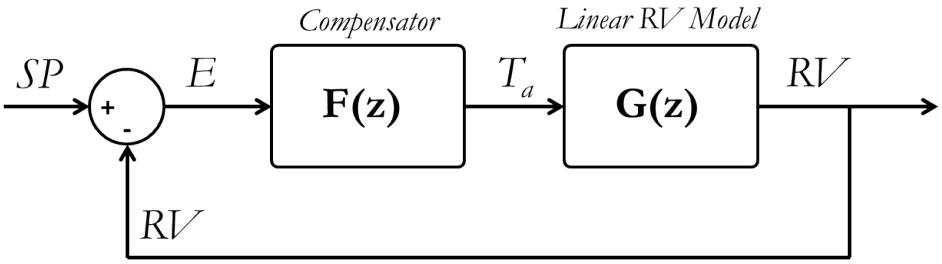

Figure 6.4: Active anodic feedback model: $G(z)$ is the linearized model of the residual voltage of one pulse, and $F(z)$ is the controller designed to correct the next anodic pulse. SP is the desired set point for the residual voltage, RV is the residual voltage signal and T_a is the anodic pulse width.

The discrete version is easier to use because the parameters of the controller are programmatically tunable. We use the discrete form of the PID control equation (Equation 6.3) to explore the effect of feedback on the residual voltage.

6.4 Experimental Methods

The experiments on anodic feedback control were performed *in vitro* 1X phosphate buffered solution (PBS) using a sputtered iridium oxide film (SIROF) electrodes. A detailed description of electrochemical measurement setups can be found in Chapter 4, Section 4.1. For the active anodic stimulation experiments, a two-electrode experimental setup was used, using a coiled platinum electrode with large surface area (Figure 6.5).

The **Bi**phasic **C**urrent stimulator with **A**ctive **F**eedback (BiCAF) system is a development board which contains a programmable, controllable high-impedance biphasic current source with provision to implement active feedback algorithms in neural stimulation systems. A relational block diagram is shown in Figure 6.6. The Arduino Micro, an open-source, cross-platform microcontroller board based on the ATmega32u4, controls the functionality of the system, and interfaces with the PC via a Serial USB protocol. The stimulation system parameters can be adjusted via a Python based graphic user interface (Figure 4.7). More details on the BiCAF system can be found in Chapter 4, Section 4.3.

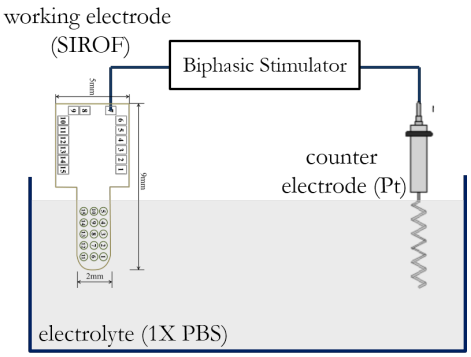

Figure 6.5: Two electrode measurement setup for stimulation: Active anodic feedback stimulation was done *in vitro* saline, using 1X PBS and the SIROF electrode array (Chapter 4, Figure 4.1) and a coiled platinum counter electrode.

The **S**puttered **Ir**idium **O**xide **F**ilm (SIROF) electrodes described in Chapter 2, Section 2.1.4 were used, which have a diameter of $400\mu m$. Our electrochemical setup comprised of a SIROF working electrode, and a coiled platinum (Pt) counter electrode, in 1X phosphate buffered solution. The water window potential limits of SIROF electrodes are -0.6V/+0.8V [18]. The stimulation parameters that were used for experimentation are shown in Table 6.1.

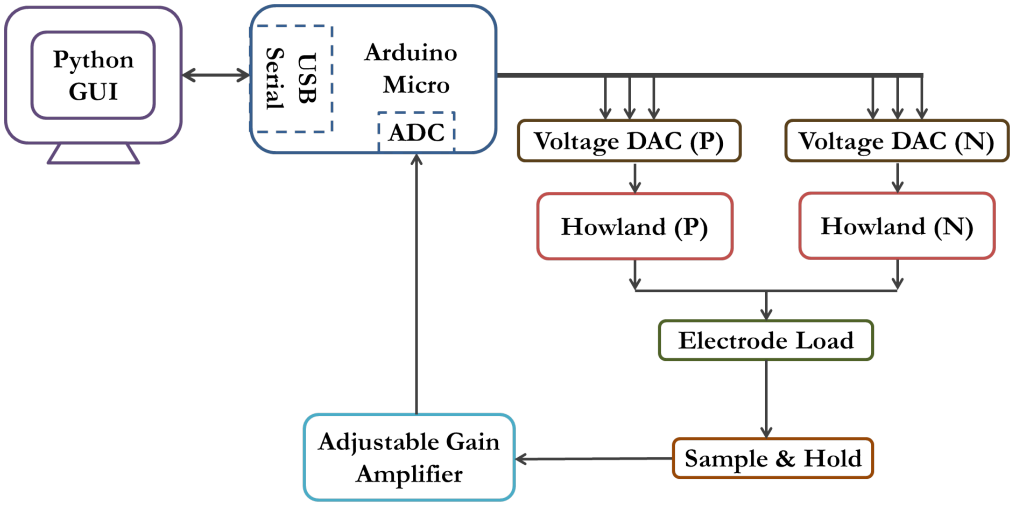

Figure 6.6: Schematic block diagram of the BiCAF board: A voltage DAC operated modified Howland current source. Residual voltage measurements were sent to eh in-built ADC of the Arduino Micro with the control algorithm, that adjusted the pulse width timing.

Table 6.1: Stimulation Parameter Values

Parameter	Symbol	Typical Value
Stimulation Frequency	$F_{stim} = 1/T_{stim}$	100 Hz
Cathodic Pulse Width	T_c	1000 μs
Anodic Pulse Width	T_a	1000 μs
Interphase Delay	T_i	100 μs
Cathodic Current Amplitude	I_c	100 μA
Anodic Current Amplitude	I_a	100 μA

6.4.1 PID Control Implementation

The output variable for active anodic feedback is the residual voltage measured after the anodic pulse. While theoretically the input variable is the charge delivered by the anodic pulse, this work uses the anodic pulse width, T_a, as the input variable. To avoid excessive memory use during each stimulation pulse, the numerical integration was performed to first-order, using the trapezoidal approximation. Assuming the residual voltage is measured once every stimulation pulse, the time between two samples of the controlled variables is the stimulation period, T_{stim}. The equations used to calculate the new anodic pulse width is,

$$\begin{aligned} e[n] &= RV[n] - SP \\ e_i[n] &= \frac{e[n] + e[n-1]}{2} \times T_{stim} \\ e_d[n] &= \frac{(e[n] - e[n-1])}{T_{stim}} \\ T_a[n] &= T_a[n-1] - (k_p e[n] + k_i e_i[n] + k_d e_d[n])\,. \end{aligned} \tag{6.4}$$

The description of the symbols of Equation 6.4 is provided in Table 6.2. The units for the controller parameters will change based on the controlled variable, which in this case is the anodic pulse width. The anodic current magnitude can also be controlled, it will not change the application of Equation 6.4. In digital control systems, it is often easier to make small changes in timing.

Table 6.2: PID Equation Variable Units

Parameter	Description	Units
RV[n]	Measured Residual Voltage	V
k_p	Proportional Constant	s/V
k_i	Integral Constant	s^2/V
k_d	Derivative Constant	1/V
SP	Set Point	V

The feedback uses a set point value of $SP = 0V$, and measured the residual voltage 1 ms after the anodic pulse. The tuning of the PID controller was done to minimize the steady-state offset voltage, reduce ringing and reduce the settling time. To demonstrate the effect of feedback, the residual voltage was initally allowed to increase for 200 pulses, with an initial anodic pulse width of 1000 μs. After 200 pulses, we introduced the feedback mechanism. In reality, the feedback mechanism would be activated before any voltage growth can occur, but allowing the residual voltage to rise allows us to examine the effect of the tuning parameters on the output voltage.

6.5 Experimental Results

The results obtained through the experiments in this work are intended to study two facets of residual voltage. Firstly, the extent to which residual voltage accumulates, in the absence of any charge balancing mechanism. Secondly, the effectiveness of active anodic feedback in controlling any residual voltage growth.

6.5.1 Residual Voltage Growth

One of the major questions that arise from [27] with regard to the first order $R_s - C_{dl} - R_{ct}$ electrode model (Chapter 2, Figure 2.2b), is its practical validity in describing complex biological systems. The validity of the electrode-electrolyte model was explored by observing the build-up of residual voltage at the end of the anodic pulse, without shorting out the elec-

trode. A first-order model should ideally reach a saturated voltage level after several pulses of stimulation, because the simplified model (Figure 2.2b) only consists of one capacitor. The residual voltage will saturate regardless of its origin.

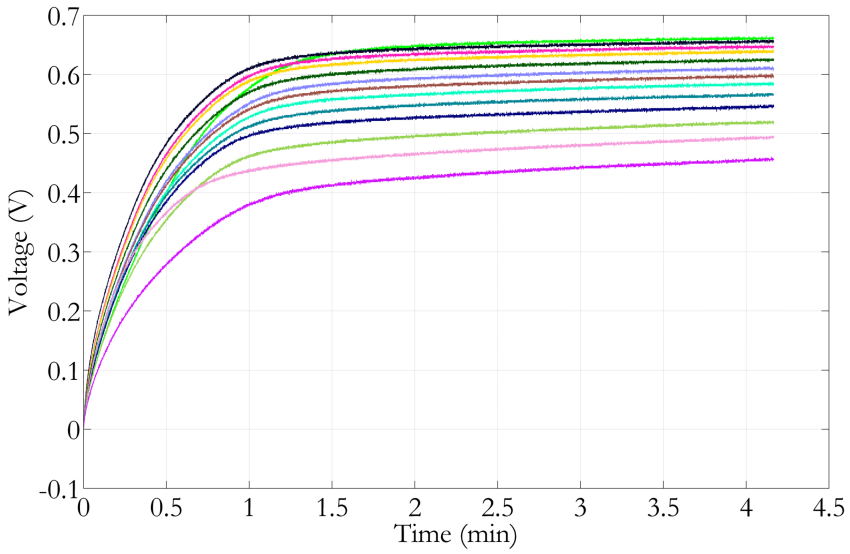

Figure 6.7: Residual voltage growth in SIROF electrodes in 1X PBS, measured for 13 electrodes. The measured residual voltage includes the intrinsic residual voltage as well as any biphasic mismatch error exhibited by the stimulator.

Observe in Figure 6.7 that the residual voltage can reach within 0.1V of the upper water window limit of the SIROF electrode (+0.8V [35]) in about 90 seconds. Relative to the life-span of an implantable device (years), this is rise time is fast. The contribution to the rise in residual voltage is due to the combination of biphasic mismatch, as well as leakage through the charge-transfer resistance, defined as the intrinsic residual voltage (Chpater 3, Section 3.2.2). A comparison of residual voltage growth curves is shown against a simulation of residual voltage growth using an ideal biphasic stimulator is shown in Figure 6.8.

6.5.2 Active Anodic Feedback

Active control of the anodic pulsewidth was implemented using PID control for SIROF electrodes in 1X PBS solution. For the purpose of demonstration, the residual voltage was allowed to grow for 200 stimulus pulses, after which feedback was turned on for 1000

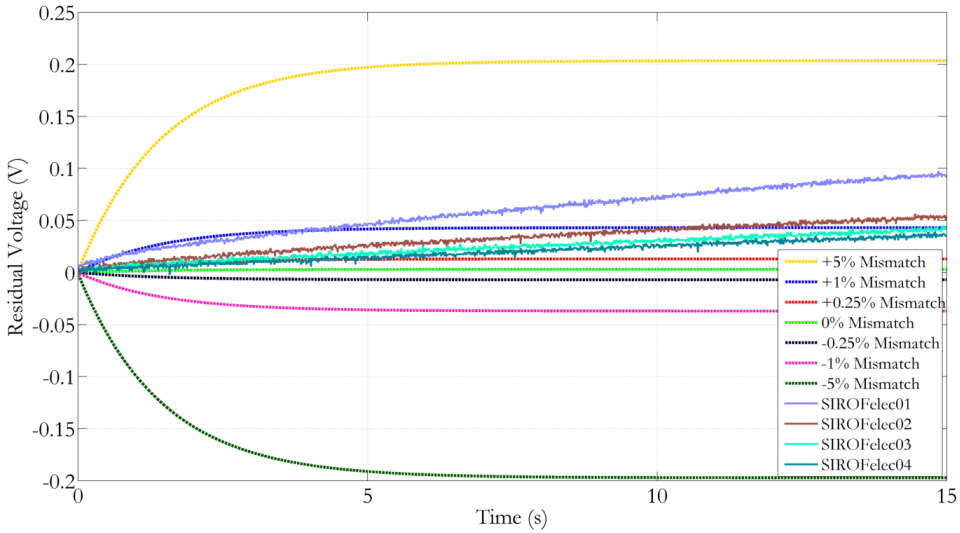

Figure 6.8: Biphasic mismatch contribution in Residual Voltage: The residual voltage growth for 4 SIROF electrodes, measured for 15 seconds, is superimposed on a simulation of the growth model for comparison.

stimulation pulses (10s). The parameters were tuned to explore the values that could achieve a stable output within 1000 pulses. The output is the residual voltage sampled by the BiCAF system.

The responses of the resulting output voltage align with typical PID tuning protocol. Increasing the proportional gain, k_p, results in a slower response, whereas decreasing k_p can increase the degree of oscillation (Figure 6.9). Integral control reduces the offset of the output response, and is usually used in conjunction with proportional control. Larger values of k_i result in more oscillations, but smaller values result is a very sluggish response (Figure 6.10). Oscillatory responses are reduced by intermediate values of k_d, this form of control is also used in tandem with proportional control. Both PI and PD control can result in unstable responses, shown in Figures 6.10, 6.11. The PID controller in this work was tuned manually to have minimal ringing and offset voltage (Figure 6.12).

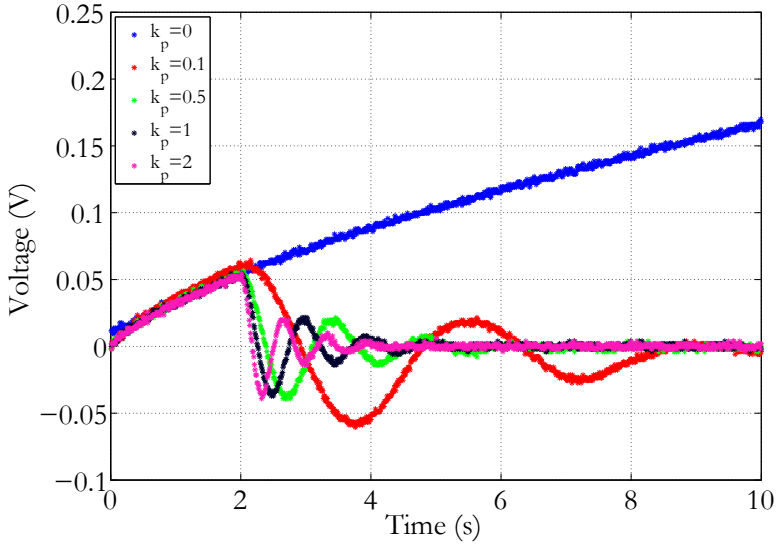

Figure 6.9: Proportional (P) control of anodic pulse width: The RV was allowed to rise for 2 seconds to demonstrate the effect of proportional control. Increasing k_p increases the ringing, but reduces the settling time and overshoot.

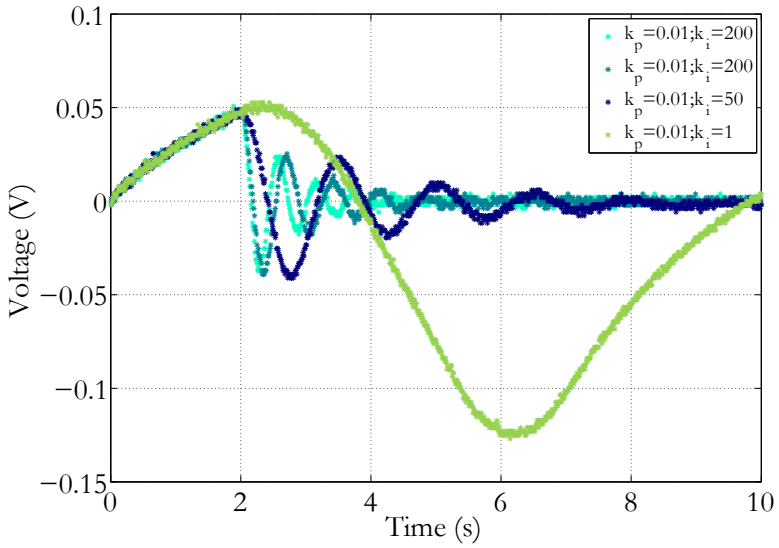

Figure 6.10: Proportional-Integral (PI) control of anodic pulse width: The RV was allowed to rise for 2 seconds to demonstrate the effect of PI control. PI control reduces the steady state offset error, but increases the settling time.

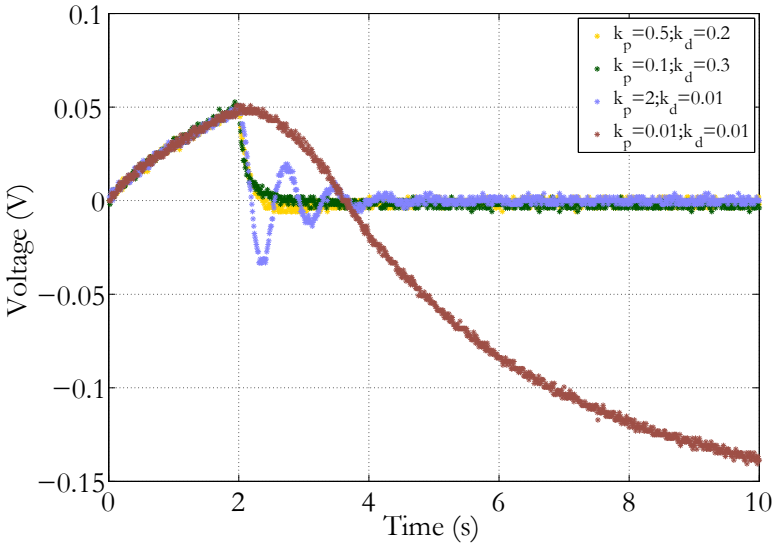

Figure 6.11: Proportional-Derivative (PD) control of anodic pulse width: The RV was allowed to rise for 2 seconds to demonstrate the effect of PD control. Introduction of the derivative control eliminates the ringing in the controlled output.

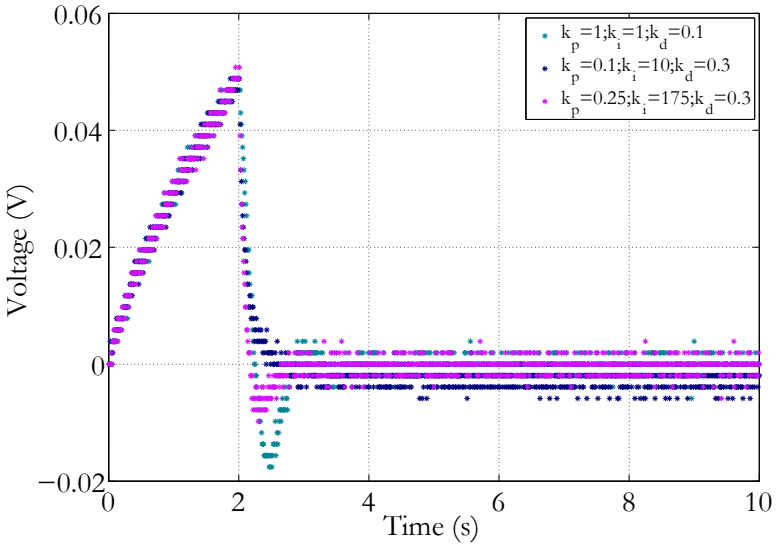

Figure 6.12: Proportional-Integral-Derivative tuning of anodic pulse width: The RV was allowed to rise for 2 seconds to demonstrate the effect of PID control.

6.6 Discussion

Electrical stimulation is typically performed with biphasic current pulses. The biphasic format allows the device designer to manipulate the signal as necessary to ensure that the tissue and electrode are within safe operating limits. The work presented in this thesis shows the practical implementation of active anodic feedback, along with an underlying basis for the method. Active anodic feedback control is built upon the hypothesis that residual voltage will exist regardless of the matching between the biphasic pulses. The method involves correcting the charge in the anodic phase in response to the measured residual voltage. While both current amplitude and timing control can be implemented in the BiCAF system, timing control was used because it is faster than amplitude control. Amplitude control of anodic pulse is suggested only when unusually large changes are required for charge balancing. The choice of timing and/or amplitude control depends on the relative resolution of each quantity available to the designer. The goal of active anodic feedback is to maintain an electrochemically neutral interface, by slightly imbalancing the biphasic stimulus pulse. A comparison of the active anodic feedback responses for different forms of control are shown in Figure 6.13.

The design of an active anodic feedback stimulation system should emphasize on the following guidelines:

Minimization of offset error: To avoid any slow electrochemical reaction at low DC offsets, the offset error should be minimized.

Minimal ringing: There should not be any large deviations during the system response for residual voltage corrections. However, if the feedback system is always turned on, the likelihood of very high overshoot is small.

Settling Time: As mentioned in [29], settling time is the time taken for the system to reach 1% of the desired steady state value, which in most cases is 0V. The feedback system must aim to reduce the number of stimulus pulses in which is settling occurs.

Gradual Correction: The controller should be tuned such that anodic pulse width is varied

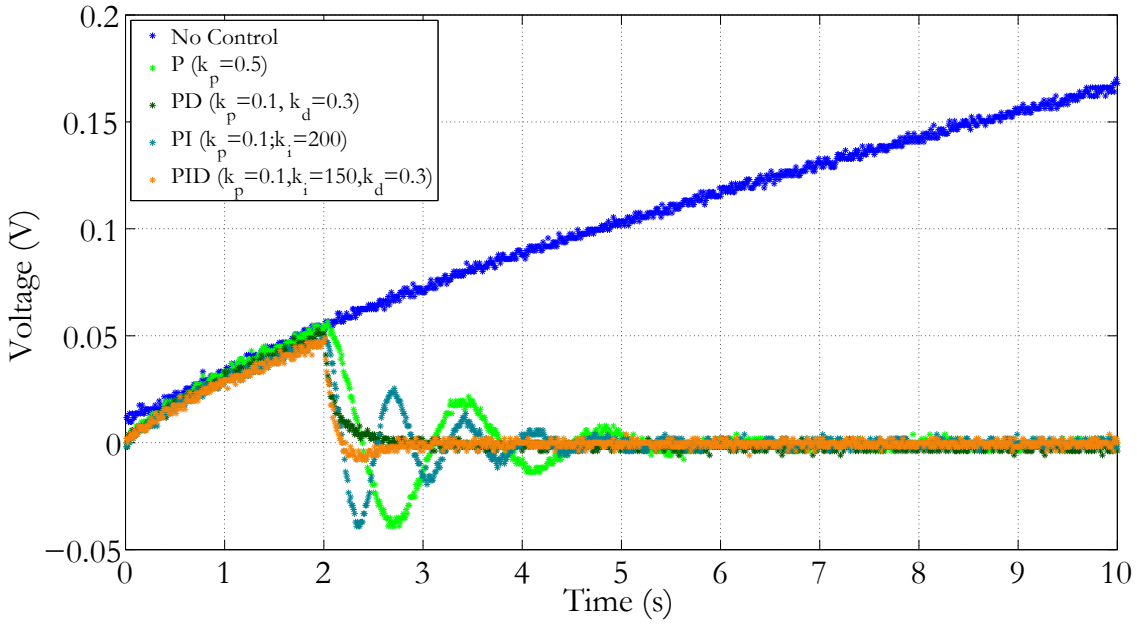

Figure 6.13: Comparison of control methods for active anodic feedback: The RV was allowed to grow for 2s to demonstrate the feedback methods. In reality, the control algorithm will be on from the first pulse, for one stimulator. Only the anodic pulse width timing was corrected, because it allows for higher resolution adjustments.

gradually in order to reach a steady state of 0V, so that unwanted physiological responses do not occur.

The main contributions of the thesis so far has been the definition of residual voltage, its usefulness as a status indicator and correction of residual voltage growth using active anodic feedback. One of the questions that arises from the experiments in saline is whether or not residual voltage growth can be a physiological problem. The preliminary *in vivo* study in rats suggests that it can definitely be a concern, the results from preliminary *in-vivo* experiments are described in Chapter 7.

Chapter 7

In Vivo Experiments

Evidence of Unsafe RV Growth

Experiments performed in physiological phosphate buffered saline allow us to mimic passive chemical environments and the dielectric properties of biological interfaces. To develop effective dynamic neural stimulators, it is imperative to observe the active nature of the electrode-tissue interface. An exploratory study *in vivo* was conducted in collaboration with Zhanhong Du from the the Neural Tissue Engineering (NTE) Lab, directed by Dr. Xinyan Cui, at the University of Pittsburgh, PA. The purpose of the experiment was to examine the effects of residual voltage *in vivo*. We observed the growth of residual voltage, and characterized the electrode-tissue interface *in vivo*. The methods and results of the experiment are described in this chapter, along with a discussion on the significance of the observations made from these preliminary experiments.

7.1 Research Questions

The work presented in this thesis thus far has defined residual voltage in biphasic electrical stimulation (Chapter 3) and presented its use as a status indicator (Chapter 5). Based on the origin of residual voltage, a method of controlling residual voltage using active anodic

feedback was presented in Chapter 6. However, there has been no evidence in prior work showing how high the residual voltage growth can be *in vivo* tissue. Another contribution of this work is to present the results of a preliminary experiment on residual voltage growth in the brain tissue of a live anesthetized rat. The residual voltage growth model is derived in Equation 3.12) and a simulated response is shown in Figure 3.6a. Experimentally, the measured residual voltage growth in 1X PBS (Figure 6.7) saturates at a value of about 200mV in saline. To obtain a realistic idea in physiological tissue, the following research questions were outlined for the *in vivo* experiments:

- How high is the residual voltage in neural tissue?
- What is the effect of prolonged exposure to uncontrolled residual voltage in neural tissue?

7.2 Experimental Methods

All the experimental and surgical procedures were approved by the Institutional Animal Care and Use Committee (IACUC) at the University of Pittsburgh, and were in compliance with the US Public Health Service policy on the human care and use of laboratory animals.

We used one Sprague-Dawley rat, which was anesthetized for the duration of the experiment. A part of the bone from the skull was removed (craniotomy) to expose the outermost membrane covering the brain — called the *dura-mater*. The SIROF electrode array (Figure 4.1) was mounted in two locations, epidural and subdural (Figure 7.1a). Epidural placement is above the dura, while sub-dural is under the dura. The electrode was placed near the visual cortex. A platinum counter electrode was placed near the working electrode. To prevent the tissue from drying, the environment is flushed with saline solution. A photograph of the experimental setup is shown in Figure 7.1b. The stimulation parameters used for these experiments are the same as those specified in Table 6.1.

The electrode-tissue interface characteristics were measured using cyclic voltammetry

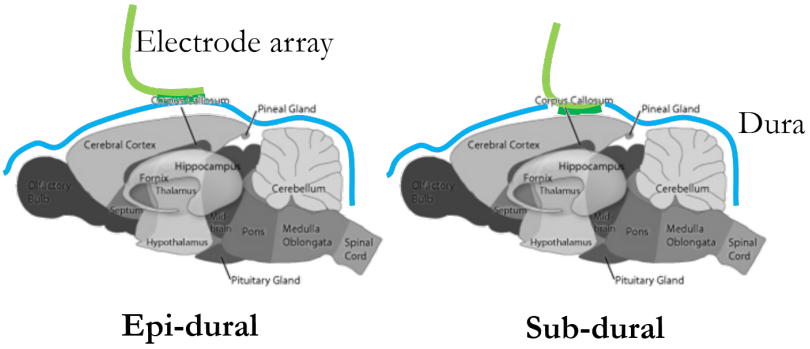

(a)

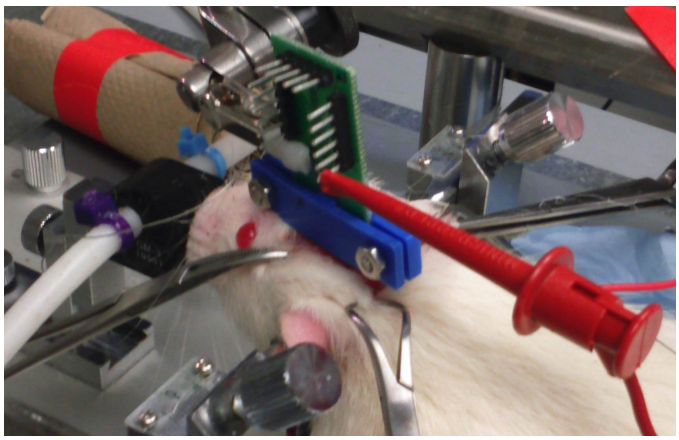

(b)

Figure 7.1: (a) Schematic of Epidural and Subdural SIROF electrode mounting in SD rat (b) Photograph of the electrode array mounted on a Sprague-Dawley rat. The location was chosen based on ease of surgical accessibility of the neural tissue.

(CV) and electrode impedance spectroscopy (EIS) using the Metrohm Autolab equipment before and after prolonged exposure to residual voltage at the epidural and subdural electrode locations. The Metrohm Autolab was used for the CV and EIS measurements. Residual voltage growth was observed in saline solution for approximately 60 minutes, in the epi-dural location for 35 minutes and in the sub-dural location for 15 minutes.

7.3 Results

The biphasic response curves for epidural and subdural locations are shown in Figure 7.2. The responses are varied because the electrodes may be in contact with either saline solution, or dura-matter or, in the case of the subdural location, brain tissue. Given the short lead of the electrode array (Figure 4.1), it can be challenging to determine which of the electrodes are making contact with brain tissue (sub-dural) versus dura-matter (epi-dural). Moreover, the tissue is constantly flushed with saline solution to ensure that it is healthy during the experiment. The electrode voltage of the SIROF electrode response in saline is between ± 0.1V (Figure 5.2). Based on these observations, it is evident that electrodes #4,#6 and #9 are responses in saline. Biphasic responses placed on top of the dura mater exhibit a response similar to saline, possibly because there is no neural tissue on the dura mater, and the environment is flushed with saline at regular intervals. Sub-dural placement of the electrodes exhibit a increased solution resistance.

The residual voltage growth curves for the epi-dural, sub-dural and saline cases are shown in Figure 7.3. A significant result from this work is the evidence that the residual voltage can grow beyond the water window limits (for SIROF electrodes). The residual voltage growth model derived in Section 3.2.3 appears to be valid in the case of *in-vivo* tissue.

The electrode-tissue interface was characterized using CV and EIS before and after exposure to the residual voltage growth, for both the epi-dural (35 minutes) and the sub-dural locations (15 minutes), shown in Figures 7.4,7.5b and 7.5a.

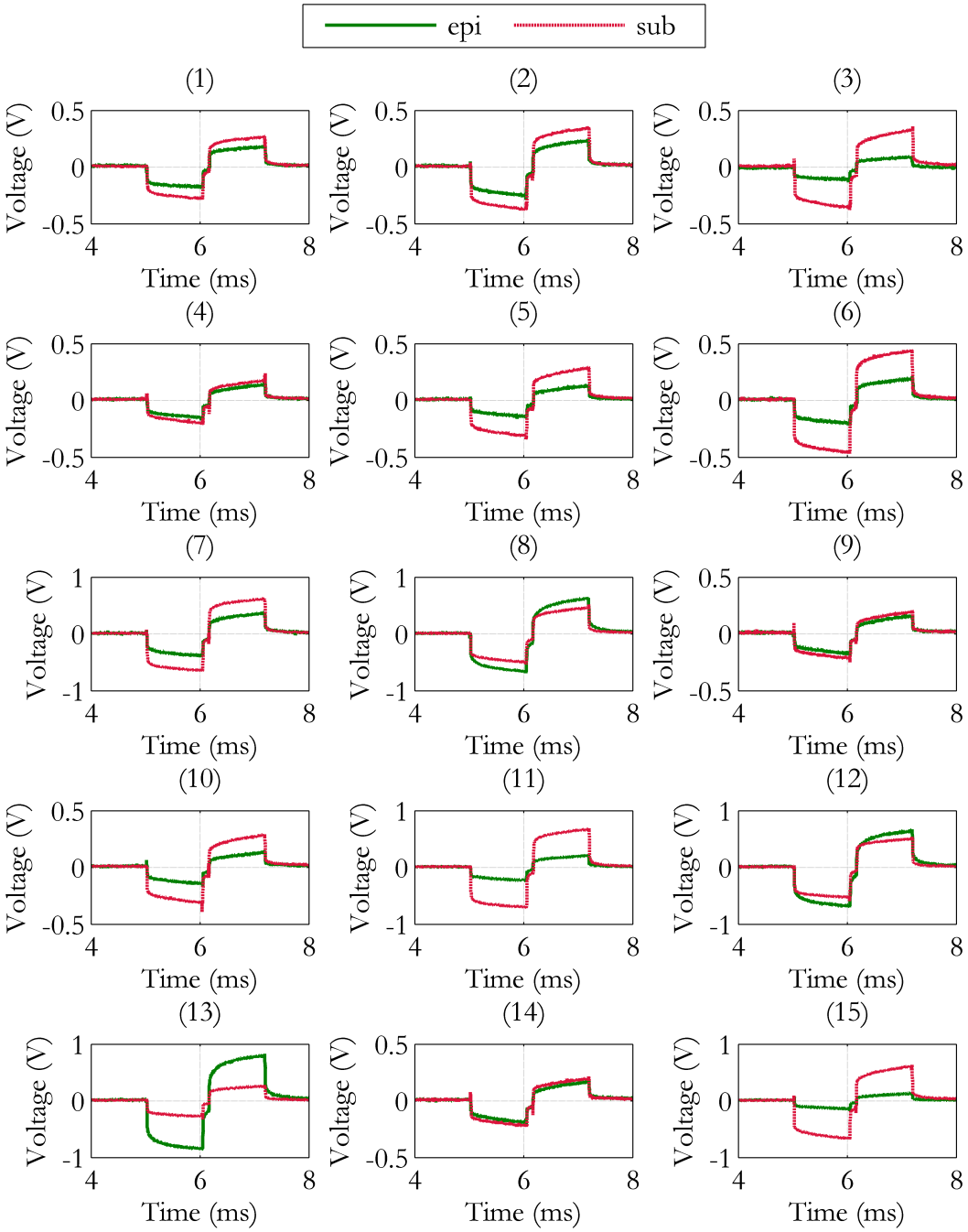

Figure 7.2: Electrode transient voltage response to biphasic stimulus for epidural and subdural locations on the visual cortex of SD rat. The sub-dural locations exhibit a high solution resistance.

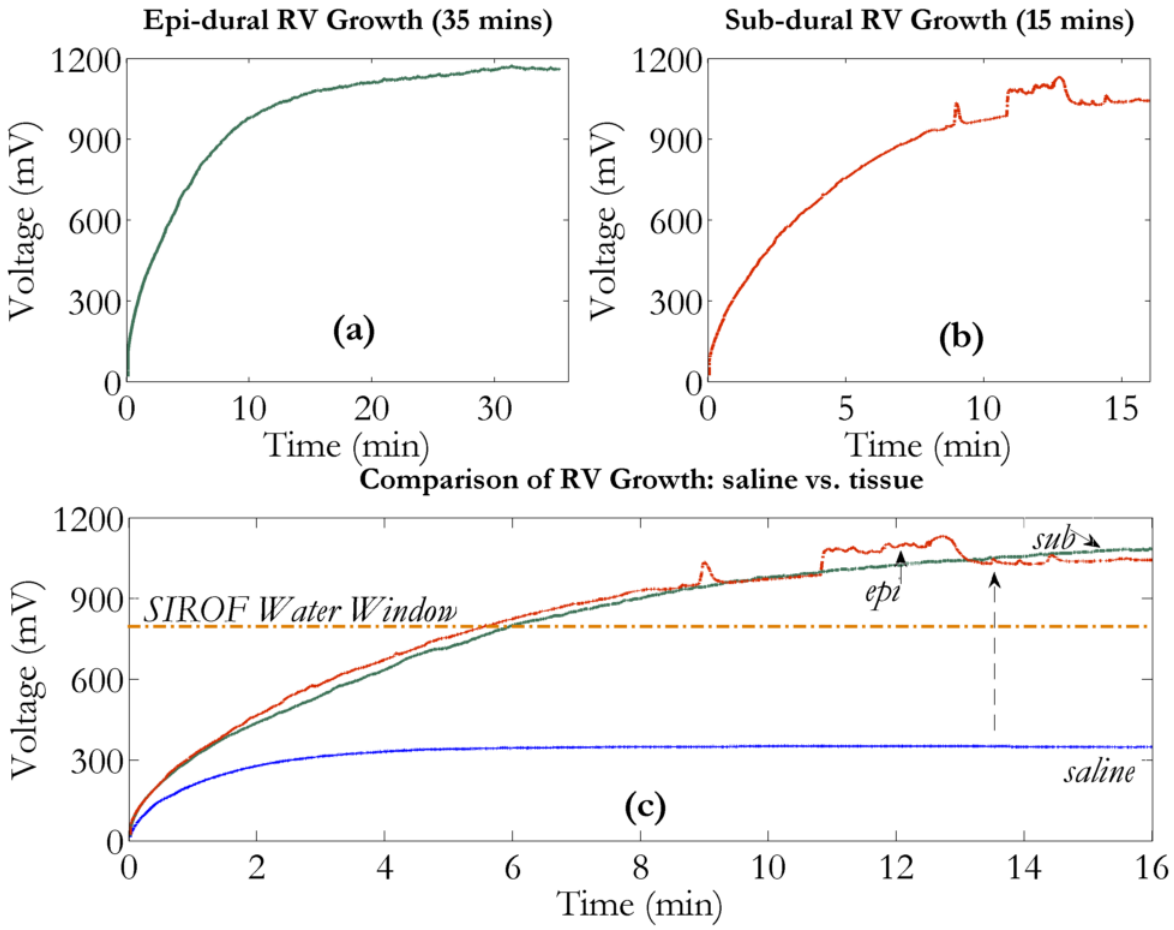

Figure 7.3: RV growth curves *in vivo*: (a) Residual voltage growth in the epi-dural location, recorded for 35 minutes (b) Residual voltage growth in the sub-dural location, recorded for 15 minutes (c) Comparison of *in-vivo* tissue RV growth with *in vitro* saline RV growth. The residual voltage growth crosses the water window limits *in vivo* tissue, resulting in a potentially unsafe environment for chronic stimulation.

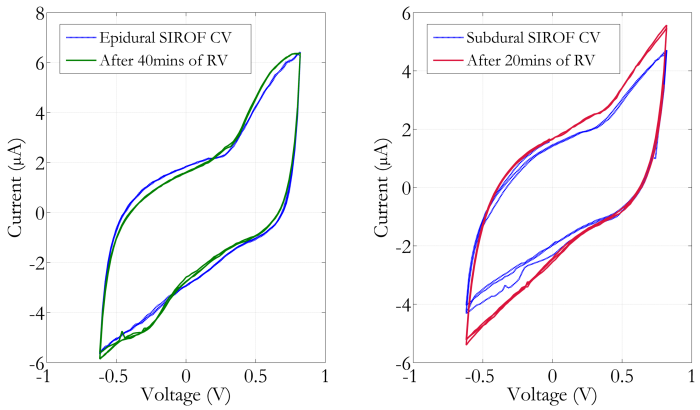

Figure 7.4: CV curves after prolonged exposure to RV *in vivo*, shows a slight increase in the charge storage capacity, but not as significant.

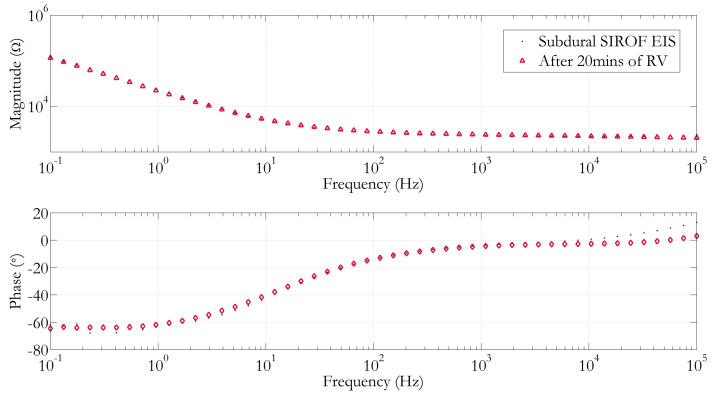

(a)

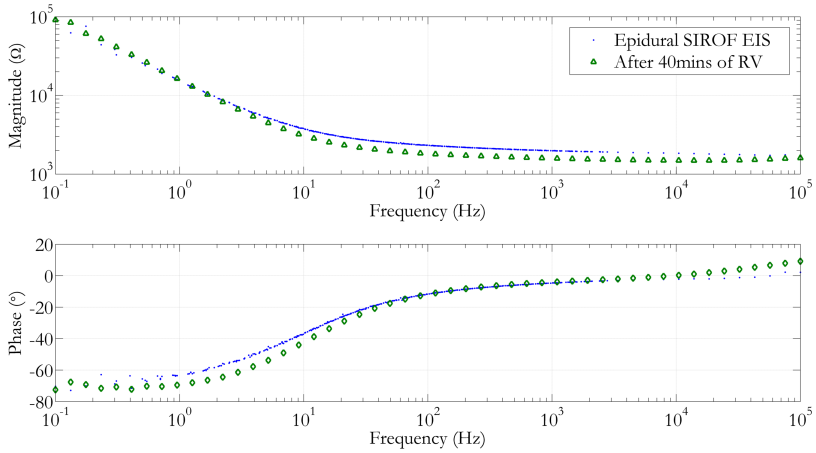

(b)

Figure 7.5: (a) Subdural EIS after 20 mins of prolonged RV exposure (b) Epidural EIS after 40 mins of prolonged RV exposure

7.4 Discussion

The *in vivo* experiments performed as part of this work give a very practical idea of the nature of residual voltage and whether we need to be concerned about its existence and growth in real animal tissue. The RV growth curves between cases *in vivo* and *in vitro* along with a model fit done using the Curve Fitting Tool in MATLAB is shown in Figure 7.6.

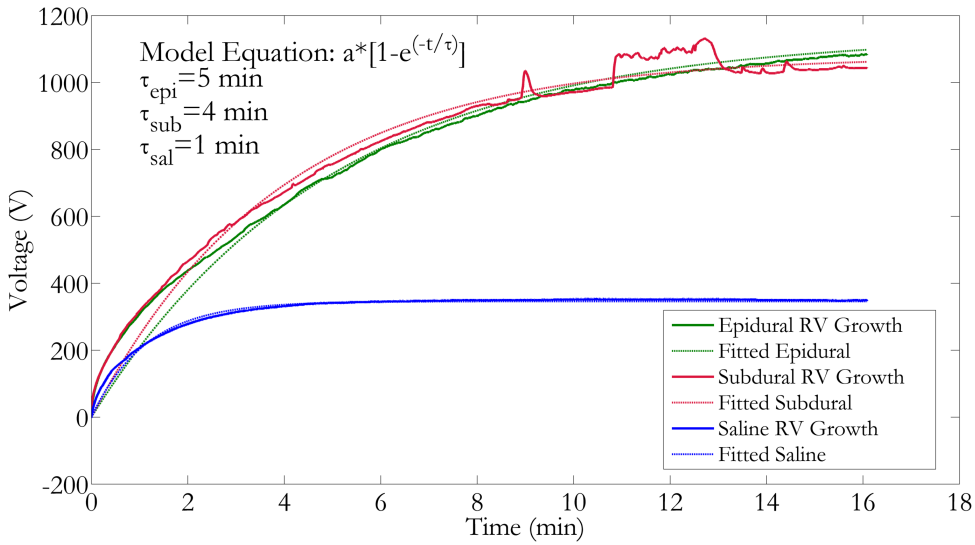

Figure 7.6: RV Growth *in vivo* model fit: The model fit using the exponential model equation shows that the relaxation time constant ($\tau = C_{dl} \times R_{ct}$) of the curves *in vivo* are larger than the case in saline. Because the final voltage is higher, it indicates a smaller capacitance and a larger charge-transfer resistance. A method of measurement of the relaxation time constant *in vitro* is suggested in Appendix I.1.

The time constant shown in the plot refers to the relaxation time constant, and the RV growth equation used for the model fit is based on Equation 3.12 (Chapter 3). There are three main observations from the plot: (1) the relaxation time constant is higher for the *in-vivo* cases and (2) the final value of the voltage is higher in the *in vivo* cases and (3) the final value is higher than the water window limits for the SIROF electrode. The increase in time constant is explained by an increase in either the double-layer capacitance (C_{dl}) or the charge-transfer resistance (R_{ct}), or both. However, the increase in the final steady state voltage indicates a reduction in the double-layer capacitance, which implies the charge-transfer resistance increases such that the relaxation time constant increases. Moreover, evidence that residual

voltage growth can grow beyond the water window limits emphasizes that charge-balancing methods are necessary for safe electrical stimulation. Prolonged exposure of residual voltage in the epidural location shows a slight change in the cyclic voltammetry plot (Figure 7.4). However, the time frame to facilitate this change is very short (40 minutes), when compared to the average life of a chronic implant device (years). A lot of physiological effects in biological systems only occur on chronic exposure, which can be more than 7 hours. While the CV shows a slight change in the characteristics, the response is not significant enough to conclusively narrow down the nature of the change, but it provides a direction for future research, a discussion of which is presented in Chapter 8.

Chapter 8

Conclusion & Future Work

Functional electrical stimulation applications such as a 1000+ electrode retinal implant are not very far into the future, and electrode monitoring can become an issue. Therefore, it is advantageous to know the status of each electrode easily, and as early as possible, before potential damage can occur. Residual voltage contains first-order information about the status of the electrode/electrolyte (tissue) interface. Measuring residual voltage presents fewer design and power constraints on integrated circuit measurement circuits, allowing for low-power circuit design as well as increased compatibility with scaling of microelectrode array. Moreover, we show through preliminary *in vivo* experiments in anesthetized rats that the residual voltage can build up to dangerous levels. An important consequence of this build-up is that if the widely-used shorting mechanism fails during operation, the electrode can get corroded, thereby becoming a potentially harmful interface with the nearby tissue. Charge balancing methods are being developed to counteract any residual voltage that appears across the electrode-tissue interface. Active anodic feedback allows us to monitor the neural interface, and compensate for any charge error that might arise during biphasic stimulation. The underlying principles of anodic correction pursued in this work are one, residual voltage exists regardless of biphasic matching, and two, the purpose of the anodic pulse is to neutralize the interface. The result of active anodic feedback is a corrected anodic pulse width that provides us with a value that can serve as meta-data about the dynamic

nature of the electrode-electrolyte (tissue) interface. Based on the work in this thesis, it is suggested that timing control of the anodic pulse width be used for small changes in RV, and current control be used for large swings. However, using both may make the design unnecessarily complicated, and harder to scale. The architecture presented in this work is not directly scalable, the next step in the design of neural stimulators is to find integrated circuit solutions that can multiplex safety features between several electrodes. The goal of high-density neural stimulation circuit design is to develop a system such as the one shown in Figure 8.1. The contributions made in this work provide insight into developing a system level implementation of monitoring and diagnosis for high density stimulation electrode arrays of safe neural stimulators.

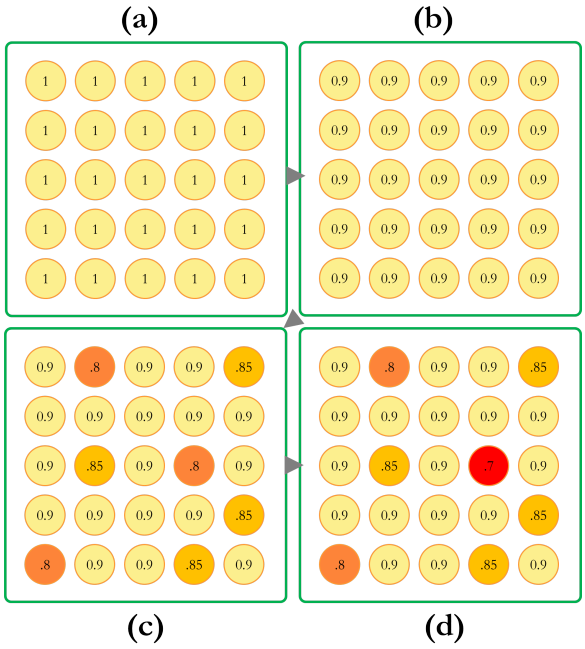

Figure 8.1: Goal of high density neural stimulation circuit design: Consider an electrode array shown in (a). Initially, the ratio of anodic charge to cathodic charge that is injected into the electrode site will be 1, indicating balanced biphasic waveforms. Due to residual voltage, the active anodic feedback mechanism operating at the electrode sites will cause the anodic to cathodic charge ratio to settle at a different value, shown in (b). Over time, as the electrode-tissue interface changes its characteristics, shown in (c), the value of the corrected anodic to cathodic charge ratio will also change. If any electrode sites show a large deviation from the initial value, it should be be possible to turn off stimulation to those sites, preventing further aggravation to the electrode-tissue site.

Chapter 9

Appendices

A Residual Voltage for an R-C-R Electrode Model

An electrode-tissue interface is modeled as shown in Figure A.1. The parameters of the model are R_s, the solution resistance; C_{dl}, the double layer capacitance. While most stimulation systems stop at using an R-C model to design stimulation systems, our approach is to evaluate the response of the circuit including the (usually very large) charge transfer resistance, R_{ct}. The electrode model is shown in Figure A.1.

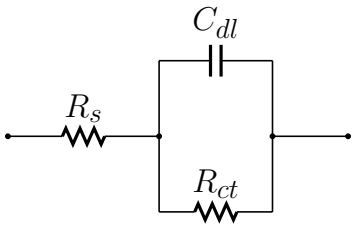

Figure A.1: Electrode Model

Consider a biphasic current input, $i(t)$, to have a waveform shown in Figure A.2.

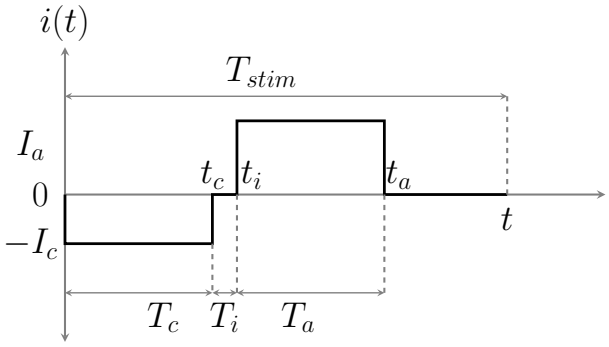

Figure A.2: Input Biphasic Current Signal

The equation to the input current signal is given by:

$$i(t) = -I_c[u(t) - u(t - t_c)] + I_a[u(t - t_i) - u(t - t_a)], \tag{1}$$

where I_c and I_a are the cathodic and anodic current amplitudes; t_c, t_i, t_a are the end of the **c**athodic pulse, **i**nterphase delay and **a**nodic pulse respectively.

For this analysis, the voltage drop across the solution resistance, R_s, does not affect the final result we require. Let the voltage across the double-layer capacitor and the charge-transfer resistance, R_{ct}, be $v_c(t)$. Using KCL at this node, we get:

$$i(t) = C_{dl}\frac{dv_c(t)}{dt} + \frac{v_c(t)}{R_{ct}} \tag{2}$$

This is a non-homogeneous first order differential equation. Here, it is pertinent to state that the initial condition of the double-layer capacitance is $v_c(0)$. This problem is easier to approach by solving for the circuit by temporally splitting the input into five regions.

Case 1: $-\infty < t \leq 0$

The initial voltage before the onset of the stimulus signal is:

$$v_c(t) = v_c(0) = 0 \tag{3}$$

Case 2: $0 < t \leq t_c$

This case shall be used to solve for a general solution of the first order differential equation. During this time interval,

$$i(t) = -I_c.$$

Initial Condition: $v_c(0) = 0$ (From Case 1)

The solution is divided into two parts, the *homogeneous* solution and the *particular* solution. The complete solution is given by,

$$v_c(t) = v_{c_h}(t) + v_{c_p}(t).$$

First, we solve for the homogeneous solution by equating the RHS of Eqn. 2 to 0.

$$
\begin{aligned}
C_{dl}\frac{dv_c(t)}{dt} + \frac{v_c(t)}{R_{ct}} &= 0 \\
C_{dl}\frac{dv_c(t)}{dt} &= -\frac{v_c(t)}{R_{ct}} \\
\frac{dv_c(t)}{dt} &= -\frac{v_c(t)}{R_{ct}C_{dl}} \\
\frac{dv_c(t)}{dt} &= -\frac{v_c(t)}{\tau} \\
\frac{dv_c(t)}{v_c(t)} &= -\frac{dt}{\tau} \\
\frac{dv_c(t)}{v_c(t)} &= -\frac{dt}{\tau}
\end{aligned} \tag{4}
$$

To get a generic solution, we integrate in the region $[t_1, t_2]$ for t.

$$
\begin{aligned}
\int \frac{dv_c}{v_c} &= \int_{t_1}^{t_2} -\frac{t}{\tau} dt \\
ln[\frac{v_c}{K}] &= -\frac{(t_2 - t_1)}{\tau} \\
v_c(t) &= Ke^{-(t_2-t_1)/\tau}
\end{aligned} \tag{5}
$$

The constant of integration is determined by using the initial condition.

We find the particular solution of Eqn. 2, because the current signal is a constant value in this interval. Because the stimulus is a constant, we can assume that $v_c(t)$ will not vary with time, that is, the solution to the ODE is also a constant. This means that we arrive at the *steady state* solution of the stimulus.

$$C_{dl}\frac{dv_c(t)}{dt} + \frac{v_c(t)}{R_{ct}} = -I_c \tag{6}$$

$$C_{dl}\cancelto{0}{\frac{dv_c(t)}{dt}} + \frac{v_c(t)}{R_{ct}} = -I_c$$

$$v_c(t) = -I_c R_{ct} \tag{7}$$

The final solution of the differential equation is:

$$v_c(t) = Ke^{-t/\tau} - I_c R_{ct} \tag{8}$$

Applying the assumed initial condition, we get the general solution to differential Eqn. 2 as:

$$v_c(0) = Ke^{-0/\tau} - I_c R_{ct} = 0$$

$$K = I_c R_{ct}$$

$$v_c(t) = I_c R_{ct}[e^{-t/\tau} - 1]$$

$$v_c(t) = (-I_c)R_{ct}[1 - e^{-t/\tau}] \tag{9}$$

Case 3: $t_c < t \leq t_i$

During this time interval,

$$i(t) = 0.$$

Initial Condition:

$$v_c(t_c+) = (-I_c)R_{ct}[1 - e^{-t_c/\tau}] \text{ (From Case 2)}$$

The final solution for this case is (only the homogenous solution, from Eqn. 5)

$$v_c(t) = v_c(t_c+)e^{-(t-t_c)/\tau} \tag{10}$$

Applying the initial condition:

$$\begin{aligned} v_c(t) &= (-I_c)R_{ct}[1 - e^{-t_c/\tau}].e^{-(t-t_c)/\tau} \\ v_c(t) &= (-I_c)R_{ct}[e^{-(t-t_c)/\tau} - e^{-t/\tau}] \end{aligned} \tag{11}$$

Case 4: $t_i < t \leq t_a$

During this time interval,

$$i(t) = +I_a.$$

Initial Condition:

$$v_c(t_i+) = (-I_c)R_{ct}[e^{-(t_i-t_c)/\tau} - e^{-t_i/\tau}] \text{ (From Case 3)}$$

The homogeneous solution for this case is (from Eqn. 5)

$$v_c(t) = Ke^{-(t-t_i)/\tau} \tag{12}$$

We find the particular solution of Eqn. 2, because the current signal is a constant value in this interval. Because the stimulus is a constant, we can assume that $v_c(t)$ will not vary with time, that is, the solution to the ODE is also a constant. This means that we arrive at the *steady state* solution of the stimulus.

$$C_{dl}\frac{dv_c(t)}{dt} + \frac{v_c(t)}{R_{ct}} = +I_a$$

$$C_{dl}\frac{dv_c(t)}{dt}^{\to 0} + \frac{v_c(t)}{R_{ct}} = +I_a$$

$$v_c(t) = I_a R_{ct} \tag{13}$$

The final solution for this case is:

$$v_c(t) = Ke^{-(t-t_i)/\tau} + I_a R_{ct} \tag{14}$$

Applying the initial condition:

$$v_c(t_i+) = Ke^{-(t-t_i)/\tau}{}^{\to 1} + I_a R_{ct} = (-I_c)R_{ct}[e^{-(t_i-t_c)/\tau} - e^{-t_i/\tau}]$$

$$K = -I_a R_{ct} - I_c R_{ct}[e^{-(t_i-t_c)/\tau} - e^{-t_i/\tau}]$$

$$\Rightarrow v_c(t) = [-I_a R_{ct} - I_c R_{ct}[e^{-(t_i-t_c)/\tau} - e^{-t_i/\tau}]][e^{-(t-t_i)/\tau}] + I_a R_{ct}$$

$$v_c(t) = I_a R_{ct}[1 - e^{-(t-t_i)/\tau}] - I_c R_{ct}[e^{-(t-t_c)/\tau} - e^{-t/\tau}] \tag{15}$$

Case 5: $t_a < t < \infty$

During this time interval,

$$i(t) = 0.$$

Initial Condition:

$$v_c(t_a+) = I_a R_{ct}[1 - e^{-(t_a-t_i)/\tau}] - I_c R_{ct}[e^{-(t_a-t_c)/\tau} - e^{-t_a/\tau}] \text{ (From Case 4)}$$

The homogeneous solution for this case is (from Eqn. 5)

$$v_c(t) = Ke^{-(t-t_a)/\tau} \tag{16}$$

Applying the initial condition:

$$\begin{aligned} v_c(t_a) &= K\cancelto{1}{e^{-(t_a-t_a)/\tau}} = I_a R_{ct}[1 - e^{-(t_a-t_i)/\tau}] - I_c R_{ct}[e^{-(t_a-t_c)/\tau} - e^{-t_a/\tau}] \\ \Rightarrow v_c(t) &= [I_a R_{ct}[1 - e^{-(t_a-t_i)/\tau}] - I_c R_{ct}[e^{-(t_a-t_c)/\tau} - e^{-t_a/\tau}]].e^{-(t-t_a)/\tau} \end{aligned} \tag{17}$$

The residual voltage for anytime, t, at the end of the biphasic current stimulus signal is,

$$v_c(t) = -I_c R_{ct}[e^{-(t-t_c)/\tau} - e^{-t/\tau}] + I_a R_{ct}[e^{-(t-t_a)/\tau} - e^{-(t-t_i)/\tau}] \tag{18}$$

The *intrinsic residual voltage* (if $Q_c = Q_a$) sampled at the end of the anodic pulse is given by,

$$RV_{t_a+} = -I_c R_{ct}[e^{-(t_a-t_c)/\tau} - e^{-t_a/\tau}] + I_a R_{ct}[1 - e^{-(t_a-t_i)/\tau}] \tag{19}$$

The intrinsic residual voltage (if $Q_c = Q_a$) in terms of stimulation pulse widths is,

$$RV|_{T_a} = -I_c R_{ct}[e^{-(T_i+T_a)/\tau} - e^{-(T_c+T_i+T_a)/\tau}] + I_a R_{ct}[1 - e^{-(T_a)/\tau}]. \tag{20}$$

B Residual Voltage Growth

The equation of residual voltage that arises from the first biphasic pulse is based on the assumption that the initial voltage on the double-layer capacitance is zero (Appendix A). While this assumption is true for the first pulse, every subsequent stimulation pulse will result in a non-zero initial condition on the double-layer capacitance. Using Equation 20, we continue the discussion on residual voltage growth with the same assumptions, and the same steps are used for residual voltage including the effects of mismatch. Accounting for

the exponential decay of the residual voltage in the time after the anodic pulse (see Case 5 in Appendix A), the intrinsic residual voltage at the *beginning* of the *second* biphasic pulse will be,

$$RV_{i0} = RV|_{t_a}.\mathbf{exp}\left(-\frac{\mathbf{T_{stim} - t_a}}{\tau}\right), \tag{21}$$

where T_{stim} is the stimulation time period. The same cases presented in Appendix A are followed, except this time, the initial condition of Case 1 will be $v_c(0) = RV_{i0}$, and not $v_c(0) = 0$. The input signal is the same biphasic signal as the first pulse. Using the same differential equation solutions from the first case, with different initial conditions, we get,

Case 1: $-\infty < t \leq 0$

The initial voltage before the onset of the stimulus signal is:

$$v_c(t) = v_c(0) = \mathbf{RV_{i0}} \tag{22}$$

Case 2: $0 < t \leq t_c$

For the first cathodic pulse,

$$i(t) = -I_c.$$

Initial Condition: $v_c(0) = 0$ (From Case 1)

The final solution of the differential equation for this case is:

$$v_c(t) = Ke^{-t/\tau} - I_c R_{ct} \tag{23}$$

Applying the new initial condition, we get the general solution to differential Equation 2 as:

$$\begin{aligned} v_c(0) &= Ke^{-0/\tau} - I_c R_{ct} = RV_{i0} \\ K &= I_c R_{ct} + RV_0 \\ v_c(t) &= (-I_c)R_{ct}[1 - e^{-t/\tau}] + RV_{i0}e^{-t/\tau} \end{aligned} \tag{24}$$

Case 3: $t_c < t \leq t_i$

During this time interval,

$$i(t) = 0.$$

Initial Condition:

$$v_c(t_c+) = (-I_c)R_{ct}[1 - e^{-t_c/\tau}] + RV_{i0}e^{-t_c/\tau} \text{ (From Case 2)}$$

The final solution for this case is (only the homogenous solution, from Eqn. 5)

$$v_c(t) = v_c(t_c+)e^{-(t-t_c)/\tau} \tag{25}$$

Applying the initial condition:

$$\begin{aligned} v_c(t) &= [(-I_c)R_{ct}[1 - e^{-t_c/\tau}] + RV_{i0}e^{-t_c/\tau}].e^{-(t-t_c)/\tau} \\ v_c(t) &= [(-I_c)R_{ct}[1 - e^{-t_c/\tau}].e^{-(t-t_c)/\tau} + RV_{i0}e^{-t/\tau} \end{aligned}$$

Case 4: $t_i < t \leq t_a$

During this time interval,

$$i(t) = +I_a.$$

Initial Condition:

$$v_c(t_i+) = [(-I_c)R_{ct}[1 - e^{-t_c/\tau}].e^{-(t_i-t_c)/\tau} + RV_{i0}e^{-t_i/\tau} \text{ (From Case 3)}$$

The final solution for this case is:

$$v_c(t) = Ke^{-(t-t_i)/\tau} + I_aR_{ct} \tag{26}$$

Applying the initial condition:

$$v_c(t_i+) = K\cancelto{1}{e^{-(t-t_i)/\tau}} + I_aR_{ct} = [(-I_c)R_{ct}[1 - e^{-t_c/\tau}].e^{-(t_i-t_c)/\tau} + RV_{i0}e^{-t_i/\tau}$$

$$K = -I_aR_{ct} + [(-I_c)R_{ct}[1 - e^{-t_c/\tau}].e^{-(t_i-t_c)/\tau} + RV_{i0}e^{-t_i/\tau}$$

$$\Rightarrow v_c(t) = [-I_aR_{ct} + [(-I_c)R_{ct}[e^{-(t_i-t_c)/\tau} - e^{-t_i/\tau}] + RV_{i0}e^{-t_i/\tau}]].e^{-(t-t_i)/\tau} + I_aR_{ct}$$

$$v_c(t) = I_aR_{ct}[1 - e^{-(t-t_i)/\tau}] + [(-I_c)R_{ct}[e^{-(t_i-t_c)/\tau} - e^{-t_i/\tau}] + RV_{i0}e^{-t_i/\tau}].e^{-(t-t_i)/\tau} \tag{27}$$

Case 5: $t_a < t < \infty$

During this time interval,

$$i(t) = 0.$$

Initial Condition (From Case 4):

$$v_c(t_a+) = I_aR_{ct}[1 - e^{-(t_a-t_i)/\tau}] + (-I_c)R_{ct}[e^{-(t_a-t_c)/\tau} - e^{-t_a/\tau}] + RV_{i0}e^{-t_a/\tau}$$

The homogeneous solution for this case is (from Eqn. 5)

$$v_c(t) = Ke^{-(t-t_a)/\tau} \tag{28}$$

Applying the initial condition:

$$v_c(t_a) = \cancelto{1}{Ke^{-(t_a-t_a)/\tau}} = I_a R_{ct}[1 - e^{-(t_a-t_i)/\tau}] + (-I_c)R_{ct}[e^{-(t_a-t_c)/\tau} - e^{-t_a/\tau}] + RV_{i0}e^{-t_a/\tau}$$

$$\Rightarrow v_c(t) = [I_a R_{ct}[1 - e^{-(t_a-t_i)/\tau}] + (-I_c)R_{ct}[e^{-(t_a-t_c)/\tau} - e^{-t_a/\tau}] + RV_{i0}e^{-t_a/\tau}].e^{-(t-t_a)/\tau} \quad (29)$$

The residual voltage at the end of the anodic phase of the second pulse is,

$$\Rightarrow v_c(t_{a+}) \quad = I_a R_{ct}[1 - e^{-(t_a-t_i)/\tau}] + (-I_c)R_{ct}[e^{-(t_a-t_c)/\tau} - e^{-t_a/\tau}] + RV_{i0}e^{-t_a/\tau}$$

Using Equation 21, the initial value for the *third* stimulation pulse can be represented using RV_0, resulting in RV_1:

$$\begin{aligned}
RV_1 &= \left[I_a R_{ct}[1 - e^{-(t_a-t_i)/\tau}] + (-I_c)R_{ct}[e^{-(t_a-t_c)/\tau} - e^{-t_a/\tau}] + RV_{i0}e^{-t_a/\tau}\right].exp\left(-\frac{(T_{stim} - t_a)}{\tau}\right) \\
&= \left[I_a R_{ct}[1 - e^{-(t_a-t_i)/\tau}] + (-I_c)R_{ct}[e^{-(t_a-t_c)/\tau} - e^{-t_a/\tau}]\right].exp\left(-\frac{-(T_{stim} - t_a)}{\tau}\right) \\
&+ [RV_{i0}e^{-t_a/\tau}].exp\left(-\frac{(T_{stim} - t_a)}{\tau}\right) \\
&= RV_{i0} + [RV_{i0}e^{-T_{stim}/\tau}] \\
RV_{i1} &= RV_{i0} + RV_{i0}e^{\frac{-T_{stim}}{\tau}} \quad (30)
\end{aligned}$$

Recursively applying Equation 30, we get,

$$\begin{aligned}
RV_{i2} &= RV_{i0} + RV_{i1}e^{\frac{-T_{stim}}{\tau}} \\
&= RV_{i0} + \left[RV_{i0} + +RV_{i0}e^{\frac{-T_{stim}}{\tau}}\right]e^{\frac{-T_{stim}}{\tau}} \\
&= RV_{i0}\left[1 + e^{\frac{-T_{stim}}{\tau}} + e^{\frac{-T_{stim}}{\tau}}\right] \\
&... \\
RV_{in} &= RV_{i0}\left[1 + e^{\frac{-T_{stim}}{\tau}} + e^{\frac{-2T_{stim}}{\tau}} + ... + e^{\frac{-nT_{stim}}{\tau}}\right] \quad (31)
\end{aligned}$$

Assuming the ratio T_{stim}/τ is to be less than 1, implies that the term $e^{-T_{stim}/\tau}$ is always less than 1. The right hand side of Equation 31 is the sum of a geometric series, with the common ratio being less than 1. The sum of such a series converges to,

$$RV_{in} = RV_{i0} \lim_{n\to\infty} \frac{1 - (exp(-T_{stim}/\tau)^{n-1}}{1 - exp(-T_{stim}/\tau} \tag{32}$$

The asympototic value, when $n \to \infty$, will be,

$$RV_{in} = RV_{i0} \left[\frac{1}{1 - exp\left(\frac{-T_{stim}}{\tau}\right)} \right] \tag{33}$$

C Biphasic Mismatch - Charge, Current and Time

This section consists of the algebraic steps that arrive at Equation 3.5, using the definitions of biphasic mismatch for charge, current, and time, presented in Section 3.2.1. The charge mismatch is expressed as,

$$\begin{aligned} \beta_Q &= \frac{Q_c - Q_a}{Q_c} \\ \Rightarrow \beta_Q &= \frac{I_c T_c - I_a T_a}{I_c T_c}, \end{aligned} \tag{34}$$

$$\tag{35}$$

The biphasic current mismatch and the pulse-width mismatch expressions are,

$$\begin{aligned} \beta_I = \ \frac{I_c - I_a}{I_c} \ &\Rightarrow \frac{I_a}{I_c} = 1 - \beta_I \\ \beta_T = \ \frac{T_c - T_a}{T_c} \ &\Rightarrow \frac{T_a}{T_c} = 1 - \beta_T \end{aligned} \tag{36}$$

where Q represents the charge in the phase, I represents the current amplitude and T represents the pulse-width of the respective phase.

$$\begin{aligned} \beta_I \times \beta_T &= \frac{I_c - I_a}{I_c} \times \frac{T_c - T_a}{T_c} \\ &= \frac{I_c T_c - I_a T_c - I_c T_a + I_a T_a}{I_c T_c} \end{aligned} \tag{37}$$

$$\tag{38}$$

Subtracting and adding the term $I_a T_a$ in the numerator of Equation 37, we get,

$$\begin{aligned} \beta_I \times \beta_T &= \frac{I_c T_c - I_a T_a + I_a T_a - I_a T_c - I_c T_a + I_a T_a}{I_c T_c} \\ &= \frac{I_c T_c - I_a T_a}{I_c T_c} + \frac{2 I_a T_a - I_a T_c - I_c T_a}{I_c T_c} \\ &= \frac{I_c T_c - I_a T_a}{I_c T_c} + 2\frac{I_a}{I_c} \times \frac{T_a}{T_c} - \frac{I_a}{I_c} - \frac{T_a}{T_c} \\ \beta_I \beta_T &= \beta_Q + 2\beta_I \beta_T - \beta_I - \beta_T \end{aligned} \tag{39}$$

The relationship between charge mismatch and the current and pulse-width mismatch errors is given by,

$$\beta_Q = \beta_T + \beta_I - \beta_I \beta_T \tag{40}$$

D Generalized Definition of Residual Voltage

As defined in Section 3.2.2, residual voltage in biphasic electrical stimulation is the voltage that appears at the end of the recovery phase of a biphasic stimulation waveform. Residual voltage occurs due to a combination of two factors: one, the mismatch in charge between the stimulation and recovery phases and two, the unidirectional leakage of the double layer capacitance across the charge-transfer resistance for the duration of the pulse. The residual

voltage equation at the end of the first biphasic pulse, including the effects of mismatch is,

$$RV|_{T,mismatch} = -I_c R_{ct}\left[exp(-\frac{-(T_i+(1-\beta_T)T_c}{\tau}) - exp\left(-\frac{-(T_i+(2-\beta_T)T_c}{\tau}\right)\right] \\ +(1-\beta_I)I_c R_{ct}\left[1-exp\left(\frac{-(1-\beta_T)Tc}{\tau}\right)\right] \quad (41)$$

E Relaxation Time Constant

The residual voltage represents the discharge of the double layer capacitance, C_{dl}, across the charge transfer resistance, R_{ct}. In order to determine the parametric values of the electrode/electrolyte (tissue) model (shown in Figure 2.2b), we analyze the transient step-down response of the first order model to observe the *relaxation* time constant of the double-layer capacitance and the charge transfer resistance. In this section, we derive the electrical equations that are used to calculate the parametric values.

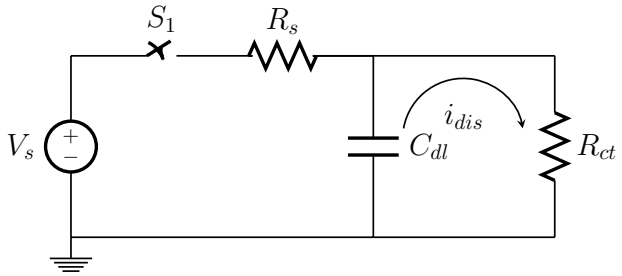

Figure E.3: Step-down switch circuit for electrode model parameter estimation

Consider the circuit shown in Figure E.3. The responses of the circuit are observed when the switch, $S1$, is closed, and when it is open. Firstly, when the switch S_1 is closed, the circuit reaches steady state, where there is no current through C_{dl}. The DC current in steady state is (Equation 42),

$$I_s = \frac{V_s}{(R_s + R_{ct})} \quad (42)$$

Once the capacitor, C_{dl}, has charged upto $V_c = V_s \times \frac{R_{ct}}{(R_s+R_{ct})}$, switch S_1 is opened and the

capacitor discharges via the charge transfer resistance. The capacitor discharge is modeled as a first order differential equation written by equating the current in the loop, which solves to the form in (43), using $v_c(0) = V_c$ as the initial condition of the capacitor.

$$\begin{aligned} C_{dl}\frac{dv_c}{dt} &= -\frac{v_c}{R_{ct}} \\ v_c(t) &= V_c e^{-\frac{t}{\tau}} \end{aligned} \tag{43}$$

F Time Constant Intercept of Exponential Decay

The time constant, τ, for a decaying exponential curve, $y = e^{-t/\tau}$, is the difference between the x-intercept of the tangent drawn at any point on the curve, and the value of the x-coordinate at that point. Consider the diagram shown in Figure F.4, it is required to prove $t_2 - t_1 = \tau$.

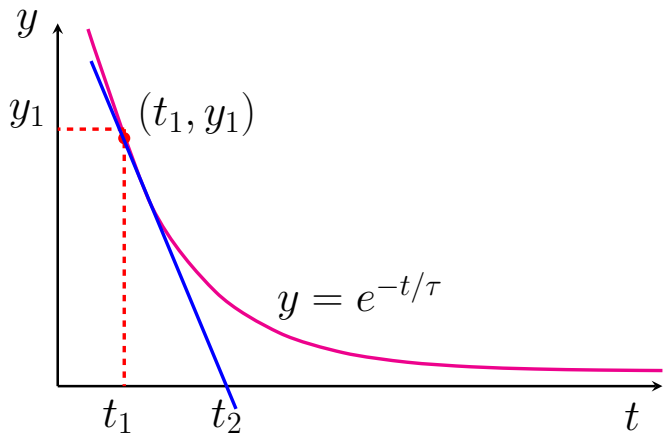

Figure F.4: Exponential curve, $y = e^{-t/\tau}$, with the tangent drawn at an arbitrary point (t_1, y_1). The intercept of the tangent line is at $(t_2, 0)$. It can be shown that $\tau = t_2 - t_1$.

Step 1: The slope of the tangent line at (t_1, y_1) is,

$$y'|_{t=t_1} = e^{-t_1/\tau}.\frac{-1}{\tau} = \frac{-y_1}{\tau}. \tag{44}$$

Step 2: The equation of the tangent line is,

$$y = \frac{-y_1}{\tau}t + t_2. \tag{45}$$

Step 3: The equation of the tangent line can also be formulated as,

$$\frac{y - y_1}{0 - y_1} = \frac{t - t_1}{t_2 - t_1}, \tag{46}$$

which can be rearranged as,

$$\begin{aligned} y - y_1 &= \frac{(-y_1)(t - t_1)}{t_2 - t_1} \\ &= \frac{-y_1}{t_2 - t_1}t + \frac{y_1 t_1}{t_2 - t_1} \\ \Rightarrow y &= \frac{-y_1}{t_2 - t_1}t + y_1\left(1 + \frac{t_1}{t_2 - t_1}\right) \\ y &= \frac{-y_1}{t_2 - t_1}t + y_1 t_2 \end{aligned} \tag{47}$$

Comparing the slopes of Equations 45 and 47, we get,

$$\tau = t_2 - t_1 \tag{48}$$

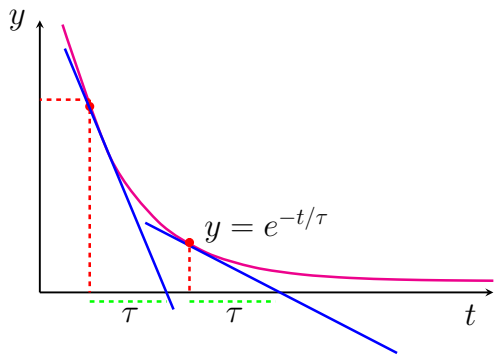

Figure F.5: Graphical intercept of exponential decay depicting Equation 48

G Simplified Feedback Model for Active Anodic Stimulation

The equation for the residual voltage, in terms of the pulse-widths, at the end of the stimulation pulse is given by,

$$\begin{aligned} RV|_{T_a} = \Bigg[& -I_c R_{ct} \left(exp(-\frac{(T_a + T_i)}{\tau}) - exp(-\frac{(T_a + T_i + T_c)}{\tau}) \right) \\ & + (1 - \beta_I) I_c R_{ct} \left(1 - exp(-\frac{T_a}{\tau}) \right) \Bigg] . exp \left(-\frac{T_{stim} - (T_a + T_i + T_c)}{\tau} \right) \end{aligned} \tag{49}$$

By taking the exponential into the square brackets, we get,

$$\begin{aligned} RV|_{T_a} = \Bigg[& -I_c R_{ct} \left(exp(-\frac{(T_{stim} + T_c)}{\tau}) - exp(-\frac{T_{stim}}{\tau}) \right) \\ & + (1 - \beta_I) I_c R_{ct} \left(exp \left(-\frac{T_{stim} - (T_a + T_i + T_a)}{\tau} \right) - exp \left(-\frac{T_{stim} - (T_c + T_i)}{\tau} \right) \right) \Bigg] \end{aligned} \tag{50}$$

The purpose of active anodic feedback is to correct the anodic pulse to reduce the residual voltage. If the residual voltage is not at 0, the controller adjusts the anodic pulse width such that it is. The residual voltage is small ($\approx 5mV$) and should be typically at 0V. In this regard, to design a feedback system, we linearize the residual voltage about an optimum anodic pulse width, $T_{a,op}$, using the Taylor series expansion,

$$RV(T_a) = RV(T_{a,op}) + RV'(T_{a,op})[T_a - T_{a,op}] \tag{51}$$

The value of $RV(T_{a,op}) = 0$, in our case, because the optimum anodic pulse width will be at a residual voltage of zero. By taking the derivative of $RV(T_a)$ with respect to T_a, we get

the linearization equation of residual voltage about an operating anodic pulse width, $T_{a,op}$,

$$RV(T_a) = \frac{-1}{\tau}(1-\beta_I)I_c R_{ct} exp\left(-\frac{T_{stim}-(T_{a,op}+T_i+T_c)}{\tau}\right)[T_a - T_{a,op}] \tag{52}$$

Let the slope of the linear equation be C_0, i.e.,

$$C_0 = \frac{-1}{\tau}(1-\beta_I)I_c R_{ct} exp\left(-\frac{T_{stim}-(T_{a,op}+T_i+T_c)}{\tau}\right). \tag{53}$$

Residual Voltage Model

Because residual voltage is sampled at a frequency of the stimulation frequency only, it is more appropriate to discuss the system of active anodic feedback in the discrete domain. Let the residual voltage that is about to be corrected be $RV[k]$. The residual voltage of the new pulse, is the RV of the previous pulse discharging over the duration of the stimulation time period, added to the linearized model of residual voltage for the new anodic pulse width from Equation 52, $T_a[k]$,

$$RV[k] = RV[k-1]exp(\frac{-T_{stim}}{\tau}) + C_0[T_a[k] - T_{a,op}] \tag{54}$$

Let the exponential decay over the stimulation time period be $C_1 = exp(\frac{T_{stim}}{\tau})$. To obtain a dynamical model for RV with respect to Ta, we write Equation 3.1 at $[k+1]$ and subtract the two equations to get,

$$\begin{aligned} RV[k+1] &= RV[k]exp(\frac{-T_{stim}}{\tau}) + C_0[T_a[k+1] - T_{a,op}] \\ RV[k+1] - RV[k] &= C_1(RV[k] - RV[k-1]) + C_0[T_a[k+1] - T_a[k]) \end{aligned} \tag{55}$$

Obtaining the z-transform of the previous equation, we get,

$$zRV(z) - RV(z) = C_1(RV(z) - z^{-1}RV(z)) + C_0[zT_a(z) - T_a(z)) \tag{56}$$

$$\Rightarrow G(z) = \frac{RV(z)}{T_a(z)} = \frac{C_0 z}{z - C_1} \tag{57}$$

Anodic Pulse Width Feedback Model

The anodic pulse width, $T_a[k]$, for the k^{th} stimulation pulse is adjusted using PID control from the previous pulse width. The control equation using negative feedback that is implemented is given by,

$$\begin{aligned} T_a[k] = T_a[k-1] - \Bigg[& k_p RV[k-1] + k_i T_{stim} \frac{(RV[k-1] + RV[k-2])}{2} \\ & + k_d \frac{RV[k-1] - RV[k-2]}{T_{stim}} \Bigg] \end{aligned} \tag{58}$$

where T_{stim} is also the sampling frequency, because the residual voltage is sampled after every stimulation pulse. The z-transform for the above difference equation is,

$$\begin{aligned} T_a(z) = z^{-1}T_a(z) - \Bigg[& k_p z^{-1} RV(z) + \frac{k_i T_{stim}}{2}(z^{-1}RV(z) - z^{-2}RV(z)) \\ & + \frac{k_d}{T_{stim}}(z^{-1}RV(z) - z^{-2}RV(z)) \Bigg] \end{aligned} \tag{59}$$

The transfer function for the feedback equation, obtained from the difference equation will be,

$$\Rightarrow F(z) = \frac{T_a(z)}{RV(z)} = \frac{a_1 z + a_0}{z^2 - z}$$

where,

$$\begin{aligned} a_0 &= k_p + \tfrac{k_i T_{stim}}{2} + \tfrac{k_d}{T_{stim}} \\ a_1 &= \tfrac{k_i T_{stim}}{2} = \tfrac{k_d}{T_{stim}} \end{aligned} \tag{60}$$

The simplified feedback system for controlling the residual voltage is given in Figure 6.4 in Chapter 6. While the model derived above closely follows the procedure implemented for practical active anodic feedback using PID control, it is imperative to highlight that a tractable theoretical model may not incorporate all aspects of the physical system.

H Post Degradation eSEM Images - 50kX Mag

Scanning electron microscope images taken at 50kX magnification for electrodes after undergoing the degradation protocol.

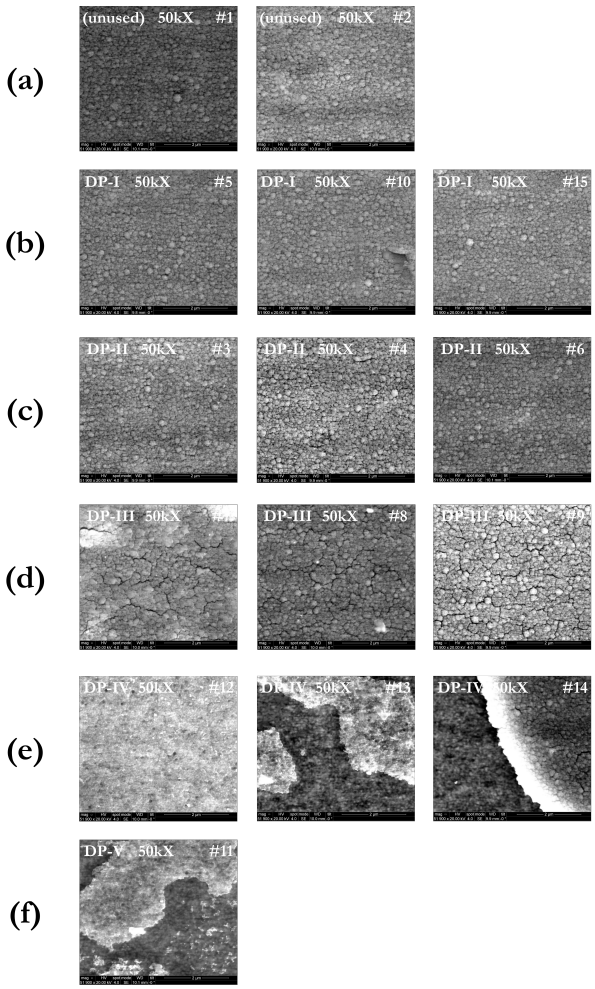

Figure H.6: Wet SEM Images after Degradation Protocol 50kX Magnification (DP, Table 5.2): (a) Unused electrodes showing the general structure of SIROF film (b) DP - I, nominal voltage range, within the water window, there is no significant texture change in all electrodes (c) DP - II, operated at the water window limits, cracks start to appear on the surface (d) DP - III, operated above the water window, the SIROF film starts to rupture (e) DP - IV, operated above the water window, shows delamination, resulting in absence of SIROF material in most areas (f) DP - V, test case with very high voltage ranges showing delamination.

I Supplementary Methods

This appendix consists of supplementary methods to substantiate evidence described in Chapters 5, 6 and 7.

I.1 Switch Circuit Measurement

The relaxation time constant for a given bias value was obtained by charging the electrode to a known bias, and measuring the open circuit voltage response of the electrode. The purpose of the relaxation time constant measurement is to obtain an estimate of the value for the product of the double-layer capacitance and the charge-transfer resistance. The measurement system is shown in Figure I.7 and the relaxation time constant is graphically estimated by calculating the intercept of the tangent at the instant of discharge, as shown in Figure I.8. For an exponential decay, assuming the circuit is opened at time $t = t_0$, the intercept of the tangent line at t_0 intercepts the time axis at one time constant (τ) from t_0 (refer Appendix F).

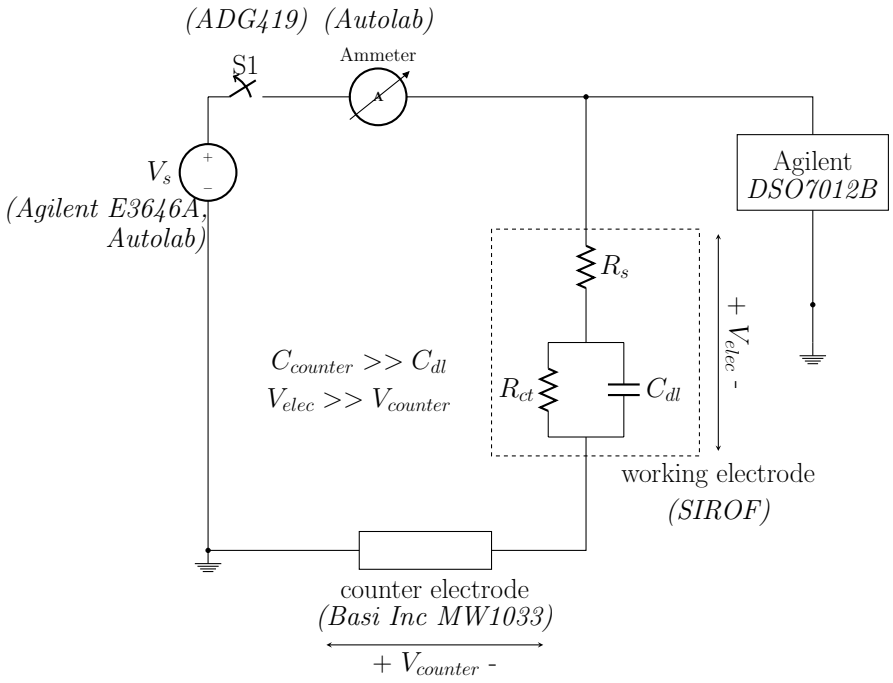

Figure I.7: Measurement setup for two electrode step response measurements. The open circuit potential (OCP) measurement module of Metrohm Autolab (instrument) and Nova 1.11 (software) was used to record the voltage when the switch, $S1$, is open.

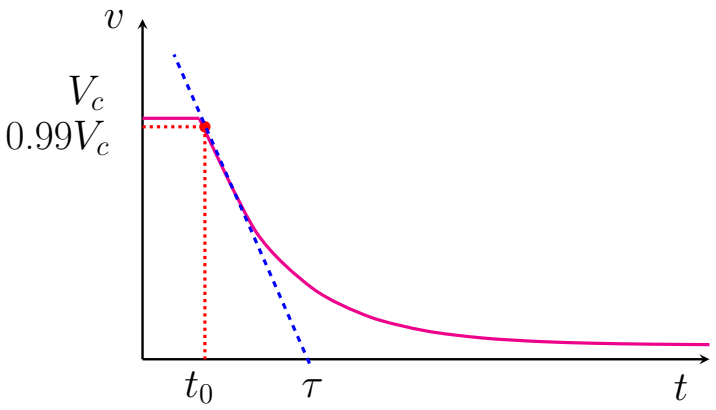

Figure I.8: Estimation of the relaxation time constant: $\tau = R_{ct} \times C_{dl}$. For an exponential decay, the intercept of the tangent line at t_0 intercepts the time axis at one time constant (τ) from t_0 (refer Appendix F).

I.2 MATLAB Pseudocode for Electrode Model Simulation

The MATLAB function used to simulate the electrode model response and generate an RV growth curve is presented in this appendix. The response to a single pulse can be used against measured data to obtain a fit by parametrically sweeping the values of R_s, C_{dl} and R_{ct}. The MATLAB function for obtaining a transient simulation for a linear transfer function model is `lsim()`, and to obtain a goodness of fit with measured data is `goodnessofFit()`.

```
function [Velec,RV,T,SAMP] = lsimRV(stimParam,elecModel,Fs)
% lsimRV generates biphasic current stimulation (parameters in stimParam)
% response curves for a first-order electrode model (elecModel)
% at sampling frequency specified by Fs.


%Biphasic Current Stimulation Waveform Parameters
Ic = stimParam(1); %Cathodic current
Ia = stimParam(2); %Anodic current
Tc = stimParam(3); %Cathodic pulse width
Ti = stimParam(4); %Anodic pulse width
Ta = stimParam(5); %Interphase pulse width
Tstim = stimParam(6); %Stimulation period
Tsamp = stimParam(7); %RV sampled point
nStim = stimParam(8); %Number of stimulation pulses

%Electrode Model Parameters
Rs = elecModel(1);
Cdl = elecModel(2);
Rct = elecModel(3);
```

```
if nargin<3
Fs = 1e6;
end

Tr = Tstim - (Ta+Ti+Tc);
Tsamp = Tc+Ti+Ta+1e-3;

%Generate one biphasic pulse
y = [Ic*ones((Tc*Fs),1);zeros((Ti*Fs),1);Ia*ones((Ta*Fs),1); ...
zeros((int32(Tr*Fs)),1);]';

%Generate transfer function for the elecModel
X = tf([Cdl*Rs*Rct (Rs+Rct)],[Cdl*Rct 1]);

%Repeat biphasic pulse (periodic) for #Stimulation Pulses
Y = repmat(y,1,nStim);
T = 0:(1/Fs):(nStim*Tstim-(1/Fs));

%Simulate response for the model
[Velec] = lsim(X,Y,T);

%Identify sampled values
SAMP = int32((Tstim*[0:(nStim-1)]+Tsamp)*Fs);
%Find the residual voltage curve from the time response
[RV] = Velec(SAMP);
```

Electrode Model Simulation

The biphasic stimulation pulse form was simulated in MATLAB, and values of R_s, C_{dl} and R_{ct} were parametrically swept to estimate model parameters for multiple arrays of SIROF electrodes. The goodness of fit with measured biphasic stimulus data was evaluated and used as a constraint for optimization. An typical fit is shown in Figure I.9. The pseudocode used in MATLAB is presented in Appendix I.2.

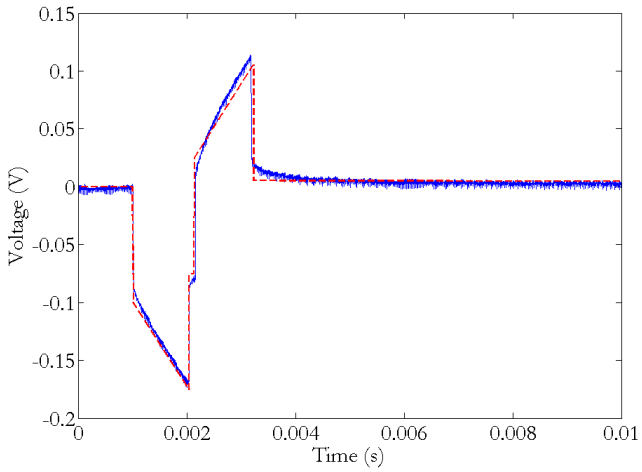

Figure I.9: Biphasic stimulation response superimposed with a model fit using the MATLAB `lsim` function. The parameter values obtained from the simulation $R_s = 0.8\text{k}\Omega$, $C_{dl} = 4\mu\text{F}$ and $R_{ct} = 1\text{M}\Omega$, with a normalized goodness of fit of 0.96.

Bibliography

[1] D. B. Shire *et al.*, "Development and implantation of a minimally invasive wireless subretinal neurostimulator," *IEEE Transactions on Biomedical Engineering*, vol. 56, pp. 2502–2511, 2009.

[2] J. F. Rizzo, "Update on retinal prosthetic research: The boston retinal implant project," *Journal of Neuro-Opthalmology*, vol. 31, no. 2, pp. 160–168, Jun 2011.

[3] V. Nutton, "Scribonius largus, the unknown pharmacologist," *Pharmaceutical History*, vol. 25, no. 1, pp. 5–8, Mar 1995.

[4] S. Finger and M. Piccolino, *The Shocking History of Electric Fishes: From Ancient Epochs to the Birth of Modern Neurophysiology.* MIT Press, 2013.

[5] G. W. Finkelstein, *Emil du Bois-Reymond: Neuroscience, Self and Society in 19th Century Germany.* Oxford University Press, 2013.

[6] A. Pascual-Leone and T. Wagner, "A brief summary of the history of noninvasive brain stimulation," *Annual Review of Biomedical Engineering*, vol. 9, pp. 527–565, 2007.

[7] P. L. Gildenberg, "History of electrical neuromodulation for chronic pain," *Pain Medicine*, vol. 7, pp. S7–S13, 2006.

[8] S. Sandrone and E. Zanin, "David ferrier (1834-1928)," *Journal of Neurology*, vol. 261, pp. 1247–1248, 2014.

[9] R. A. Wilson and F. C. Keil, Eds., *MIT Encyclopedia of Cognitive Science.* MIT Press, 1999.

[10] J. C. Lilly, J. R. Hughes, E. C. A. Jr., and T. W. Galkin, "Brief, noninjurious electric waveform for stimulation of the brain," *Science*, vol. 121, pp. 468–469, 1955.

[11] M. Riordan and L. Hoddeson, *Crystal Fire: The Invention of the Transistor and the Birth of the Invention Age.* W. W. Norton and Co., 1998.

[12] W. Greatbatch and C. F. Holmes, "History of implantable devices," *IEEE Engineering in Medicine and Biology*, vol. 10, pp. 38–41.

[13] A. Mudry and M. Mills, "The early history of the cochlear implant," *JAMA Otolaryngol Head Neck Surg.*, vol. 139, pp. 446–453.

[14] L. Mertz, "Sight restoration comes into focus: Versions of visual prosthesis," *IEEE Pulse Magazine*, vol. 12, pp. 2154–2287, 2012.

[15] M. Inc., "Reveal LINQ Insertable Cardiac Monitor," https://www.medtronic.com/patients/fainting/device/our-insertable-cardiac-monitors/reveal-linq-icm/, 2008, [Online; accessed 5-November-2015].

[16] K. Deisseroth, "Optogenetics," *Nature Methods*, vol. 8, pp. 26–29, 2011.

[17] D. Braeken *et al.*, "Local electrical stimulation of single adherent cells using three-dimensional electrode arrays with small interelectrode distances," *31st Annual Conference of the IEEE Engineering in Medicine and Biology Society*, pp. 2756–2759, Sep. 2009.

[18] S. F. Cogan, "Neural stimulation and recording electrodes," *Annual Review of Biomedical Engineering*, vol. 10, pp. 275–309, 2008.

[19] W. F. Agnew and D. B. McCreery, *Neural Prosthesis: Fundamental Studies.* Prentice Hall, 1990.

[20] D. R. Merrill, M. Bikson, and J. G. R. Jefferys, "Electrical stimulation of excitable tissue: design of efficacious and safe protocols," *Journal of Neuroscience Methods*, vol. 141, no. 141, pp. 171–198, October 2005.

[21] L. A. Geddes, "Historical evolution of circuit models for the electrode-electrolyte interface," *Annals of Biomedical Engineering*, vol. 25.

[22] S. Kelly and J. Wyatt, "A power-efficient neural tissue stimulator with energy recovery," *IEEE Transactions on Biomedical Circuits and Systems*, vol. 5, pp. 20–29, 2011.

[23] V. J. Jose and M. Ghovanloo, "Towards a switched-capacitor based stimulator for efficient deep-brain stimulation," in *32nd Annual International Conference of the IEEE Engineering in Medicine and Biology Society*, Sept, pp. 2927–2930.

[24] X. Liu, A. Demostheous, and N. Donaldson, "In vitro evaluation of a high-frequency current-switching stimulation technique for fes applications," in *13th Annual Conference of the International Functional Electrical Stimulation Society*, Sept 2008, pp. 291–293.

[25] M. Ortmanns, "Charge balancing in functional electrical stimulators: A comparative study," *IEEE International Symposium on Circuits and Systems*, pp. 573 – 576, 2007.

[26] F. Rattay, "Analysis of models for extracellular fiber stimulation," *IEEE Transactions on Biomedical Engineering*, vol. 36.

[27] A. Krishnan and S. Kelly, "On the cause and control of residual voltage generated by electrical stimulation of neural tissue," in *34th Annual International Conference of the Engineering in Medicine and Biology Society*, August 2012.

[28] S. Moradi, E. Maghsoudloo, and R. Lotfi, "New charge balancing method based on imbalanced biphasic current pulses for functional electrical stimulation," in *20th Iranian Conference on Electrical Engineering*, May 2012.

[29] L. Zheng, S. Shin, and S.-M. Kang, "Design of a neural stimulator system with closed loop charge cancellation," in *IEEE 20th International Conference on VLSI and System-on-Chip (VLSI-SoC)*, Oct 2012.

[30] K. Sooksood, T. Stieglitz, and M. Ortmanns, "An active approach for charge balancing in functional electrical stimulation," *IEEE Transactions on Biomedical Circuits and Systems*, vol. 4, pp. 162 – 170, 2010.

[31] H. Chun, Y. Tang, and T. Lehmann, "Required matching accuracy of biphasic current pulse in multi-channel current mode bipolar stimulation for safety," in *34th Annual International Conference of the IEEE Engineering in Medicine and Biology Society*, August 2012.

[32] Fisher Scientific, "PBS 10X Solution - Safety Data Sheet," 2014.

[33] A. J. Bard and L. R. Faulkner, *Electrochemical Methods: Fundamentals and Applications*. John Wiley and Sons, Inc., 2001.

[34] F. Scholz, Ed., *Electroanalytical Methods: Guide to Experiments and Applications*. Springer, 2010.

[35] S. F. Cogan *et al.*, "Potential-biased, asymmetric waveforms for charge-injection with activated iridium oxide (airof) neural stimulation electrodes," *IEEE Transactions on Biomedical Engineering*, vol. 53, pp. 327 – 332, 2006.

[36] D. R. Merrill and P. A. Tresco, "Impedance characterization of microarray recording electrodes in vitro," *IEEE Transactions on Biomedical Engineering*, vol. 52, pp. 1960–1965, 2005.

[37] J. O. Bockris, A. K. N. Reddy, and M. Gamboa-Aldeco, *Electrodics*. Kluwer Academic Publishers, 2002.

[38] S. Negi, R. Bhandari, R. van Wagenen, and F. Solzbacher, "Factors affecting degradation of sputtered iridium oxide used for neuroprosthetic applications," in *IEEE 23rd International Conference on Micro Electro Mechanical Systems*, Jan 2010.

[39] A. Krishnan and S. Kelly, "On using residual voltage to estimate electrode model parameters for damage detection," in *IEEE Biomedical Circuits and Systems Conference*, October 2015.

[40] S. F. Cogan *et al.*, "Sputtered iridium oxide films (sirofs) for neural stimulation electrodes," *IEEE Engineering in Medicine and Biology Conference*, pp. 4153–4156, 2004.

[41] J. Mozota and B. E. Conway, "Surface and bulk processes at oxidized iridium electrodes – i. monolayer stage and transition to reversible multilayer oxide film behaviour," *Electrochimica Acta*, vol. 26.

[42] D. B. McCreery, W. F. Agnew, T. G. Yuen, and L. Bullara, "Charge density and charge per phase as cofactors in neural injury induced by electrical stimulation," *IEEE Transactions on Biomedical Engineering*, vol. 37, pp. 996–1001, 1990.

[43] R. V. Shannon, "A model for safe levels of electrical stimulation," *IEEE Transactions on Biomedical Engineering*, pp. 424–426, Apr. 1992.

[44] K. Sooksood, T. Stieglitz, and M. Ortmanns, "An active approach for charge balancing in functional electrical stimulation," in *IEEE International Symposium on Circuits and Systems*, May 2009, pp. 341–344.

[45] A. Scheiner, J. T. Mortimer, and U. Roessmann, "Imbalanced biphasic electrical stimulation: Muscle tissue damage," *Annual International Conference of the IEEE Engineering in Medicine and Biology Society*, vol. 12, pp. 1486 – 1487, 1990.

[46] D. E. Seborg, T. F. Edgar, and D. A. Mellichamp, "Process dynamics and control," 1989.

[47] T. F. Weiss, *Cellular Biophysics, Volume II, Electrical Properties.* MIT Press, 1996.

[48] C. J. Schwiening, "A brief historical perspective: Hodgkin and huxley," *Journal of Physiology*, vol. 590, pp. 2571–2575.

[49] E. J. Tehovnik, "Electrical stimulation of neural tissue to evoke behavioral responses." *Journal of Neuroscience Methods*, vol. 65, no. 1, pp. 1–17, Mar. 1996.

[50] A. Horsager and I. Fine, *The perceptual effects of chronic retinal stimulation*, G. Dagnelie, Ed. Springer, 2011.

[51] S. F. Cogan *et al.*, "Sputtered iridium oxide films for neural stimulation electrodes," *Journal of Biomedical Materials Research Part B*, vol. 89B, pp. 353–361, 2009.

[52] J.-U. Chu *et al.*, "Feedback control of electrode offset voltage during functional electrical stimulation," *Journal of Neuroscience Methods*, vol. 218, pp. 55–71, 2013.

[53] E. Margalit *et al.*, "Can vision be restored by electrical stimulation?" in *Neuroprosthetics: Theory and Practice*, G. S. D. Kenneth W. Horch, Ed. World Scientific, 2004, pp. 1067–1093.

[54] S. Kelly, "A system for efficient neural stimulation with energy recovery," Ph.D. dissertation, Massachusetts Institute of Technology, 2003.

[55] K. L. Roach, "Electrochemical models for electrode behavior in retinal prosthesis," Ph.D. dissertation, Massachusetts Institute of Technology, 2003.

[56] D. R. Merrill, *The Electrochemistry of Charge Injection at the Electrode/Tissue Interface*, D. D. Zhou and E. Greebaum, Eds. Springer, 2010.

[57] R. White, "System design of a cochlear implant," *IEEE Engineering in Medicine and Biology Magazine*, vol. 6, pp. 42–46, 1987.

[58] J. Patrick, P. Seligman, D. Money, and J. Kuzma, "Engineering, in cochlear prosthesis," *IEEE Engineering in Medicine and Biology Magazine*, vol. 6, pp. 42–46, 1987.

[59] J.-J. Sit and R. Sarpeshkar, "A low-power blocking-capacitor-free with less than 6 na dc error for 1-ma," *IEEE Transactions on Biomedical Circuits and Systems*, vol. 1, pp. 172–183, 2007.

[60] M. Sivaprakasam, W. Liu, M. S. Humayun, and J. D. Weiland, "A variable range bi-phasic current stimulus driver circuitry for an implantable retinal prosthetic device," *IEEE Journal of Solid State Circuits*, vol. 40, pp. 763–771, 2005.

[61] S. R. Taylor and E. Gileadi, "Physical interpretation of the warburg impedance," *Corrosion Science*, vol. 51.